NASA Contractor Report 156882

# A Global Atlas of GEOS-3 Significant Waveheight Data and Comparison of the Data with National Buoy Data



J. D. McMillan

November 1981

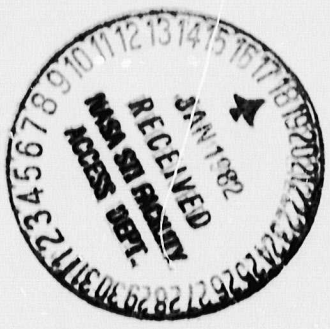


National Aeronautics and Space Administration

**Wallops Flight Center**
Wallops Island, Virginia 23337
AC 804 824-3411

NASA Contractor Report 156882

# A Global Atlas of GEOS-3 Significant Waveheight Data and Comparison of the Data with National Buoy Data

J. D. McMillan

EG&G Washington Analytical Services Center, Inc.
P. O. Box 476
Pocomoke City, MD 21851

Prepared Under Contract No. NAS6-2639

National Aeronautics and
Space Administration

**Wallops Flight Center**
Wallops Island, Virginia 23337
AC 804 824-3411

TABLE OF CONTENTS

PAGE

LIST OF ILLUSTRATIONS . . . . . vi

LIST OF TABLES . . . . . vii

CHAPTER 1 - INTRODUCTION . . . . . 1

1.1 Background . . . . . 1

1.2 General Description of GEOS-3 Spacecraft . . . . . 2

1.3 Lineage of the GEOS-3 Altimeter . . . . . 8

1.4 Description of the GEOS-3 Altimeter . . . . . 9

1.5 GEOS-3 Significant Waveheight Estimation . . . . . 14

1.6 Application of Satellite Significant Waveheight Estimates . . . . . 16

1.7 Scope of the Investigation . . . . . 20

CHAPTER 2 - SIGNIFICANT WAVEHEIGHT FROM SATELLITE ALTIMETERS . . . . . 23

2.1 Waveform Geometry for Negligible SWH . . . . . 23

2.2 Waveform Geometry for Non-Negligible SWH . . . . . 29

2.3 Choice of Model . . . . . 31

2.4 Derivation . . . . . 34

2.5 Convergence Considerations . . . . . 39

2.6 Error Sources . . . . . 46

2.7 Description of Navy SWH Estimation Algorithms . . . . . 51

2.8 Comparison of Other SWH Estimation Algorithms . . . . . 53

CHAPTER 3 - THE DATA SET . . . . . 57

3.1 GEOS Data Set . . . . . 57

3.2 Buoy Data Set . . . . . 62

3.3 Seasat Data Set . . . . . 67

CHAPTER 4 - COMPARISON OF THE GEOS-3 SWH ESTIMATES WITH BUOY AND SEASAT SWH ESTIMATES . . . . . 68

4.1 Computation of GEOS-3 SWH Standard Deviation . . . . 69

4.2 Computation of SWH Mean Difference . . . . . 76

4.3 Linear Regression . . . . . 80

4.4 GOASEX Comparison . . . . . 87

CHAPTER 5 - GLOBAL ATLAS OF SWH DATA . . . . . 90

5.1 Description of the SWH Global Atlas . . . . . 90

5.2 Comparison with the Navy Climatic Atlas . . . . . 93

5.2.1 December Through February Comparison . . . . 96

5.2.2 March Through May Comparison . . . . . 98

5.2.3 June Through August Comparison . . . . . 100

5.2.4 September Through November Comparison . . . . 101

5.3 Discussion of the Contour Comparisons . . . . . 103

CHAPTER 6 - CONCLUSIONS AND RECOMMENDATIONS . . . . . 106

BIBLIOGRAPHY . . . . . 110

APPENDIX A - GLOBAL ATLAS OF GEOS-3 SIGNIFICANT WAVEHEIGHT DATA

# LIST OF ILLUSTRATIONS


| FIGURE | | PAGE |
|---|---|---|
| 1.1 | GEOS-3 Spacecraft Cutaway | 3 |
| 1.2 | GEOS-3 Telemetry Coverage | 4 |
| 1.3 | Intensive Mode Gate Timing | 11 |
| 1.4 | NDBO Buoy Locations | 21 |
| 2.1 | Square Pulse Impinging Upon a Flat Sea Surface | 24 |
| 2.2 | Idealized Mean Return Pulse Shape | 25 |
| 2.3 | Square Pulse Impinging Upon a Rough Sea Surface | 30 |
| 2.4 | Idealized Mean Return Pulse Shape for Several Values of SWH | 32 |
| 2.5 | Algebraic Relationship Between SWH and Estimated Value of c | 42 |
| 3.1 | Data Taken During GEOS-3 Mission | 58 |
| 3.2 | NDBO Buoy Measurement Reporting Periods | 65 |
| 4.1 | Distribution of $SWH_{GEOS} - SWH_{BUOY}$ | 78 |
| 4.2 | Linear Regression with Buoy SWH as Independent Variable | 82 |
| 4.3 | Linear Regression with GEOS SWH as Independent Variable | 83 |
| 4.4 | $SWH_{GEOS} - SWH_{BUOY}$ As a Function of PCA Distance | 86 |
| 5.1 | U. S. Navy Atlas Contour Map of SWH < 1.5 Meters and SWH < 2.5 Meters for January | 94 |

LIST OF TABLES


| TABLE | | PAGE |
|---|---|---|
| 1.1 | NASA Telemetry Stations | 5 |
| 1.2 | Defense Mapping Agency Telemetry Stations | 6 |
| 2.1 | ARS Relative Times | 45 |
| 2.2 | ARS Amplitude Biases | 45 |
| 3.1 | GEOS/BUOY Comparison Data Set | 66 |
| 4.1 | GEOS/BUOY Comparison Results | 70 |
| 4.2 | Statistics of $SWH_{GEOS} - SWH_{BUOY}$ | 77 |
| 4.3 | GEOS-3/Seasat Comparison Statistics for Sub-Track Crossings | 89 |

# CHAPTER 1

# INTRODUCTION

## 1.1 Background

The ability to measure certain ocean wave characteristics over large areas and long periods of time could conceivably have significant impact upon open ocean and coastal activities. Ship routing, search and rescue operations, meteorological research and recreational activities are just a few of the areas where quick and reliable sea state information is desired.

With the advent of satellite altimetry, it is now possible to estimate many ocean wave characteristics with a degree of accuracy which equals or exceeds previous techniques. Specifically, the altimeter on board the Geodynamics Experimental Ocean Satellite (GEOS-3) sampled the radar return waveform from which the ocean significant waveheight (SWH) could be inferred. The ocean significant waveheight, which is sometimes referred to as H-1/3, is defined as the average of the one-third highest waves in a long sequence of waves observed at a point (Neuman and Pierson, 1966).

Satellite significant waveheight measurements taken in the more remote regions of the earth's oceans are of particular interest since local estimates of significant waveheight are made almost entirely from ships at infrequent intervals. The small number of

ships passing through such remote regions, combined with the inherent inaccuracies of human "eyeball" estimates, make global significant waveheight measurements from satellites highly desirable.

The GEOS-3 estimates of significant waveheight were made on a near-global basis and in near-real-time. Although preliminary estimates of the measurement accuracy have been made (McMillan and Roy, 1977, and Parsons, 1977 and July, 1979), a formal determination of the accuracy of these estimates has yet to be presented.

## 1.2 General Description of GEOS-3 Spacecraft

The GEOS-3 spacecraft (see Figure 1.1) was launched from the Air Force Western Test Range on April 9, 1975, as part of the National Geodetic Satellite Program, with the specific objectives of improving man's knowledge of the earth's gravitational field, the size and shape of the terrestrial geoid, the deep ocean tides, sea state, current structure, crustal structure, solid earth dynamics and remote-sensing technology (Stanley, 1979). The spacecraft orbited the earth with a period of 101.8 minutes in a near-circular orbit with an inclination to the equator of $115^{\circ}$. Data were collected and archived from the satellite until November 30, 1978, when active operations were terminated.

GEOS-3 telemetry data were acquired from four sources: the NASA STDN (Space Tracking and Data Network) VHF telemetry sites,

ORIGINAL PAGE IS
OF POOR QUALITY

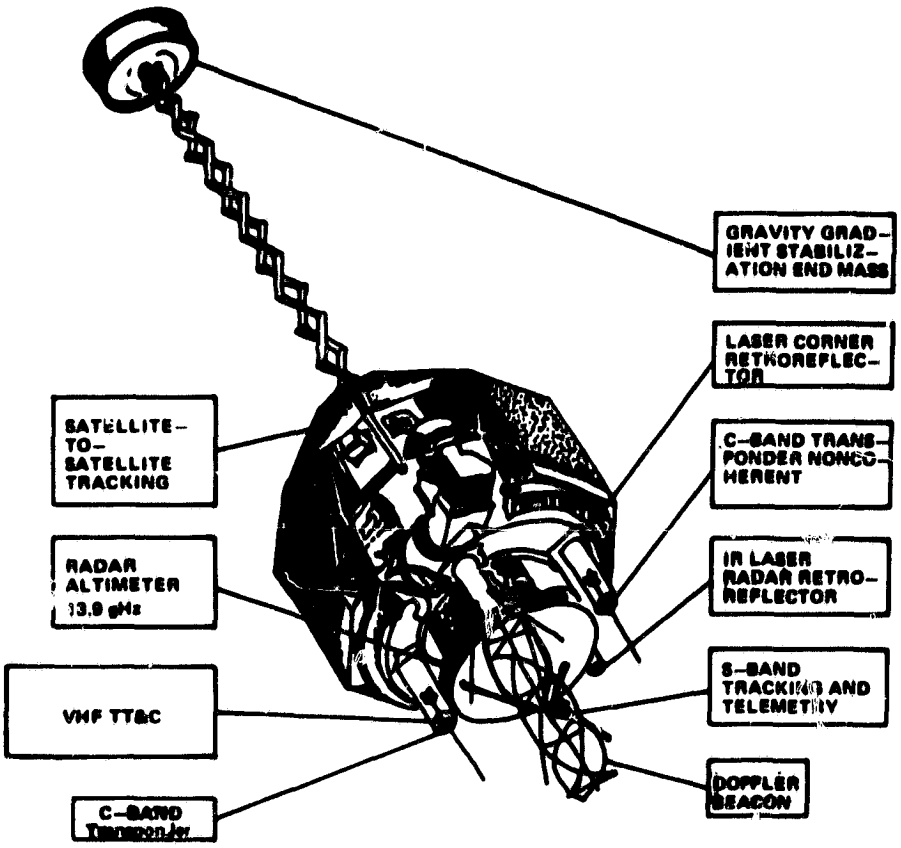


FIGURE 1.1. GEOS-3 SPACECRAFT CUTAWAY

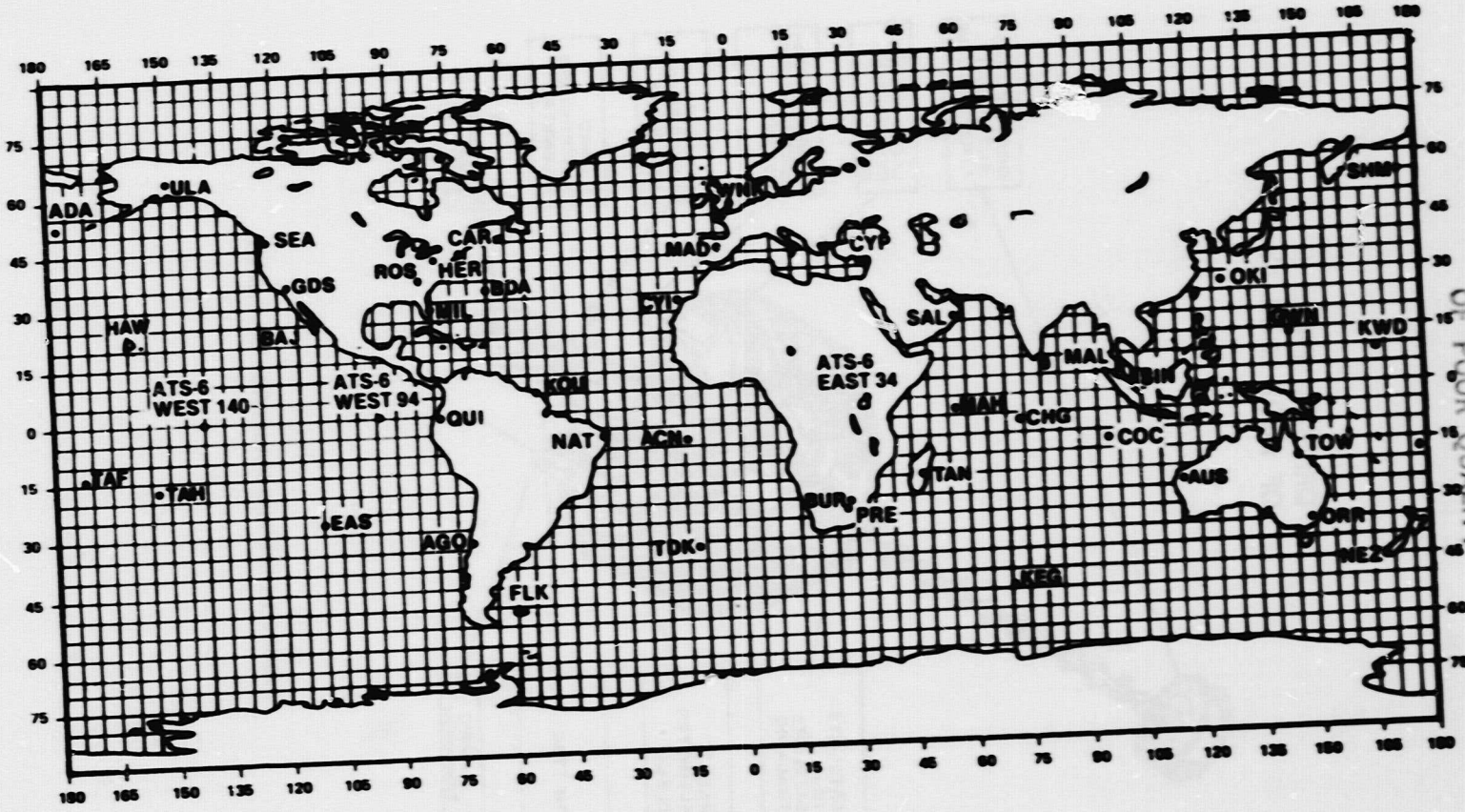


FIGURE 1.2. GEOS–3 TELEMETRY COVERAGE

| STATION | TOTAL NUMBER OF GOOD PASSES | OPERATIONAL DATES START | STOP |
|---|---|---|---|
| Merritt Islands, Florida (MIL) | 1181 | April 10, 1975 | Dec. 1, 1978 |
| Rosman, North Carolina (ROS) | 641 | April 10, 1975 | Dec. 1, 1978 |
| Winkfield, United Kingdom (WNK) | 1221 | April 10, 1975 | Dec. 1, 1978 |
| Bermuda Islands (BDA) | 398 | April 10, 1975 | Dec. 1, 1978 |
| Madrid, Spain (MAD) | 122 | April 10, 1975 | Dec. 1, 1978 |
| Ascension (ACN) | 457 | April 10, 1975 | Dec. 1, 1978 |
| Johannesburg (BUR) | 118 | April 10, 1975 | Oct. 31, 1975 |
| Guam (GWM) | 410 | April 10, 1975 | Dec. 1, 1978 |
| Orroral, Australia (ORR) | 482 | April 10, 1975 | Dec. 1, 1978 |
| Hawaii (HAW) | 706 | April 10, 1975 | Dec. 1, 1978 |
| Fairbanks, Alaska (ULA) | 1051 | April 10, 1975 | Dec. 1, 1978 |
| Goldstone, California (GDS) | 486 | April 10, 1975 | Dec. 1, 1978 |
| Quito, Ecuador (QUI) | 383 | April 10, 1975 | Dec. 1, 1978 |
| Santiago, Chile (AGO) | 395 | April 10, 1975 | Dec. 1, 1978 |
| Tananarive, Madagascar (TAN) | 12 | April 10, 1975 | July 11, 1975 |
| Mahe, Seychelles (MAH) | 79 | March 1, 1976 | May 9, 1976 |
| Rosman (via ATS-6 94° West) | 78 | April 10, 1975 | June 12, 1975 |
| Rosman (via ATS-6 140° West) | 347 | Sept. 3, 1976 | Dec. 1, 1978 |
| Madrid, Spain (via ATS-6 34° East) | 34 | May 26, 1975 | Oct. 22, 1976 |

TABLE 1.1. NASA TELEMETRY STATIONS

| STATION | TOTAL NUMBER OF GOOD PASSES | OPERATIONAL DATES START | STOP |
|---|---|---|---|
| Herndon, Virginia (HER) | | April 20, 1975 | July 1, 1975 |
| Perth, Australia (AUS) | 82 | July 14, 1975 | Aug. 17, 1975 |
| Tafuna, Samoa (TAF) | 120 | Aug. 12, 1975 | Nov. 30, 1975 |
| Shemya, Alaska (SHM) | 234 | Aug. 18, 1975 | Dec. 6, 1975 |
| Napier, New Zealand (NEZ) | 89 | Aug. 29, 1975 | Oct. 24, 1975 |
| Easter Island (EAS) | 222 | Nov. 8, 1975 | Feb. 1, 1976 |
| Baja, Mexico (BAJ) | 137 | Dec. 12, 1975 | Feb. 1, 1976 |
| Kerguelen Island (KEG) | 137 | March 2, 1976 | May 16, 1976 |
| Cocos Islands (COC) | 113 | March 13, 1976 | May 26, 1976 |
| Falkland Islands (FLK) | 165 | April 21, 1976 | June 20, 1976 |
| Canary Islands (CYI) | 128 | July 4, 1976 | Sept. 7, 1976 |
| Natal, Brazil (NAT) | 63 | July 14, 1976 | Nov. 15, 1976 |
| Tristan Da Cunha (TDK) | 32 | Aug. 3, 1976 | Oct. 14, 1976 |
| Caribou, Maine (CAR) | 346 | Sept. 6, 1976 | Dec. 11, 1976 |
| Kwajalein (KWA) | 37 | Jan. 16, 1977 | April 17, 1977 |
| Seattle, Washington (SEA) | 166 | Jan. 18, 1977 | April 3, 1977 |
| Rangiroa, Tahiti (TAH) | 73 | Jan. 22, 1977 | Feb. 23, 1977 |
| Townsville, Australia (TOW) | 72 | March 16, 1977 | July 20, 1977 |
| Cyprus (CYP) | 161 | April 18, 1977 | July 22, 1977 |
| Mahe, Seychelles (MAH) | 101 | Aug. 10, 1977 | Nov. 13, 1977 |
| Salalah, Oman (SAL) | 233 | Aug. 15, 1977 | Nov. 25, 1977 |
| Pretoria, South Africa (PRE) | 206 | Aug. 27, 1977 | Nov. 30, 1977 |
| Adak Island, Alaska (ADA) | 99 | Jan. 20, 1978 | March 26, 1978 |
| Kourou, French Guiana (KOU) | 62 | May 5, 1978 | June 20, 1978 |
| Papeete, Tahiti (TAH) | 9 | Dec. 16, 1977 | Jan. 20, 1978 |
| Pinang, Malaysia (MAL) | 32 | May 8, 1978 | July 2, 1978 |
| Okinawa (OKI) | 48 | May 2, 1977 | July 24, 1977 |

TABLE 1.2. DEFENSE MAPPING AGENCY TELEMETRY STATIONS

the portable DOD (Department of Defense) VHF facilities, the NASA STDN S-band telemetry sites and the NASA ATS-6 satellite telemetry data relay link (see Tables 1.1 and 1.2 and Figure 1.2, reproduced from Stanley and Dwyer, 1980).

The primary instrument on board the GEOS-3 spacecraft was a radar altimeter, developed for NASA by the General Electric Corporation. This altimeter operated at a single frequency of 13.9 GHz and transmitted 100 radar pulses per second. The pulses transmitted by the altimeter were reflected from the earth's surface and received by the spacecraft. The time interval required for a pulse to make the round-trip could be used to determine the altitude of the spacecraft above the mean earth surface. In addition, the slope of the return pulse received at the spacecraft could be used to determine the characteristics of the surface.

The GEOS-3 altimeter was instrumented with 16 sample and hold gates (see Section 1.3), which provided information about the shape and amplitude of the return waveform. This information could be used to determine a number of interesting and useful parameters, including the spacecraft attitude, water/land and water/ice boundaries, surface wind speed and significant waveheight. Significant waveheight was determined through analysis of the return waveform at the NASA Wallops Flight Center (WFC), Wallops Island, Virginia, during the entire active mission of the spacecraft.

The GEOS-3 spacecraft structure, which was patterned after the GEOS-2 structure, was an octahedron topped by a truncated pyramid. Extending from the pyramid was a gravity-gradient boom with an end mass, which was extended after insertion into orbit. The spacecraft was oriented in a stable gravity-gradient attitude, where the direction was defined by the gravitational force acting on the spacecraft (approximately radial).

The radar altimeter was mounted on the octrahedron opposite from the pyramid and the boom (facing radially inward toward the earth's surface). The altimeter antenna was required to be aligned within 1.2 degrees of the local vertical at all times. This pointing precision was maintained by the gravity-gradient boom and end mass configuration and by a constant speed, angular momentum wheel. Estimates of the pointing angle error have been made using the radar return waveform and were found to comply with the 1.2 degree pointing requirement (McMillan, November 1980).

Also included in the instrument package were coherent and non-coherent C-Band transponders, laser retroflectors, doppler transmitters and S-Band instrumentation for earth tracking and satellite-to-satellite experiments.

## 1.3 Lineage of the GEOS-3 Altimeter

The Skylab S-193 altimeter was the first in the series of

satellite altimeters that were planned to progressively achieve the goal of 10 cm resolution in the satellite altitude above the ocean surface. That experimental altimeter was designed primarily to obtain the radar measurements necessary for designing improved altimeters. The GEOS-3 altimeter, second in the series of satellite altimeters, was the first altimeter system applied to global operation. The Advanced Applications Flight Experiments (AAFE) Altimeter, an aircraft system which first collected data in October 1975, was a developmental effort directed at bridging the technology gap between the capabilities of the GEOS-3 altimeter and the rather stringent requirements imposed on the Seasat altimeter, as well as providing surface truth in support of the Seasat altimeter calibration activities. The Seasat spacecraft, launched June 26, 1978, carried the third in the series of satellite altimeters and represented the first attempt to achieve 10 cm altimetric precision from orbit. It was conceptually identical to the AAFE altimeter. The Seasat spacecraft also carried other sensors which were dedicated to ocean applications (IEEE Journal of Oceanic Engineering, April 1980).

## 1.4 Description of the GEOS-3 Altimeter

The GEOS-3 altimeter operated in two distinct data gathering modes; namely, the intensive or short-pulse mode and the global or long-pulse mode. The global mode was the original mode designed

for GEOS. However, the National Oceanic and Atmospheric Administration (NOAA) and the Department of Defense (DOD) also decided to support the intensive mode, which used pulse compression (at that time unproven over oceans). The intensive mode proved to be so accurate and reliable that it was used for the vast majority of the GEOS-3 data segments.

The global mode transmitter consisted of a magnetron tube with a 200 nanosecond pulse width capable of measuring height to a precision of 1 meter. It also provided a measurement of the backscatter signal intensity but did not use the 16 sample and hold gates that the intensive mode employed. Therefore, it provided minimal information about the return pulse shape.

The intensive mode transmitter consisted of a traveling wave tube (TWT) with a pulse compression to 12 nanoseconds and provided improved accuracy derived from a shorter pulse width, a more stable transmitter and waveform samples. The receiver was coherent with both transmitters.

The intensive mode gate timing and positioning is illustrated in Figure 1.3 (reproduced from Hofmeister and Keeney, 1977). As can be seen from that figure, four tracking gates were positioned at various points along the waveform in order to define the waveform shape. These tracking gates were:

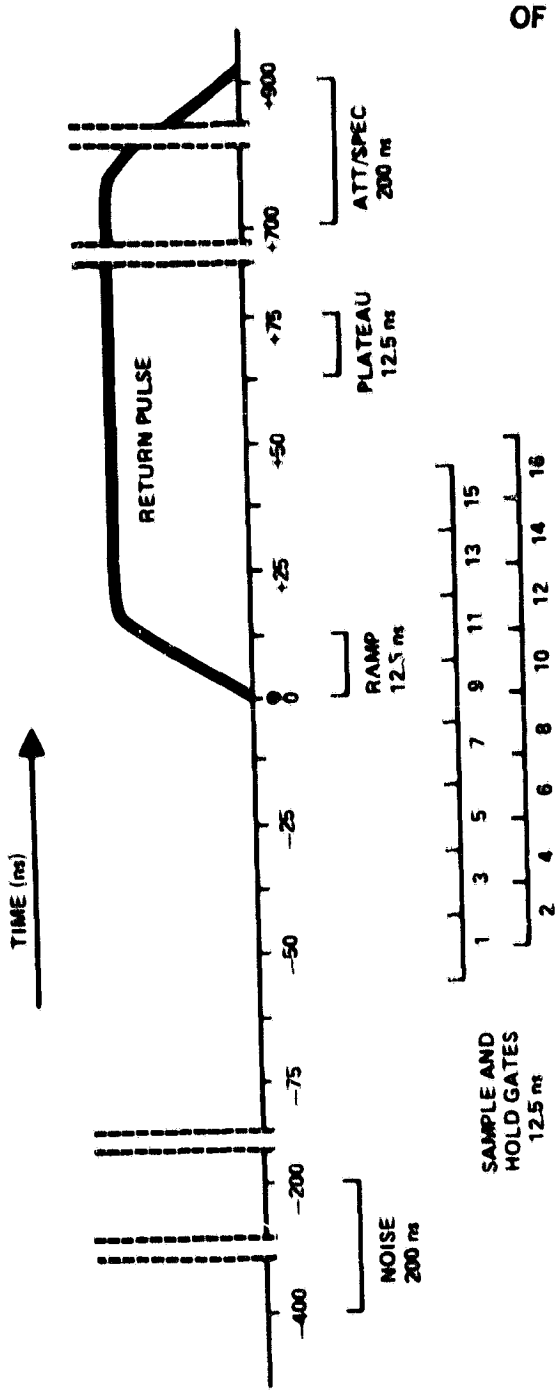


FIGURE 1.3. INTENSIVE MODE GATE TIMING

1. The Noise Gate. This gate had a width of 200 ns with a leading edge 400 ns in front of the leading edge of the return pulse and provided a reference for measuring the amplitude of the return waveform.

2. The Ramp Gate. This gate had a width of 12.5 ns and was located on the leading edge of the return pulse. It was used as a time reference for the other gates.

3. The Plateau Gate. This gate had a width of 12.5 ns and was located 62.5 ns after the leading edge of the return pulse. It was used to determine the magnitude of AGC attenuation necessary to normalize the waveform.

4. The Attitude/Specular Gate. This gate had a width of 200 ns with a leading edge 700 ns after the leading edge of the waveform. It was used to provide information about antenna bandwidth effects, wind speed and pointing angle.

In addition, a waveform sampling system of sample and hold gates was included in the intensive mode to provide detailed information concerning the shape of the altimeter return waveform. Sixteen sample and hold gates were provided and positioned fixed in time with respect to the tracking gates (see Figure 1.3). The width of the gates was designed such that the leading edge of the average impulse response of the ocean surface could be obtained for

waveheights up to 10 meters to withnin ± 20%. As will be demonstrated in this investigation, this accuracy requirement was met and exceeded. More specific information conerning the function and positioning of the gates can be obtained from Hofmeister, et al (1976).

The mean return waveforms were normalized using an automatic gain control (AGC) system. While tracking, the AGC attenuation was adjusted to hold the average plateau gate output to a constant value. The other tracking gates and the sample and hold gates were adjusted by the same amount. The return waveform could then be analyzed to determine some of the characteristics of the reflecting surface (the sea surface).

Telemetry data were transmitted in three formats for each of the two altimeter modes. The telemetry (TM) formats are summarized below:

TM #1 - 2.0 seconds per data record with altitude data frequency of 10 per second

TM #2 - 3.2 seconds per data record with altitude data frequency of 10 per second

TM #3 - 3.2 seconds per data record with altitude data frequency of 100 per second

It should be noted that, due to the power constraints of the spacecraft, the altimeter was not operational at all times. Altimeter data segments were generally limited to tracks over water and were scheduled several weeks in advance of the actual data acquisition. This complexity of scheduling was not merely an inconvenience, since data from local weather disturbances, such as hurricanes, could not be acquired unless the altimeter had been scheduled weeks earlier to take data at that time and place.

For more information concerning the GEOS-3 spacecraft hardware subsystems see GEOS-C Mission Plan, NASA, 1974.

## 1.5 GEOS-3 Significant Waveheight Estimation

The initial GEOS-3 significant waveheight estimation algorithm was developed by G. S. Hayne (Hayne, 1977) and programmed by J. D. McMillan (McMillan, 1975) at WFC for use as a quality control check on the GEOS-3 altimeter preprocessing software. Various improvements and refinements of the algorithm by McMillan and Roy (1977) led to the achievement of a high degree of agreement between the GEOS-3 estimates and ship-based measurements of SWH.

Eventually, the SWH estimate was distributed to GEOS-3 principal investigators as an integral part of the altimeter data set. Various experiments performed at WFC by McMillan and Roy (1977) and by Fedor, et al (1979) indicated that the estimate of

significant waveheight produced by the GEOS-3 altimeter preprocessing software compared favorably with other estimates and measurements of sea state.

The first comprehensive comparison of GEOS-3 significant waveheight estimates with independently derived sea state information was presented by McMillan and Roy (1977) at the GEOS-3 Final Investigators' Meeting in New Orleans, Louisiana, in November, 1977. That study presented several variations of the original significant waveheight algorithm and included results obtained using different convergence criteria, different risetime coefficients and different ARS timing and amplitude biases (see Chapter 2). In that investigation, the accuracy of the GEOS-3 SWH estimate was determined to be 55 cm.

The significant waveheight estimate proved to be so useful that, in 1978, NASA established the GEOS-3 Near-Real-Time Data System (McMillan, 1978) for disseminating significant waveheight and wind speed estimates. This system employed the significant waveheight algorithm which was developed by McMillan and Roy.

In the near-real-time system, the GEOS-3 altimeter data were acquired through the NASA Space Tracking and Data Network locations (see Table 1.1) or the ATS-6 satellite and transmitted to the NASA Goddard Space Flight Center in Greenbelt, Maryland, where they were buffered to magnetic tape in real-time. The buffered data were

then transmitted to the Computer Sciences Corporation INFONET center in Beltsville, Maryland, where significant waveheight was computed and made available to user-supplied terminals on a call-up basis.

During February, 1976, near-real-time GEOS-3 significant waveheight estimates in the North Atlantic Ocean were closely monitored and compared to other significant waveheight measurements provided by the Spaceflight Meteorology Group of the National Weather Service and the Navy Fleet Numerical Weather Central. In Parsons (1976), comparisons were made between the data sets, and it was found that the inherent consistency of the GEOS-3 data makes the satellite product the best representation of the true sea state.

Even though the significant waveheight estimation algorithm as developed by McMillan and Roy was employed on thousands of GEOS-3 passes, no definitive study has been undertaken to establish the accuracy of the estimates. This investigation will establish the accuracy of the significant waveheight estimates contained on the GEOS-3 data tapes (which are archived at the National Oceanographic Data Center in Suitland, Maryland) and will present a global atlas of all of the significant waveheight data processed during the GEOS-3 mission.

## 1.6 Applications of Satellite Significant Waveheight Estimates

The global coverage and established accuracy of the altim-

eter significant waveheight measurements make the data set preferable to other sources of information, which rely almost entirely upon infrequent and sometimes unreliable "eyeball" measurements that are typically in error by two to three meters. Consequently, the formulation of a global atlas of SWH has potential use by government and private industry to augment the information currently being implemented in climatic models. These models typically describe the oceans and the atmosphere in three dimensions but require information concerning the air/sea interface. While the near-real-time data discussed previously would be extremely useful in short-term forecasts, the historical data presented in a global atlas could help define more accurately the relationship between the ocean and atmospheric models for which data have already been taken.

For example, the U. S. Navy and the Coast Guard have expressed interest in the significant waveheight data to assist in the planning and execution of search and rescue operations. Again, the near-real-time data have been requested for real-time search operations and will be available from future spacecraft. The historical contour information, however, is also highly desirable for the study of the statistical probability of locating an object at sea in a given area at a given time of year.

The Bureau of Land Management, as well as the petroleum industry, has expressed an interest in the data for use in the design of offshore facilities. Of particular interest is the

relationship between significant waveheight and the structural stress endured by offshore drilling equipment. An historical atlas of this type could help determine the statistical probability of high stress situations and, therefore, the design of equipment for particular areas. For example, drilling equipment in the North Sea has completely different structural requirements than does drilling equipment in the Baltimore Canyon (see, for example, McMillan, December, 1980).

According to NOAA, significant waveheight data in some parts of the world are virtually nonexistent. This problem is particularly acute in the southern hemisphere, where the lack of data has prevented the establishment of well-defined shipping lanes. Through the use of a significant waveheight atlas, the accuracy of waveheight measurements in the southern hemisphere would be greatly enhanced. The result would be a much more accurate data base from which to determine shipping lanes on a seasonal basis.

The U. S. Coast Guard is charged with the responsibility of controlling oil spills in the ocean areas near the United States coastline. Since significant waveheight is typically depressed from 0.5 to 1.0 meters in the oil spill region, the measurement of significant waveheight is closely coupled with the analysis of oil spills. The Coast Guard is currently developing a three-dimensional model for oil spill distribution, and historical significant waveheight data are used as an input to that model.

Naval architects, sea engineers and ship builders also need historical waveheight data. Since ships and ocean structures are designed to withstand the structural stresses that they might reasonably be expected to encounter, a history of waveheight by geographical area and season could be quite helpful. A GEOS-3 atlas of SWH is believed to be the most accurate source of historical waveheight data currently available and is, therefore, the best source for design information. Although subtle differences between the GEOS-3 significant waveheight atlas and other SWH data bases might not seem to be of sufficient magnitude to affect the design of ships and offshore structures, the opposite may be true. Dr. Herb Austin of the Virginia Institute of Marine Science has stated that the GEOS-3 atlas would be "extremely useful" in this context (Austin, 1979).

As previously mentioned, some areas of the world's oceans are so remote that significant waveheight data from these regions is virtually nonexistent. No ocean buoys are located in these areas and ships rarely traverse through them. The U. S. Coast Guard has expressed interest in analyzing significant waveheight contour data from these remote areas, with particular interest in how meteorological features move through these rarely traveled regions.

Oceanographers, meteorologists, and climatologists frequently plan their research, field trips, etc., based upon the statistical probability of locating certain climatic conditions. The

GEOS-3 atlas could be used by scientists to plan research when prediction of significant waveheight is important.

Finally, the GEOS-3 near-real-time significant waveheight estimate has already gained wide acceptance in the scientific community as an accurate and timely data set to which other significant waveheight measurements can be compared. The GEOS-3 historical significant waveheight contour atlas presented in this report could similarly be used as a reference point for comparison of other results.

## 1.7 Scope of the Investigation

The first part of this study attempts to document the accuracy of the GEOS-3 altimeter derived significant waveheight estimates. The estimates, which were obtained from a statistically representative sampling of GEOS-3 passes, were compared with independent measurements of significant waveheight. These independent measurements were obtained from the NOAA Data Buoy Office (Hadsell, 1974) which maintains a number of ocean stations (see Figure 1.4) that routinely measure significant waveheight and other sea state and atmospheric parameters at 3-hour intervals. The accuracy of the buoy measurements of significant waveheight has been established to be 55 cm (Steele and Johnson, 1977).

For the purposes of this part of the investigation, it was

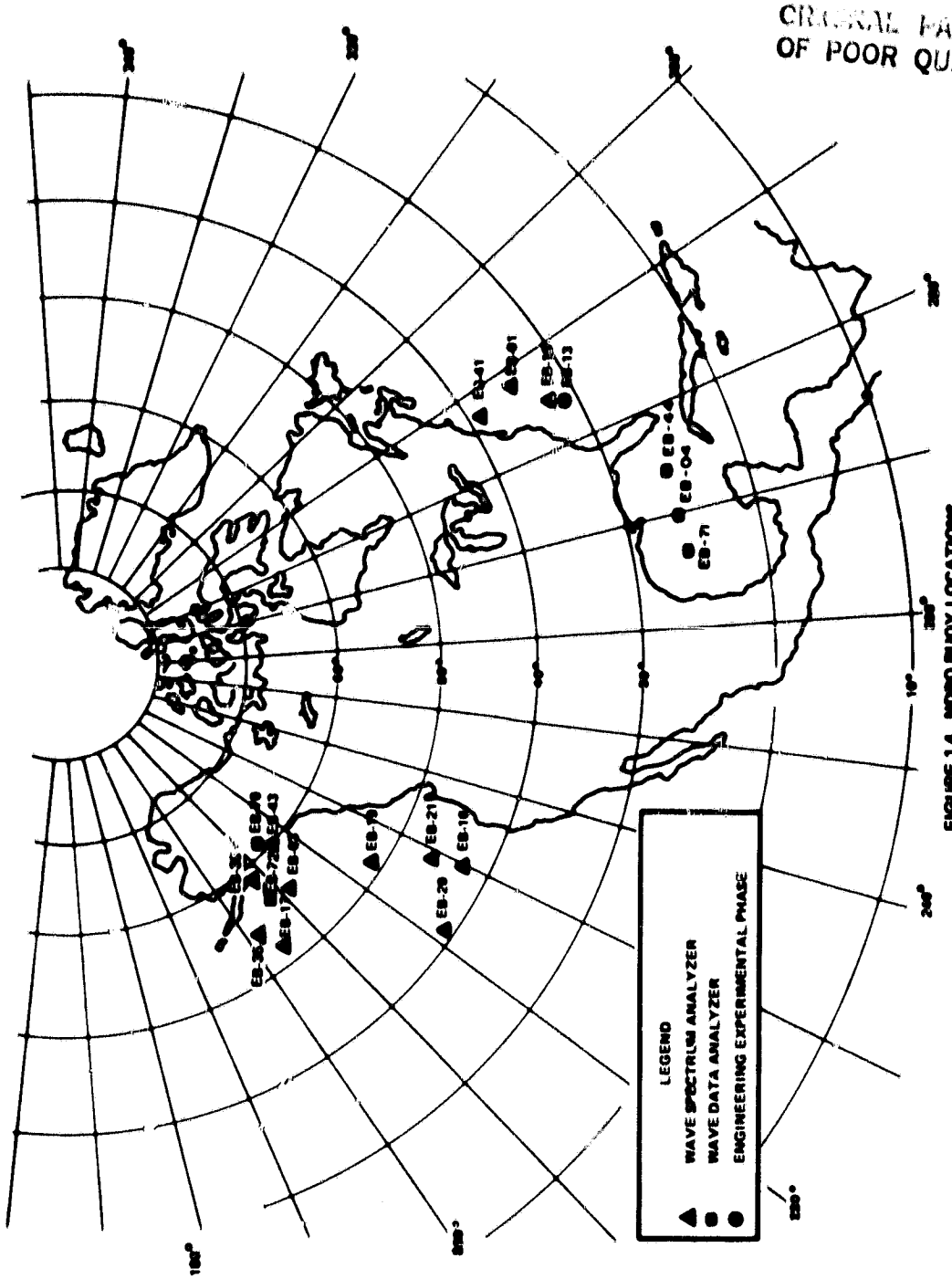


FIGURE 1.A. NDBO BUOY LOCATIONS

necessary to identify

1. all GEOS-3 passes whose ground tracks came arbitrarily close to one of the NOAA buoy locations, and

2. those passes identified in (1.) where the altimeter was tracking in the intensive mode.

It was decided that in order to satisfy both of the above conditions the GEOS-3 data must have been taken within 90 minutes of a buoy measurement and must have passed within one equatorial degree (111 kilometers) of the buoy making the measurement (see Section 3.1). The estimates of significant waveheight from these GEOS-3 passes and the corresponding buoy measurement of significant waveheight form the data set for the first part of the investigation.

Finally, the GEOS-3 significant waveheight estimates for the entire mission are presented in the form of a global atlas. This atlas, patterned after the significant waveheight results illustrated in the U. S. Navy Marine Climatic Atlas (U. S. Navy, 1974), presents global significant waveheight contour maps for both low and high sea state.

# CHAPTER 2

# SIGNIFICANT WAVEHEIGHT FROM SATELLITE ALTIMETERS

## 2.1 Waveform Geometry for Negligible SWH

The geometry of a square pulse emitted from an altimeter antenna which impinges upon an idealized flat sea surface is illustrated in Figure 2.1. This figure depicts the distances from the spacecraft to the subsatellite point (the point on the surface of the earth lying on the line between the spacecraft and the center of mass of the earth) and to a general point P near the subsatellite point.

In Figure 2.2, a pulse of duration $\tau$ is observed leaving the spacecraft at time $t = 0$ and returning from the sea surface at time $t = t_2$, after traversing a distance H each way. At the surface, it is reflected (at time $t = t_1$) back to the satellite where it is received at the antenna. Assuming that any vertical motion of the spacecraft has negligible effect upon the signal transit time,

$$t_2 = \frac{2H}{c} \tag{2.1}$$

where c is the speed of light. At time $t = t_3 = t_2 + \delta$, where $\delta$ is some time increment less than $\tau$, the square pulse is

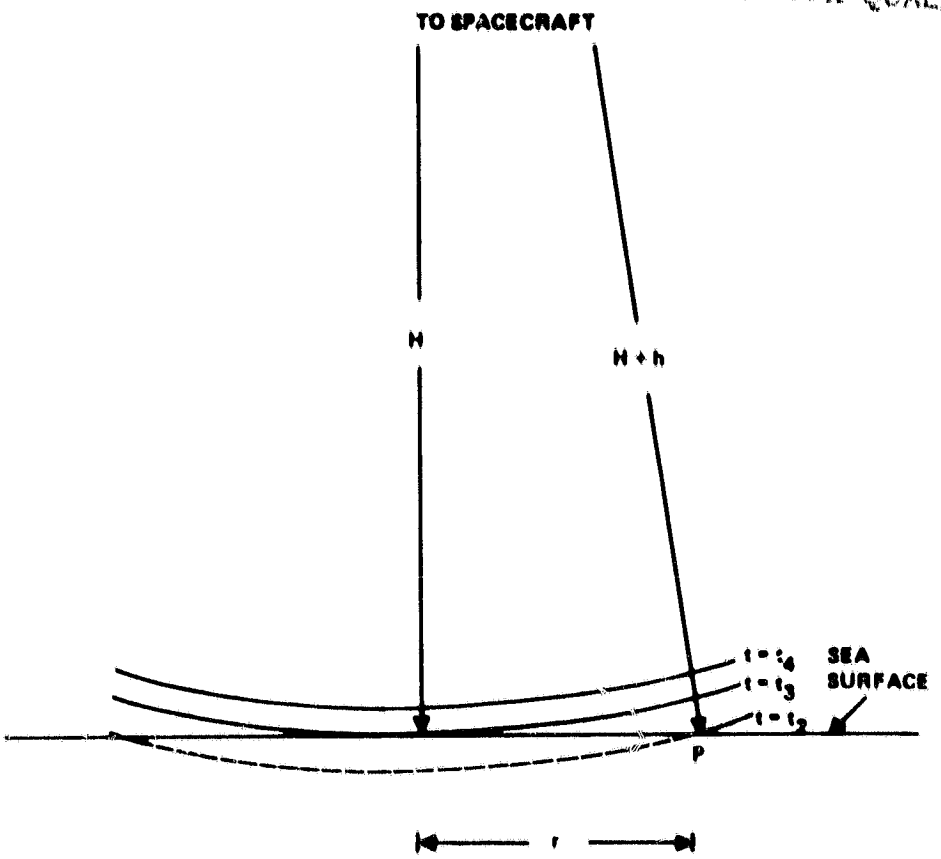


FIGURE 2.1. SQUARE PULSE IMPINGING UPON A FLAT SEA SURFACE

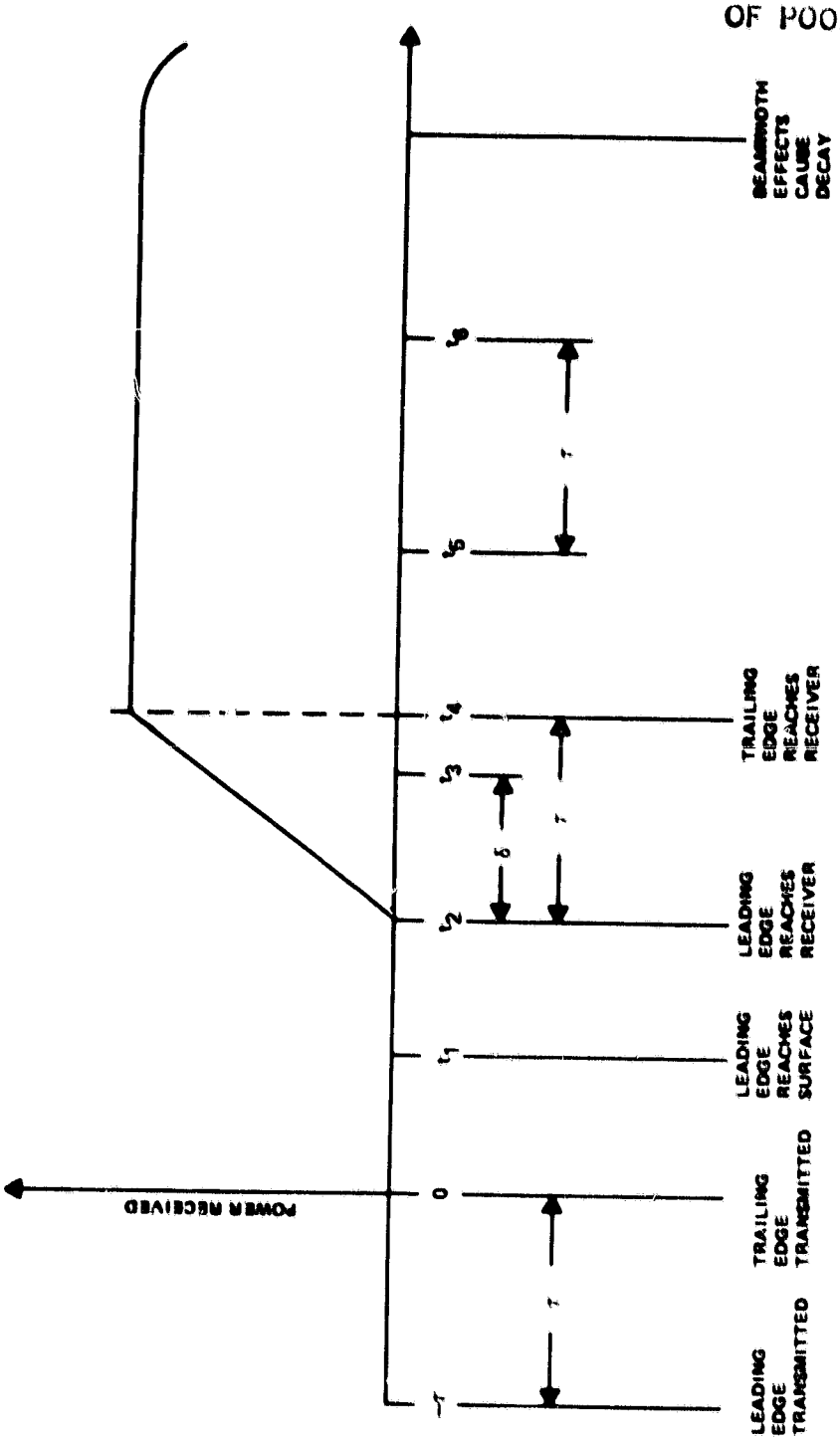


FIGURE 2.2 IDEALIZED MEAN RETURN PULSE SHAPE

observed impinging upon the sea surface. The observed area illuminated by the pulse expands circularly until the trailing edge of the waveform is received at the satellite. If the distance from the spacecraft to point P on the edge of the illuminated circle (see Figure 2.1) is H+h, then the radius r of the illuminated area is related to H by

$$r^2 = (H + h)^2 - H^2 \simeq 2Hh \tag{2.2}$$

since $h << H$ and therefore $h^2 << 2Hh$ .

The time $t = t_3$ is given by

$$t_3 = t_2 + \delta = \frac{2H}{c} + \delta \tag{2.3}$$

and corresponds to the two-way travel time between the satellite and point P on the surface. Therefore,

$$\frac{1}{2}\left(\frac{2H}{c} + \delta\right) = \frac{H + h}{c} \tag{2.4}$$

or

$$\frac{H}{c} + \frac{\delta}{2} = \frac{H}{c} + \frac{h}{c} \tag{2.5}$$

which yields

$$h = \frac{c\delta}{2} \tag{2.6}$$

Combining Equations (2.2) and (2.6) yields

$$r^2 = Hc\delta \tag{2.7}$$

and the area of the illuminated region is given by

$$A = \pi r^2 = \pi Hc\delta \tag{2.8}$$

Note that the observed area of the illuminated region, or equivalently the power received by the satellite, increases linearly with time.

At $t = t_4$, the trailing edge of the pulse is received at the satellite. At time $t = t_5$ where $t_5 > t_4$, the observed illuminated area becomes an annulus with inner radius $r_I$ and outer radius $r_0$ given by

$$r_I^2 = Hc(t_5 - t_4) \tag{2.9}$$

$$r_0^2 = Hc(t_5 - t_2) \tag{2.10}$$

and width $W$ and area $A$ given by

$$W = r_0 - r_I = [Hc(t_5-t_2)]^{1/2} - [Hc(t_5-t_4)]^{1/2} \tag{2.11}$$

$$A = \pi r_0^2 - \pi r_I^2 = \pi Hc\tau \tag{2.12}$$

From Equation (2.12), the area of the annulus remains constant. Therefore, the power received at the satellite remains constant until antenna beamwidth effects cause the power received to decay. This is due to the increasing size of the annulus and the limited antenna beamwidth (which for GEOS-3 was $2.3^o$).

The character of a square pulse impinging upon a sea surface with negligible significant waveheight as seen from the satellite can be summarized as follows:

1. no power is received until the leading edge of the pulse strikes the sea surface and is reflected back to the satellite;

2. after the leading edge of the pulse is received at the spacecraft and before the trailing edge is, the power received increases linearly with time;

3. after the trailing edge of the pulse is received at the spacecraft, the power received remains at a constant plateau value; and

4. after the antenna beamwidth effects become non-negligible, the power received begins to decay.

These four stages are depicted in Figure 2.2, which represents the idealized mean return pulse shape. However, due to the scattering properties of the surface, the instantaneous power received fluctuates, making it necessary to average a large number of pulses in order to determine the mean pulse shape.

The GEOS-3 satellite received the return pulses in 16 waveform sampling gates (see Figure 1.3). These 16 values, called Instantaneous Return Samples, or IRS's, were collected 100 times per second by the spacecraft and averaged onboard in an attempt to

construct an accurate representation of the mean pulse shape, which was characterized by the four stages described in the previous paragraph. The 16 values of averaged IRS's were called Average Return Samples, or ARS's, and were computed using an RC filter with a 2-second time constant (Leitao and Purdy, 1975). It will be shown in Section 2.2 that the significant waveheight can be determined by observing the departure of the leading edge slope of the ARS's from the leading edge slope that the ARS's would have in the ideal calm sea case.

## 2.2 Waveform Geometry for Non-Negligible SWH

In the case where a square pulse impinges upon an ocean surface with non-negligible significant waveheight, the shape of the mean return pulse will be altered. The geometry of a square pulse impinging upon a sea surface with non-negligible significant waveheight is illustrated in Figure 2.3. Note that the crests of the waves are illuminated prior to the time at which the calm sea would have been illuminated. Similarly, the troughs of the waves are not illuminated until after the time at which the calm sea would have been illuminated. The net result of these effects is that the mean power received for non-negligible sea state does not reach its full plateau value until after the time at which the mean power received from a calm sea would have reached its plateau value. This effect causes the slope of the leading edge of the ARS's to diminish.

FIGURE 2.3 SQUARE PULSE IMPINGING UPON A ROUGH SEA SURFACE

The leading edge of an idealized mean pulse shape for negligible sea state and for several non-negligible sea states is characterized in Figure 2.4. From this figure it can be seen that the slope of the mean return pulse is related to significant waveheight. If the mean pulse shape for negligible sea state is known precisely, then the significant waveheight can be determined by analyzing the departure of the mean return pulse shape for the non-negligible sea state from the mean return pulse shape for calm sea.

## 2.3 Choice of Model

It has been shown (Brown, 1977) that the mean return waveform can be conceived of as a convolution of

1. the system point-target impulse response,
2. the non-coherent surface impulse response,
3. the ocean surface height probability density function, and
4. the tracking loop jitter.

The first component is the composite of the transmitted pulse and the transmitter and receiver bandwidth effects. Its distribution is a complicated function which can be modeled as a Gaussian distribution. The second component is the calm sea response, which can be modeled as a step function. The third component represents the

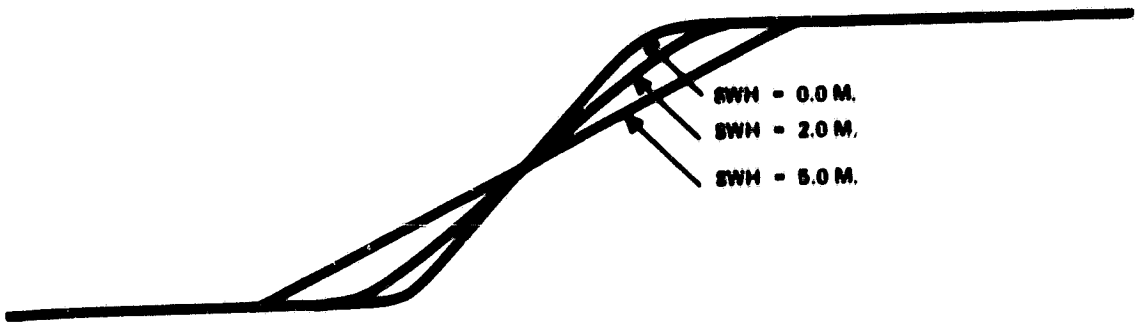


FIGURE 2.4. IDEALIZED MEAN RETURN PULSE SHAPE FOR SEVERAL VALUES OF SWH

rough sea distribution, which is modeled in this investigation as a Gaussian distribution. The fourth component is assumed to be unaffected by sea state in this investigation. (See Section 2.6 for a discussion of the errors associated with assuming these distributions.)

Assuming that pointing angle errors have negligible effect upon the leading edge of the waveform (see Section 2.6), Brown and Miller (1974) have shown that a good approximation for the return power as a function of time is the Gaussian function

$$y(t) = aP(\frac{t-b}{c}) + d \tag{2.13}$$

where

a = return waveform amplitude

b = time origin

c = return waveform standard deviation

d = return waveform baseline amplitude

and where $P(\frac{t-b}{c})$ is the Probability Integral

$$P(z) = \int_{-\infty}^{z} Z(q)dq \tag{2.14}$$

and $Z(q)$ is the Gaussian function

$$Z(q) = \frac{1}{(2\pi)^{1/2}} e^{-q^2/2} \tag{2.15}$$

$P(z)$ is determined (from Abramowitz and Segun, 1968) by

$$P(z) = 1 - Z(z)(b_1 t + b_2 t^2 + b_3 t^3 + b_4 t^4 + b_5 t^5) + \varepsilon(z) \quad (2.16)$$

where

$$t = \frac{1}{1+p} \quad (2.17)$$

$$|\varepsilon(z)| < 7.5 \times 10^{-8} \quad (2.18)$$

$$p = 0.2316419 \quad (2.19)$$

$$b_1 = 0.319381530 \quad (2.20)$$

$$b_2 = -0.356563782 \quad (2.21)$$

$$b_3 = 1.781477937 \quad (2.22)$$

$$b_4 = -1.821255978 \quad (2.23)$$

$$b_5 = 1.330274429 \quad (2.24)$$

In this model it is necessary to estimate the four parameters a, b, c and d from which the significant waveheight can be determined. The technique used to estimate the four-parameter function y(t) is the method of least squares.

## 2.4 Derivation

Equation (2.13) can be expanded in a first-order Taylor Series approximation about a point $y_o = y(a_o, b_o, c_o, d_o)$ (see Hayne, 1977) to yield

$$\bar{y}_i = y_o + y_a(a-a_o) + y_b(b-b_o) + y_c(c-c_o) + y_d(d-d_o) + \cdots \quad (2.25)$$

where

$$y_a = \frac{\partial y}{\partial a}\bigg|_{y=y_o} = P\left(\frac{t-b_o}{c_o}\right) \tag{2.26}$$

$$y_b = \frac{\partial y}{\partial b}\bigg|_{y=y_o} = -\frac{a_o}{c_o} Z\left(\frac{t-t_o}{c_o}\right) \tag{2.27}$$

$$y_c = \frac{\partial y}{\partial c}\bigg|_{y=y_o} = -\frac{a_o}{c_o}\left(\frac{t-b_o}{c_o}\right) Z\left(\frac{t-b_o}{c_o}\right) \tag{2.28}$$

$$y_d = \frac{\partial y}{\partial d}\bigg|_{y=y_o} = 1 \tag{2.29}$$

and where $y_i$ are the observed values of $y$, $\bar{y}_i$ are the computed values of $y$, and higher order terms have been neglected, thereby assuming that $y_o$ is sufficiently close to $y_i$ to permit convergence while neglecting the complications introduced by including higher order terms in the Taylor Series expansion. The traditional least squares estimate of $y(t)$ is obtained by minimizing the sum of the errors squared over the 16 gates

$$E = \sum_{i=1}^{16} (\bar{y}_i - y_i)^2 \tag{2.30}$$

with respect to $(a-a_o)$, $(b-b_o)$, $(c-c_o)$ and $(d-d_o)$. When this is done, the following four equations are generated:

$$\frac{\partial E}{\partial (a-a_o)} = 0 = 2\sum_{i=1}^{16} (\bar{y}_i - y_i)\frac{\partial (\bar{y}_i - y_i)}{\partial (a-a_o)} = 2\sum_{i=1}^{16} (\bar{y}_i - y_i) y_a \tag{2.31}$$

$$\frac{\partial E}{\partial(b-b_o)} = 0 = 2\sum_{i=1}^{16}(\bar{y}_i-y_i)\frac{\partial(\bar{y}_i-y_i)}{\partial(b-b_o)} = 2\sum_{i=1}^{16}(\bar{y}_i-y_i)y_b \qquad (2.32)$$

$$\frac{\partial E}{\partial(c-c_o)} = 0 = 2\sum_{i=1}^{16}(\bar{y}_i-y_i)\frac{\partial(\bar{y}_i-y_i)}{\partial(c-c_o)} = 2\sum_{i=1}^{16}(\bar{y}_i-y_i)y_c \qquad (2.33)$$

$$\frac{\partial E}{\partial(d-d_o)} = 0 = 2\sum_{i=1}^{16}(\bar{y}_i-y_i)\frac{\partial(\bar{y}_i-y_i)}{\partial(d-d_o)} = 2\sum_{i=1}^{16}(\bar{y}_i-y_i)y_d \qquad (2.34)$$

Substituting Equations (2.26) through (2.29) into Equations (2.31) through (2.34) yields

$$0 = \sum_{i=1}^{16} y_o y_a + \sum_{i=1}^{16} y_a^2(a-a_o) + \sum_{i=1}^{16} y_a y_b(b-b_o) + \sum_{i=1}^{16} y_a y_c(c-c_o) + \sum_{i=1}^{16} y_a y_d(d-d_o) - \sum_{i=1}^{16} y_i y_a \qquad (2.35)$$

$$0 = \sum_{i=1}^{16} y_o y_b + \sum_{i=1}^{16} y_a y_b(a-a_o) + \sum_{i=1}^{16} y_b^2(b-b_o) + \sum_{i=1}^{16} y_b y_c(c-c_o) + \sum_{i=1}^{16} y_b y_d(d-d_o) - \sum_{i=1}^{16} y_i y_b \qquad (2.36)$$

$$0 = \sum_{i=1}^{16} y_o y_c + \sum_{i=1}^{16} y_a y_c(a-a_o) + \sum_{i=1}^{16} y_b y_c(b-b_o) + \sum_{i=1}^{16} y_c^2(c-c_o) + \sum_{i=1}^{16} y_c y_d(d-d_o) - \sum_{i=1}^{16} y_i y_c \qquad (2.37)$$

$$0 = \sum_{i=1}^{16} y_o y_d + \sum_{i=1}^{16} y_a y_d(a-a_o) + \sum_{i=1}^{16} y_b y_d(b-b_o)$$

$$+ \sum_{i=1}^{16} y_c y_d (c-c_o) + \sum_{i=1}^{16} y_d^2 (d-d_o) - \sum_{i=1}^{16} y_i y_d \qquad (2.38)$$

Equations (2.35) through (2.38) can be written in matrix form as

$$\begin{bmatrix} \sum_{i=1}^{16} y_a^2 & \sum_{i=1}^{16} y_a y_b & \sum_{i=1}^{16} y_a y_c & \sum_{i=1}^{16} y_a y_d \\ \sum_{i=1}^{16} y_a y_b & \sum_{i=1}^{16} y_b^2 & \sum_{i=1}^{16} y_b y_c & \sum_{i=1}^{16} y_b y_d \\ \sum_{i=1}^{16} y_a y_c & \sum_{i=1}^{16} y_b y_c & \sum_{i=1}^{16} y_c^2 & \sum_{i=1}^{16} y_c y_d \\ \sum_{i=1}^{16} y_a y_d & \sum_{i=1}^{16} y_b y_d & \sum_{i=1}^{16} y_c y_d & \sum_{i=1}^{16} y_d^2 \end{bmatrix} \begin{bmatrix} a-a_o \\ b-b_o \\ c-c_o \\ d-d_o \end{bmatrix} = \begin{bmatrix} \sum_{i=1}^{16} y_a (y_i - y_o) \\ \sum_{i=1}^{16} y_b (y_i - y_o) \\ \sum_{i=1}^{16} y_c (y_i - y_o) \\ \sum_{i=1}^{16} y_d (y_i - y_o) \end{bmatrix} \qquad (2.39)$$

For this problem, the technique of least squares is applied to a truncated Taylor series (Equation 2.25), which is linear in the corrections to the guessed values of $a_o$ , $b_o$ , $c_o$ and $d_o$ and, therefore, separable. Accordingly, iteration is required because of the linearization.

It should be noted that in order to solve for a, b, c and d, a 4 x 4 symmetric matrix must be inverted. This matrix has been examined and found to be well conditioned. In particular, the accuracy of the matrix inversion has been examined for a wide range of waveheights and was determined to be satisfactory.

The convolutional model for the mean return waveform (see Section 2.3) assumes that the standard deviation, c (sometimes referred to as the risetime coefficient which should not be confused

with the speed of light), is a composite of four elements which can be grouped in the following way:

1. the ocean surface height probability density function, and

2. the composite of a) the transmitter and receiver effects, b) the noncoherent impulse response and c) the tracking loop jitter.

The first of these two groups can be referred to as the "rough sea" contribution to the return power and the second as the "calm sea" contribution to the return power. Since both distributions are assumed to be Gaussian and since the convolution of two Gaussian distributions is itself a Gaussian distribution,

$$c^2 = \sigma_s^2 + \sigma_c^2 \qquad (2.40)$$

where $\sigma_c$ is the calm sea standard deviation, and $\sigma_s$ is the rough sea standard deviation, both expressed in nanoseconds.

According to Neumann and Pierson (1966)

> The significant waveheight is defined as the average of the heights of the one-third highest waves in a long sequence of waves observed at a point. It is more or less equal to four times the square root of the variance of the wave record. Tests of wind-sea records, by first averaging the heights of the one-third highest waves and then estimating $m_o$ (the wave record variance) and computing $4[m_o]^{1/2}$, yield the same value within perhaps 5 per cent.

Using Equation (2.40) and converting to units of meters by multiplying by the two-way speed of light yields:

$$SWH = 4\,\sigma_s = 0.6\,[c^2 - c_o^2]^{1/2} \qquad (2.41)$$

The implementation of the estimation algorithm proceeds as:

1. Provide initial guesses for $a_o$ , $b_o$ , $c_o$ and $d_o$

2. Estimate a, b, c and d using Equation (2.39)

3. Compute E using Equation (2.30)

4. If E has converged, go to Step #6

5. Replace $a_o$ , $b_o$ , $c_o$ and $d_o$ with the new estimates of a, b, c and d and return to Step #2

6. Compute SWH using Equation (2.41).

## 2.5 Convergence Considerations

Since Equation (2.25) neglected higher order terms, the estimation algorithm must be iterated. The convergence criteria for the estimation algorithm was that the relative error in Equation (2.30) for two consecutive iteratives be less than 0.1%. Significant waveheight has been computed in this way on thousands of passes of GEOS-3 data, and it has been found that the algorithm nearly always converges within 2 or 3 iterations. In addition, it has been determined that the final converged estimate of significant waveheight is not particularly sensitive to the initial guesses of $a_o$ , $b_o$ , $c_o$ and $d_o$ . In practice, the following initial guesses

are used for all passes:

$$a_o = 84.500 \tag{2.42}$$

$$b_o = -0.902 \tag{2.43}$$

$$c_o = 8.500 \tag{2.44}$$

$$d_o = 5.800 \tag{2.45}$$

For each significant waveheight estimate after the first frame of data, the converged values of a, b, c and d for the previous frame of data are used as the initial guesses for $a_o$ , $b_o$ , $c_o$ and $d_o$ .

As was discussed in Section 2.2, it is necessary to have an accurate estimate of the calm sea standard deviation, $\sigma_c$ , in order to calculate significant waveheight using Equation (2.41). Early in the GEOS-3 mission, many arcs of the satellite which passed over areas where ship measurements indicated the presence of calm seas were analyzed in order to determine that value of $\sigma_c$ which would yield an estimate of SWH = 0 for those passes. The value arrived at was

$$\sigma_c = 7.49 \text{ nsec} \tag{2.46}$$

This value, which accounts for the effects of tracking loop jitter in an average sense, was examined by McMillan and Roy (1977) and found to produce better agreement with ground truth measurements than did any other tested value. Gower (1979) estimated that

removing the effects of tracking loop jitter would yield

$$\sigma_c = 6.25 \pm 0.25 \text{ nsec} \tag{2.47}$$

Because rough sea scattering behaves as if it were a collection of incoherent, discrete scatterers and the statistical properties of the scattering are assumed to be Rayleigh (see, for example, Walsh, 1974), the mean return represented by the ARS's contains noise. Although individual waveforms exhibit these Rayleigh fluctuations, the data points are all scattered about the mean return for some averaging interval (Hammond, et al, 1977). Nevertheless, the waveforms from two adjacent data records of ARS's can differ substantially, even though the altimeter is receiving data from ocean areas only a few kilometers apart. This, combined with the numerical errors associated with the estimation process, produce an estimate of $\sigma_c$ which sometimes causes the term under the radical in Equation (2.41) to become negative if the true sea state is very calm.

Figure 2.5 illustrates the algebraic relationship between significant waveheight and the estimated value of $\sigma_c$. It should be noted that for moderate to large values of significant waveheight, small errors in the estimate of $\sigma_c$ do not cause large errors in the calculated value of significant waveheight. However, the estimate of significant waveheight is very sensitive to even small errors in $\sigma_c$ for calms seas, i.e., for significant waveheight less than about 1 meter.

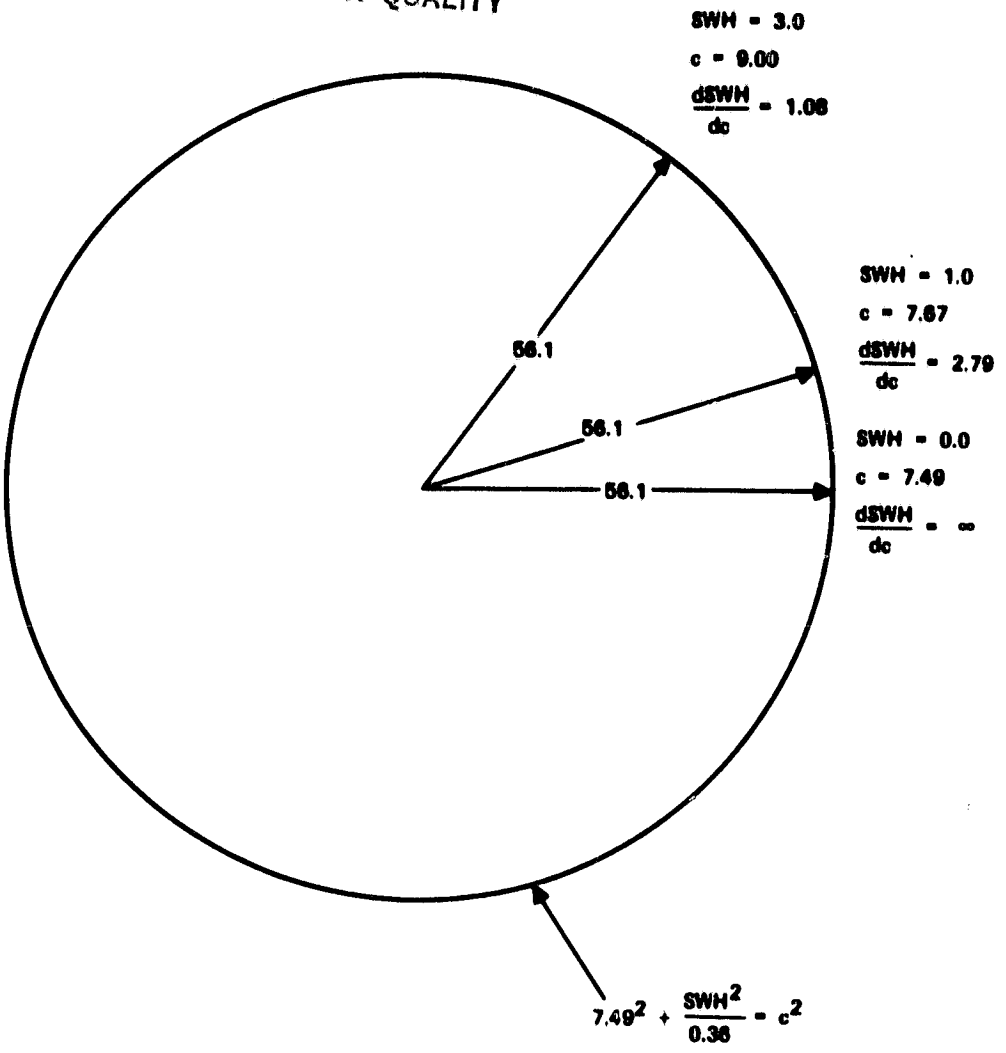


FIGURE 2.5. ALGEBRAIC RELATIONSHIP BETWEEN SWH AND ESTIMATED VALUE OF c

When the scattering properties of the surface, the noise characteristics of the altimeter, the estimation errors and the algebraic sensitivity of the estimate to c are combined, it is obvious that smoothing the estimate should provide more confidence in its accuracy, especially when the sea state is calm. The longest segment over which the sea state can be assumed to be correlated has been empirically determined (Apel, 1975) to be 150 kilometers (or 21 seconds for GEOS-3). Therefore, a sliding 21-second rectangular filter was employed by the significant waveheight estimation software.

Either the estimate of c or the calculated value of SWH can be smoothed and the results were shown by McMillan and Roy (1977) to be identical to within the numerical precision of the computer. For computational ease, the estimate of c is smoothed in this investigation. However, even when the estimate is smoothed, the term under the radical in Equation (2.41) still occasionally becomes negative due to the effects of noise in the measured waveforms and the algebraic sensitivity demonstrated previously in this section. Such estimates had no physical meaning and a value of SWH = 0 was assumed.

The first few weeks after the launch of GEOS-3 were designated the calibration phase of the mission and were designed to

eliminate known errors and inconsistencies in the preprocessing of the altimeter data. During this phase, it was determined that two important corrections were required for the ARS's.

First, due to limitations of current circuitry and to timing difficulties, the 16 sample and hold gates should not have been assumed to be equally spaced in time. Accordingly, General Electric supplied WFC with the timing corrections necessary to properly time tag the ARS's (see Table 2.1) based upon correlation analysis of the ARS's.

Second, it became evident that amplitude biases needed to be determined for the ARS's. In subsequent weeks, several sets of ARS amplitude biases were determined by G. S. Hayne and by E. J. Walsh at WFC (Walsh, March 1979). McMillan and Roy (1977) determined that the most consistent agreement between the estimated value of significant waveheight and direct measurements of significant waveheight made by buoys and ships was produced when the Walsh amplitude biases were employed (see Table 2.2). Since the ship and buoy measurements of significant waveheight constituted a statistically representative sampling population, it was assumed that "tuning" the estimation algorithm to that particular set of ground truth data would not cause an estimation bias. The validity of this assumption was later demonstrated when several independent estimation algorithms were compared (Fedor, et al, 1979) and were found to produce essentially equivalent estimates.

| ARS GATE | TIME (ns) | ARS GATE | TIME (ns) |
|---|---|---|---|
| 1 | −52.19 | 9 | − 6.88 |
| 2 | −46.00 | 10 | + 0.00 |
| 3 | −43.63 | 11 | + 6.50 |
| 4 | −37.50 | 12 | +12.69 |
| 5 | −31.81 | 13 | +15.19 |
| 6 | −24.88 | 14 | +25.69 |
| 7 | −17.12 | 15 | +31.69 |
| 8 | −12.31 | 16 | +38.38 |

TABLE 2.1. ARS RELATIVE TIMES

| ARS GATE | BIAS (mv) | ARS GATE | BIAS (mv) |
|---|---|---|---|
| 1 | + 2.3 | 9 | + 1.3 |
| 2 | − 2.7 | 10 | − 2.0 |
| 3 | + 0.8 | 11 | + 3.6 |
| 4 | − 1.8 | 12 | + 1.3 |
| 5 | + 2.5 | 13 | + 0.9 |
| 6 | − 0.1 | 14 | − 0.5 |
| 7 | − 0.8 | 15 | − 0.3 |
| 8 | − 1.2 | 16 | − 4.0 |

TABLE 2.2. ARS AMPLITUDE BIASES

The algorithm derived in this chapter, together with the smoothing technique and ARS timing and amplitude bias corrections detailed above, was used at the Wallops Island facility in preprocessing the GEOS-3 altimeter data (McMillan, 1975). The same techniques were used by the Goddard Space Flight Center in the near-real-time data network (McMillan, 1978) described in Chapter 1.

## 2.6 Error Sources

The error sources affecting the estimation of significant waveheight can be divided into three general categories:

1. modeling errors associated with the waveform shape
2. measurement errors associated with the return power
3. mathematical errors associated with the estimation of the slope of the ARS's

Each of these categories will be examined separately.

The first category of error sources includes the errors associated with the modeling of the waveform shape. As presented in Section 2.3, the mean return waveform is modeled as a convolution of

1. the system point-target response,
2. the noncoherent surface impulse response,

3. the ocean surface height probability density function, and

4. the tracking loop jitter.

The first of these terms, which represents a composite of the transmitted pulse and the transmitter and receiver bandwidth effects, resembles a Gaussian distribution and is therefore modeled as such, introducing a model error. The second term is the calm sea impulse response, which resembles a step function and is so modeled, introducing another error. The third term is the radar observed distribution of the ocean surface. The distribution is assumed to be Gaussian in nature. If the distribution is not Gaussian, i.e., if the probability density function must be characterized by higher order terms (skewness and kurtosis), then the estimation process becomes more complicated. The skewness has been accounted for by Walsh (1979). Nevertheless, Fedor, et al (1979) found that the Walsh algorithm and the Wallops algorithm produced nearly identical estimates. For a further discussion of the surface elevation probability distribution, see Huang and Long (1981).

Additionally, the radar observed ocean distribution is not the true geometrical distribution. This difference might be accounted for through the use of a correction called the electromagnetic bias (EM bias), which is currently being investigated (Jackson, 1979) for use in reducing the altimeter data of future spacecraft. The effect of the EM bias is that (McMillan, et al, 1980),

the relative radar cross section tends to increase below mean sea level and decrease above mean sea level in the presence of waves. Its effect is to shift the centroid of the radar return away from mean sea level toward the wave troughs so that the altimeter tracks long. Recent experimental data from the Surface Contour Radar at 36 GHz and the NRL 10 GHz adaptive radar altimeter indicate that the EM bias is in the range of 0 to 3 percent of the SWH.

Each of the first three components in the convolutional model of the return waveform is assumed to have a defined functional form which can easily be incorporated into an overall model of the waveform. Actually, each of these modeled functional forms introduces an error into the estimation process, but a more accurate model for the estimation of significant waveheight from GEOS-3 data remains to be established.

As discussed in Section 2.3, the tracking loop jitter is assumed to be independent of sea state and is not accounted for directly in the GEOS-3 significant waveheight algorithm. It is accounted for, in an average sense, in the determination of the calm sea pulse width, $\sigma_c$ (see Section 2.5). Any error introduced in the estimate by not properly accounting for tracking loop jitter would tend to be more significant for high sea states than for low sea states (Hayne, 1976). Walsh (1979) and others have eliminated the effects of tracking loop jitter in their SWH estimation algorithms. Fedor, et al (1979) examined both actual and simulated GEOS-3 data and determined that this additional numerical procedure did not appreciably alter the estimate (see Section 2.8).

Additionally, the Gaussian distribution used to model the return power is presented as a function of four parameters, each of which must be determined in the least squares estimation process. Other Gaussian functions with a different number of unknowns could be used to model the return waveform, but one would expect that no significant variation in the estimated SWH would result by altering the algorithm in this manner.

The second general category of error sources includes the errors associated with the measurement of the return power. In Section 2.5, the ARS amplitude and timing biases were presented. McMillan and Roy (1977) examined several sets of ARS amplitude and timing biases and concluded that results varied by as much as 15% when using different bias sets. Both of these bias corrections to the measured return waveform are somewhat arbitrary, especially the amplitude biases. Nevertheless, these corrections are the most accurate biases currently known.

Certain other instrument-related error sources can be enumerated under the general category of errors associated with the measurement of the return waveform. They include the effects of pointing angle, pulse width, gate position, AGC fluctuation, power and timing variations and gate saturation. For GEOS-3, the estimated standard deviation, $\sigma_c$, was assumed to be insensitive to variations in pointing angle. The validity of this assumption has been proven by G. S. Hayne at WFC using simulated waveform data with

varying pointing angles. The pulse width is a limiting factor in the resolution of the estimate, with a smaller pulse width yielding higher resolution. The position of the sample and hold gates (see Figure 1.3) was not optimum for the estimation of significant waveheight, and therefore is a potential error source. A more optimum gate configuration would include more sample and hold gates, especially in the ramp portion of the waveform, which is the portion most sensitive to sea state. AGC fluctuation, power and timing variations and gate saturation could and did occur at certain times during the mission, but these effects were assumed to cause only noise in the SWH estimation algorithm (Stanley, 1980).

The third and final category of error sources includes the mathematical errors associated with the significant waveheight estimation process itself. These include all numerical estimation errors such as matrix inversion errors, roundoff errors and truncation errors. All of these errors are assumed negligible. The validity of this assumption is supported by the facts that the Wallops algorithm determined equivalent SWH estimates on at least three different computers, and the Wallops algorithm compared favorably with the other estimation algorithms examined by Fedor, et al (1979). Additionally, the accuracy of the matrix inversion has been substantiated over a variety of sea state conditions. Finally, it should be pointed out that G. S. Hayne at WFC is currently investigating the contributions of the various error sources in the significant

waveheight estimation. That investigation is based upon the examination of simulated waveform data.

## 5.7 Description of Other SWH Estimation Algorithms

The problem of calculating ocean significant waveheight based upon the altimeter waveform measurements of the GEOS-3 spacecraft has been addressed by a number of other GEOS-3 principal investigators (Fedor and Barrick, 1978; Gower, 1979; Hayne, 1977; Rufenach and Alpers, 1979; and Walsh, July 1979). The various techniques used by the GEOS-3 principal investigators were reviewed during the design of the Seasat altimeter. As a consequence, the significant waveheight was calculated onboard the Seasat spacecraft using the altimeter return waveforms in much the same fashion as has been presented in this study. Although the purpose of this investigation is not to compare the accuracy of various algorithms but to establish the accuracy of the WFC and real-time significant waveheight algorithm, a description of these other algorithms is included here for the sake of completeness. A more detailed comparison of the algorithms is given by Fedor, et al, (1979).

Although the different algorithms solve for different sets of parameters, use different weighting and best fit criteria and even differ as to whether IRS or ARS data are used as input, they all fit a model function to the detected waveform. Thus, the differences in the accuracy of the algorithms are essentially due to

the curve fitting techniques employed. Accordingly, the comparison study (Fedor, et al, 1979) found that "individual differences between the algorithms were small when compared to the general good agreement among them."

As previously noted, several of the algorithms employ the ARS's as the input to the curve fit technique, while the other algorithms use the IRS's. For 3.2 seconds of data, a fit through the ARS data requires the determination of a curve passing through only 16 points, whereas the use of IRS data requires the determination of a function which best represents 5120 (320 x 16) points. Not only does the use of IRS data slow down the estimation process due to the requirements of reading and storing so many variables and burdening the curve fit software with such a cumbersome number of data points, it precludes the use of telemetry mode #1 data (low data rate data) which does contain ARS's but does not contain IRS's.

The GEOS-3 altimeter mode could be

1. Global
2. Intensive
    a. none of the IRS's reported
    b. half of the IRS's reported
    c. all of the IRS's reported

If the altimeter were operating in the global mode, no waveform information was reported so that significant waveheight could not be estimated. If the altimeter was operating in intensive mode, ARS's

were always reported, but IRS's may or may not have been reported. Thus, the algorithms that processed IRS data were not only limited to intensive high data rate but were also limited to those intensive high data rate modes where all of the IRS's were reported.

It should also be noted that the different algorithms treat the effects of tracking loop jitter in different ways. Although the WFC significant waveheight algorithm (as well as several of the other estimation algorithms) treat tracking loop jitter in an average sense by including its effects in the calm sea risetime (see Equation 2.46) and assuming that it is unaffected by the magnitude of significant waveheight, several of the algorithms, i.e., Walsh (July, 1979), have attempted to account for the contribution of tracking loop jitter in a more rigorous way. These techniques involve a realignment of the IRS's based upon the residuals between the actual altitude measurements and smoothed altitude measurements. Since they use IRS data, the TM Mode 2 (high data rate) must be used. Nevertheless, the close agreement between these methods of estimation and the methods which accounted for jitter in an average sense seems to indicate that jitter need not be determined rigorously.

## 2.8 Comparison of Other SWH Estimation Techniques

Of the six significant waveheight estimation algorithms presented by Fedor, et al (1979), three of the algorithms solve for

four or more parameters by fitting a curve to the leading edge of the return waveform. Four of the algorithms use a least squares technique to achieve convergence of the curve fit, and four of the six employ the IRS's instead of the ARS's, although one of those models uses an abbreviated set of IRS's. The major characteristics of each of the algorithms is summarized in the following:

Wallops Algorithm. The WFC significant waveheight algorithm presented previously in this chapter employs a least squares fit of a four-parameter function to the ARS data. Tracking loop jitter is accounted for in an average sense. This algorithm was used for the computation of SWH for all archived GEOS-3 data and for the real-time estimation of SWH.

Walsh Algorithm (Walsh, July 1979). The Walsh significant waveheight algorithm performs a five-parameter least squares fit to the IRS data. Tracking loop jitter is accounted for by a time realignment of the IRS's based upon the residuals between the actual altitude measurements and smoothed altitude measurements.

Gower Algorithm (Gower, 1979). The Gower significant waveheight algorithm performs a modified maximum likelihood estimation of a four-parameter fit to the IRS data. Time realignment of the IRS's is used to account for tracking loop jitter.

Rufenach and Alpers Algorithm (Rufenbach and Alpers, 1979). The Rufenach and Alpers algorithm performs a least squares estimation of a two-parameter fit to IRS 8 through IRS 12, which is the rise-time portion of the return waveform. Realignment is performed to account for tracking loop jitter.

Fedor Algorithm (Fedor and Barrick, 1978). The Fedor significant waveheight algorithm fits a three-parameter function to the first differences of the IRS's after a time-realignment correction for tracking loop jitter. An iterative procedure then computes a correction to account for the difference between first differences and true point derivatives. The best-fit function is determined by the method of least squares.

Godbey Algorithm. The Godbey significant waveheight algorithm is based upon a monotonically increasing function of the ARS's and thus accounts for tracking loop jitter in only the average sense. The algorithm estimates only one parameter and does not require iteration. This computational simplicity is a real advantage, especially over the algorithms which process IRS data. However, some of the contributors to the Fedor, et al (1979) investigation (Hayne, 1980) believed that the Godbey algorithm simplified the estimate too much and that the actual shape of the waveform should be estimated.

Fedor, et al (1979) concluded that all of the algorithms

agreed well with each other and with a small amount of ground truth data which was available for their evaluation. The study established the following standard deviations for all of the algorithms:

$$\sigma < 0.75 \text{ m, for } 0.0 < \text{SWH} \leq 4.0 \text{ m} \tag{2.48}$$

$$\sigma < 0.50 \text{ m, for=4.0} < \text{SWH} \leq 8.0 \text{ m} \tag{2.49}$$

From the results presented in this chapter and later in Chapter 4, it can be deduced that since the significant waveheight estimated by the Wallops algorithm agrees well with NOAA buoy data and since the six algorithms presented in the above study all agree with each other, that all of the algorithms are providing satisfactory estimation accuracy. Therefore, simplicity of operation becomes an overriding concern. This would seem to indicate that the algorithms which process ARS data are not only preferable because they allow processing of low data rate data, but also because they achieve comparable accuracy without the computer time and storage requirements necessary for processing IRS data.

# CHAPTER 3

# THE DATA SET

## 3.1 GEOS Data Set

For the purpose of estimating the SWH measurement accuracy, it was necessary to select those passes of GEOS-3 altimeter data from the entire set of GEOS-3 data segments (see Figure 3.1) which could be compared to the independent buoy measurements of significant waveheight. The GEOS-3 ground tracks, which were computed at GSFC to a radial accuracy of 1 to 1.5 meters (Lerch, et al, 1978), must have passed near one of the buoy locations (see Section 3.2) at about the time when the buoy waveheight measurements were made.

As was discussed in Section 1.4, the GEOS-3 altimeter did not operate continuously but was subjected to the power constraints of the spacecraft. Accordingly, the first criterion for matching a GEOS-3 data pass with a buoy observation was that the altimeter be operational at the time that the ground track passed the buoy. In addition, the altimeter must have been operating in a mode which allowed significant waveheight to be estimated.

Since the magnitude of wind generated waves in the open ocean varies slowly with respect to time and distance, it can be

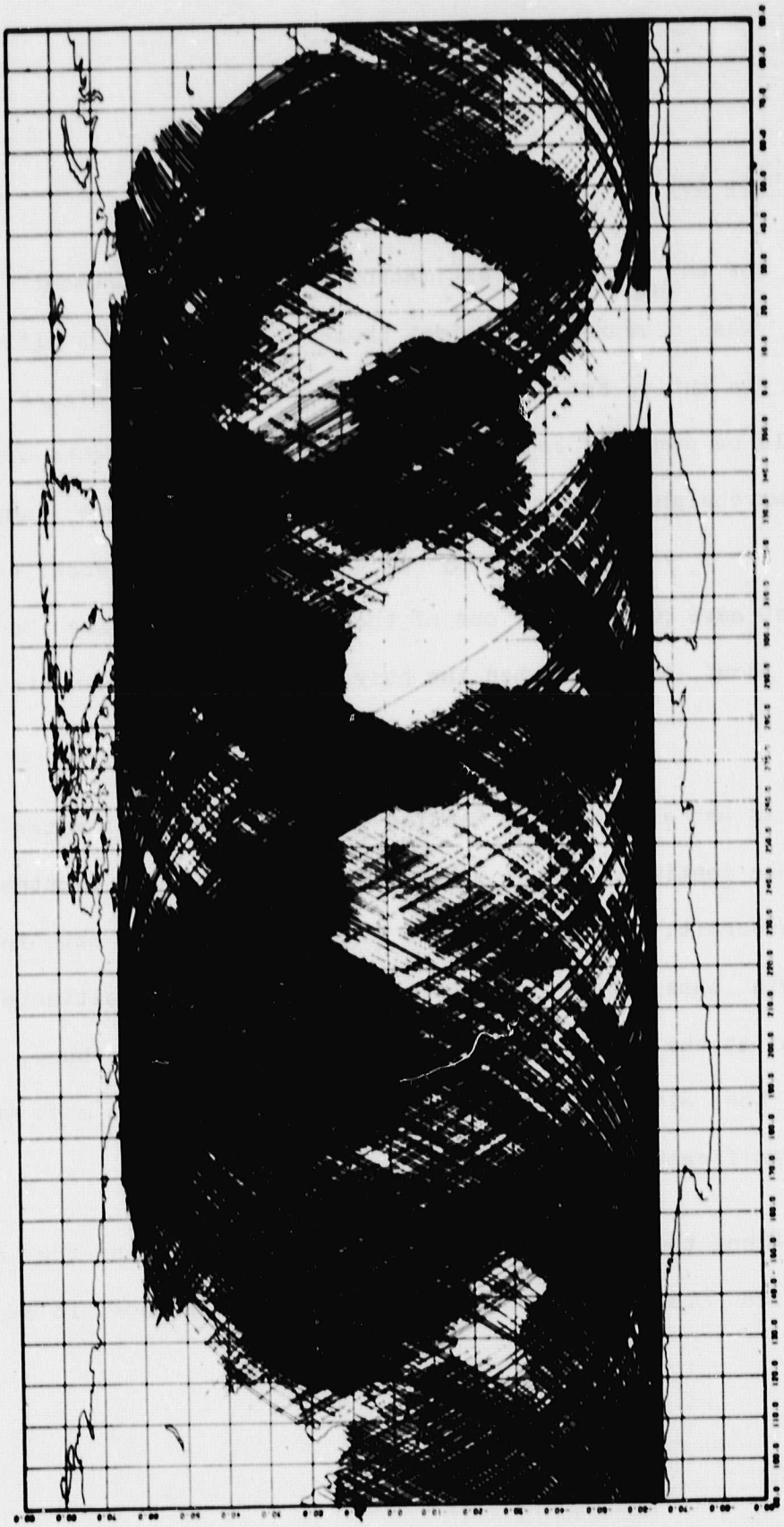

FIGURE 3.1 DATA TAKEN DURING THE GEOS-3 MISSION

assumed to be unchanged over areas of moderate size surrounding the buoys. Therefore, the radius of the search area about the buoy location is somewhat arbitrary. A search area corresponding to one equatorial degree (about 111 kilometers) in radius was assumed to be sufficiently small such that the significant waveheight was unchanged throughout the entire area under reasonably normal conditions. The validity of this assumption, which has been verified by Apel (1975), will be considered in Section 3.2. Additionally, a search area with a radius of one degree is large enough to identify a statistically representative (but not cumbersome) sample population of altimeter data passes.

The mere passing of the satellite ground track through any of the buoy search areas did not qualify that pass as a member of the comparison data set. Since the buoys were often irregular in measuring significant waveheight and since all of the buoy measurements during the GEOS-3 mission were not readily available (see Section 3.2), it was necessary to identify those altimeter data segments passing through the search area at a time when the buoy was measuring significant waveheight and at a time when the buoy measurement was available for reduction.

If the altimeter data set was restricted to data segments whose ground tracks passed through the search area at the exact time when the buoy measurement was being made, there would be only a small number of passes to be reduced. Fortunately, waveheight is

normally a slowly varying parameter in the absence of storm conditions. Therefore, any altimeter data segment which passed through the search area and which occurred within some reasonable period of the buoy measurement could be accepted in the altimeter comparison data set. This period was chosen to be 90 minutes, since the buoy SWH measurements are normally made at 3-hour intervals and any pass entering the search area during a period when the buoy was operating would do so within 90 minutes of a buoy significant waveheight measurement. The 90-minute measurement window is justifiable since wave conditions vary slowly. In fact, most of the buoys measured other data, such as wind speed, every hour. However, NOAA determined that, due to power constraints, it was sufficient to measure SWH every three hours (Steele, 1980). It was assumed, however, that no storm fronts entered the search area in the interval between the time of the buoy measurement and the time of the altimeter estimate.

After the altimeter passes which entered one or more of the search areas within 90 minutes of a buoy measurement were identified, it was necessary to ascertain the status of the altimeter data. When the altimeter was not locked in the tracking mode (this usually occurred during and shortly after the time when the satellite passed over land), the data segment could not be included in the set of data to be compared with the buoy data. Had any of the SWH estimation algorithms which process IRS data been used, the altimeter data would also have had to be in TM Mode 2 with all IRS's

reported. This would have reduced the size of the data set by more than half.

The SWH estimate which occurred at the point of closest approach to the buoy was used in the comparison study. As discussed in Chapter 2, the GEOS-3 significant waveheight estimates were based upon a 21-second sliding rectangular filter of the ARS's and the ARS's were averages of the instantaneous waveforms, which were reported 100 times per second. Therefore, the SWH used for comparison with the buoy measurements was based upon over 2100 instantaneous waveforms. This smoothing removed most of the variability in the estimate in the vicinity of the point of closest approach (PCA) to the buoy.

The same mode and status requirements were employed in identifying those segments of altimeter data to be included in the global atlas of significant waveheight. The proximity requirement in time and location to a NOAA buoy, however, did not apply to the part of the investigation concerned with generating the global atlas of significant waveheight. Therefore, the size of the data set used for the global atlas was vastly larger than the data set used for the buoy comparison. The size of the buoy comparison data set was 126 passes, while the size of the data set used for the global atlas was approximately 8000 passes. The actual processing, which included several other algorithms besides the SWH estimation algorithm, required the use of two computers, operating 24 hours per

day, 7 days per week, for several months.

## 3.2 Buoy Data Set

During the preliminary stages of the investigation, a computer program was written to select all GEOS-3 altimeter passes whose ground tracks passed near one of the NOAA buoys (see Figure 1.4). The data from those buoys (Hadsell, 1974) which matched the GEOS-3 altimeter passes was then identified and requested from NOAA. Unfortunately, at this early stage, a search area radius of 1/4 degree was used to identify the desired buoy data. Some time later, it was determined that a one-degree search area could have been used to select the buoy data. Although the search area was changed to one degree and additional matches were found to have occurred between the buoy data already received and the entire GEOS-3 altimeter data set, the number of matching passes of altimeter data and buoy data would have been increased by approximately 300% if the requested buoy data had been based upon a one-degree search area radius. However, due to budgetary constraints, it was not possible to obtain additional buoy data at a later time.

The NDBO measurements of significant waveheight were made by three different types of buoys. These types were:

1. EEP - Engineering Experimental Phase

2. WSA - Wave Spectrum Analyzer

3. WDA - Wave Data Analyzer

The Engineering Experiment Phase type buoy was the first system developed by NDBO and is described in Steele, et al (1975). Although the system performed acceptably, the hardware was not operationally reliable, and the measurements displayed relatively high noise levels (Steele and Johnson, 1977). Currently only one EEP type buoy is deployed, and that buoy is used only for the purpose of evaluating the performance of the more advanced WSA and WDA type buoys. Only one EEP measurement was used in this investigation.

Most of the buoy data used in this investigation (about 80%) were reported by WSA type buoys, which are described in Remond (1976). WSA buoys consist of 12 analog filters, each with a separate center frequency. The output from a strapped down accelerometer is fed into the filters, and a system of 12 equations with 12 unknowns is solved to produce the estimate of significant waveheight. However, the filters were not precisely calibrated and tended to estimate significant waveheight which was 15% lower than the true waveheight (Steele, 1980). The only other measurement error thought to be of consequence is the measurement error of the accelerometer (Steele, 1980). NDBO estimates that the WSA determination of significant waveheight has a measurement error of 50 to

100 cm (Withee and Blassingame, 1976).

About 20% of the buoy data used in this investigation were reported by WDA type buoys, which are currently the most advanced buoys deployed by NDBO. These buoys are described by Steele, et al (1976). In this system, data from a vertical strapped down accelerometer is passed through an analog filter, digitized and transformed into the equivalent of covariances (Steele, et al, 1975, and Steele, et al, 1976), from which significant waveheight is calculated. NDBO is very confident in the quality of the WDA measurements, but Steele (1980) estimates that the significant waveheight reported by the WDA type buoys is 10 to 20 cm low. As was the case with the WSA type buoys, the only other significant error source is thought to be the measurement error of the accelerometer (Steele, 1980). NDBO estimates that the WDA determination of significant waveheight has a measurement accuracy of 30 to 50 cm (Steele, 1980).

Many of the altimeter passes which entered one of the search areas could not be matched to buoy data. This occurred because the buoys were often deployed for several months, then recovered and not deployed again until some time later (see Figure 3.2). Additionally, more than half of the buoy data was reported containing atmospheric measurements, such as wind speed, temperature and pressure, but not significant waveheight measurements. Table 3.1 lists all of the passes which satisfy both the altimeter data set requirements and which were requested and received from the NOAA

FIGURE 3.2. NDBO BUOY MEASUREMENT REPORTING PERIODS

| CASE | REV | UNIQ | BUOY | CASE | REV | UNIQ | BUOY | CASE | REV | UNIQ | BUOY |
|---|---|---|---|---|---|---|---|---|---|---|---|
| 1 | 581 | 526 | EB13 | 54 | [illegible] | 114 | EB70 | 107 | 12028 | 171 | EB20 |
| 2 | 1111 | 86 | EB03 | 55 | [illegible] | 141 | EB19 | 108 | 12031 | 174 | EB41 |
| 3 | 1438 | 345 | EB03 | 56 | [illegible] | 147 | EB16 | 109 | 12068 | 121 | EB41 |
| 4 | 2291 | 525 | EB03 | 57 | 9275 | [illegible] | EB41 | 110 | 12169 | 121 | EB01 |
| 5 | 2389 | 62 | EB16 | 58 | 9310 | 154 | EB41 | 111 | 12210 | 177 | EB16 |
| 6 | 2870 | 502 | EB41 | 59 | 9355 | 170 | EB16 | 112 | 12217 | 184 | EB71 |
| 7 | 3032 | 593 | EB41 | 60 | 9644 | 174 | EB43 | 113 | 12230 | 186 | EB41 |
| 8 | 3069 | 617 | EB41 | 61 | 9709 | 136 | EB41 | 114 | 12336 | 160 | EB41 |
| 9 | 3361 | 789 | EB03 | 62 | 9836 | 167 | EB41 | 115 | 12409 | 182 | EB01 |
| 10 | 3473 | 841 | EB16 | 63 | 9998 | 132 | EB41 | 116 | 12486 | 141 | EB01 |
| 11 | 3558 | 882 | EB41 | 64 | 10039 | 172 | EB70 | 117 | 12671 | 139 | EB16 |
| 12 | 3595 | 905 | EB41 | 65 | 10057 | 187 | EB16 | 118 | 12864 | 129 | EB16 |
| 13 | 4213 | 423 | EB04 | 66 | 10080 | 115 | EB16 | 119 | 12868 | 134 | EB17 |
| 14 | 4525 | 200 | EB16 | 67 | 10110 | 140 | EB03 | 120 | 12870 | 137 | EB16 |
| 15 | 4590 | 240 | EB16 | 68 | 10110 | 140 | EB17 | 121 | 12884 | 153 | EB41 |
| 16 | 4917 | 127 | EB16 | 69 | 10128 | 153 | EB03 | 122 | 12921 | 199 | EB41 |
| 17 | 4921 | 132 | EB03 | 70 | 10128 | 153 | EB16 | 123 | 12998 | 157 | EB16 |
| 18 | 5116 | 389 | EB16 | 71 | 10157 | 174 | EB17 | 124 | 13063 | 128 | EB16 |
| 19 | 5136 | 414 | EB41 | 72 | 10163 | 103 | EB41 | 125 | 13120 | 182 | EB41 |
| 20 | 5443 | 227 | EB16 | 73 | 10166 | 105 | EB19 | 126 | 13197 | 161 | EB16 |
| 21 | 6026 | 121 | EB41 | 74 | 10167 | 106 | EB70 | | | | |
| 22 | 6367 | 155 | EB01 | 75 | 10208 | 134 | EB16 | | | | |
| 23 | 6515 | 120 | EB41 | 76 | 10227 | 148 | EB70 | | | | |
| 24 | 6552 | 159 | EB41 | 77 | 10240 | 157 | EB16 | | | | |
| 25 | 6623 | 129 | EB16 | 78 | 10256 | 166 | EB16 | | | | |
| 26 | 6629 | 135 | EB16 | 79 | 10305 | 134 | EB16 | | | | |
| 27 | 6879 | 185 | EB41 | 80 | 10334 | 151 | EB71 | | | | |
| 28 | 7021 | 127 | EB16 | 81 | 10366 | 106 | EB43 | | | | |
| 29 | 7867 | 175 | EB70 | 82 | 10366 | 106 | EB70 | | | | |
| 30 | 7874 | 179 | EB16 | 83 | 10384 | 117 | EB16 | | | | |
| 31 | 7896 | 118 | EB03 | 84 | 10433 | 146 | EB16 | | | | |
| 32 | 7924 | 146 | EB70 | 85 | 10439 | 149 | EB16 | | | | |
| 33 | 7935 | 154 | EB70 | 86 | 10533 | 159 | EB71 | | | | |
| 34 | 7938 | 160 | EB43 | 87 | 10535 | 163 | EB16 | | | | |
| 35 | 7938 | 160 | EB70 | 88 | 10597 | 126 | EB19 | | | | |
| 36 | 7967 | 187 | EB19 | 89 | 10632 | 155 | EB16 | | | | |
| 37 | 8008 | 127 | EB16 | 90 | 10654 | 101 | EB03 | | | | |
| 38 | 8066 | 181 | EB70 | 91 | 10654 | 101 | EB16 | | | | |
| 39 | 8279 | 102 | EB71 | 92 | 10703 | 134 | EB01 | | | | |
| 40 | 8422 | 135 | EB03 | 93 | 10820 | 147 | EB19 | | | | |
| 41 | 8606 | 125 | EB71 | 94 | 10831 | 153 | EB16 | | | | |
| 42 | 8649 | 159 | EB70 | 95 | 10959 | 108 | EB16 | | | | |
| 43 | 8660 | 168 | EB70 | 96 | 10965 | 112 | EB16 | | | | |
| 44 | 8848 | 156 | EB70 | 97 | 10979 | 123 | EB01 | | | | |
| 45 | 8859 | 162 | EB70 | 98 | 11357 | 107 | EB16 | | | | |
| 46 | 8861 | 165 | EB16 | 99 | 11505 | 135 | EB41 | | | | |
| 47 | 8877 | 107 | EB16 | 100 | 11542 | 154 | EB41 | | | | |
| 48 | 8946 | 155 | EB41 | 101 | 11556 | 106 | EB01 | | | | |
| 49 | 8948 | 160 | EB21 | 102 | 11633 | 148 | EB01 | | | | |
| 50 | 9075 | 105 | EB04 | 103 | 11741 | 153 | EB41 | | | | |
| 51 | 9076 | 106 | EB03 | 104 | 11832 | 149 | EB01 | | | | |
| 52 | 9129 | 135 | EB03 | 105 | 11855 | 110 | EB04 | | | | |
| 53 | 9132 | 138 | EB71 | 106 | 11883 | 130 | EB01 | | | | |

TABLE 3.1. GEOS/BUOY COMPARISON DATA SET

Data Buoy Office.

It should be noted that NOAA's philosophy is (Steele, 1980) that a high degree of accuracy in measuring sea state is not as important for low sea state as it is for high sea state. For example, an estimate of SWH = 2 meters in error by a meter or more is less important than an estimate of SWH = 5 meters which is in error by a meter or more. Additionally, ships and ocean platforms are designed to be able to endure certain maximum stresses. Since high sea state may cause stresses that approach structural limits, a precise determination of SWH in high sea state conditions is imperative.

## 3.3 Seasat Data Set

During September and October of 1978, the Gulf of Alaska Seasat Experiment (GOASEX) was performed to aid in the accuracy determination of the Seasat geophysical parameters. Part of that experiment contained altimeter parameter accuracy determination. The results of that determination were published in the Seasat Gulf of Alaska Workshop II Report (1979). In that report, 17 ground track crossings of Seasat and GEOS-3 were compared for the purpose of verifying the accuracy of the significant waveheight determinations of each of the altimeters. The Seasat and GEOS-3 data for those 17 passes make up the Seasat data set, which is examined in Chapter 4.

# CHAPTER 4

## COMPARISON OF GEOS-3 SWH ESTIMATES WITH BUOY AND SEASAT SWH MEASUREMENTS

The GEOS-3 significant waveheight estimates and the NOAA buoy significant waveheight measurements constitute two independent determinations of the same phenomenon. Some information about the accuracy of the buoy estimates is available from NOAA, and these data, combined with statistical analysis of the difference between the GEOS-3 and the buoy determinations, can be used to infer the accuracy of the GEOS-3 significant waveheight estimate.

The analysis that follows assumes that the two estimates are independent and that they have independent error sources. Although there is no reason to believe that these assumptions are violated, it should be noted that the statistical analysis which determines the accuracy of the GEOS-3 significant waveheight phenomenom could be corrupted slightly if the GEOS-3 and buoy determinations had error contributions from the same indirect source. An example of this phenomenom is the degradation of the buoy measurement due to wind speed and direction. Since the wind affects the motion of the buoys and since the significant waveheight measured by the buoys is related to the motion of the platform, both wind speed and direction could cause an error in the measurement of significant waveheight by

the buoy. Although the GEOS-3 estimate was assumed to be independent of wind effects, the existence of such dependence, along with a similar dependence by the buoy data, would influence the altimeter SWH accuracy estimates which follow.

Table 4.1 lists all of the altimeter passes which could be matched with buoy data. If the standard deviation of the differences between the GEOS-3 significant waveheight estimates and the NOAA buoy significant waveheight measurements is computed, it can be seen that the difference between the two estimates for revolution number 10227 is noticeably larger in absolute value and in fact is greater than three times the standard deviation (3-sigma) of the differences of the entire comparison data set. It can therefore be legitimately edited from the data set leaving 125 passes of data on which the following analysis is based.

## 4.1 Computation of the GEOS-3 SWH Standard Deviation

As has been stated earlier, one of the primary objectives of this investigation is to establish the accuracy of the Wallops SWH estimation algorithm. Table 4.1 presents the differences between the SWH computed using that algorithm and the SWH measured by buoys. Using the statistics of those diferences and the statistics of the buoy measurement permits the statistics of the GEOS-3 estimate to be inferred.

| CASE | REV | UNIQ | BUOY | PCA | | | SWH (M) | | |
|---|---|---|---|---|---|---|---|---|---|
| | | | | DATE | TIME | KM | GEOS | BUOY | DIFF |
| 1 | 581 | 526 | EB13 | 750521 | 13720 | 64.0 | .50 | 1.05 | -.55 |
| 2 | 1111 | 86 | EB03 | 750627 | 12[illegible]453 | 30.9 | .23 | .90 | -.67 |
| 3 | 1438 | 346 | EB03 | 750720 | 151129 | .6 | .00 | .90 | -.90 |
| 4 | 2291 | 526 | EB03 | 750918 | 222[illegible]53 | 28.1 | 2.21 | 2.20 | .01 |
| 5 | 2389 | 62 | EB16 | 750925 | 204060 | 11.1 | 3.05 | 2.16 | .89 |
| 6 | 2870 | 502 | EB41 | 751029 | 204039 | 28.2 | 1.35 | 1.10 | .25 |
| 7 | 3032 | 593 | EB41 | 751110 | 70332 | 13.1 | 1.67 | .47 | 1.20 |
| 8 | 3069 | 617 | EB41 | 751112 | 221552 | 21.4 | 1.30 | 1.10 | .20 |
| 9 | 3361 | 789 | EB03 | 751203 | 131657 | 3.8 | 2.94 | 3.16 | -.22 |
| 10 | 3473 | 841 | EB16 | 751211 | 110818 | 25.2 | 2.11 | 4.13 | -2.02 |
| 11 | 3558 | 882 | EB41 | 751217 | 112209 | 14.4 | 2.05 | [illegible].10 | .95 |
| 12 | 3595 | 905 | EB41 | 751220 | 23431 | 22.9 | 2.26 | 1.30 | .96 |
| 13 | 4213 | 423 | EB04 | 760201 | 182639 | 22.1 | 5.60 | 4.37 | 1.23 |
| 14 | 4525 | 200 | EB16 | 760223 | 194520 | 18.3 | 4.45 | 3.17 | 1.28 |
| 15 | 4590 | 240 | EB16 | 760228 | 103154 | 20.9 | .00 | .70 | -.70 |
| 16 | 4917 | 127 | EB16 | 760322 | 131513 | 28.2 | 1.89 | 1.26 | .63 |
| 17 | 4921 | 132 | EB03 | 760322 | 195351 | 21.2 | 3.27 | 3.02 | .25 |
| 18 | 5116 | 389 | EB16 | 760405 | 145020 | 27.3 | 4.54 | 2.49 | 2.05 |
| 19 | 5136 | 414 | EB41 | 760407 | 1735 | 28.5 | 2.14 | .69 | 1.45 |
| 20 | 5443 | 227 | EB16 | 760428 | 173336 | 22.3 | 1.52 | .50 | 1.02 |
| 21 | 6026 | 121 | EB41 | 760608 | 223129 | 1.7 | 2.55 | .60 | 1.95 |
| 22 | 6367 | 156 | EB01 | 760703 | 10056 | 12.1 | 1.31 | 1.83 | -.52 |
| 23 | 6515 | 120 | EB41 | 760713 | 113720 | 6.5 | 1.31 | 1.73 | -.42 |
| 24 | 6552 | 159 | EB41 | 760716 | 24941 | 12.7 | .44 | .50 | -.06 |
| 25 | 6623 | 129 | EB16 | 760721 | 31814 | 105.9 | 1.23 | .61 | .62 |
| 26 | 6629 | 135 | EB16 | 760721 | 125836 | 18.8 | 1.77 | .67 | 1.10 |
| 27 | 6879 | 185 | EB41 | 760808 | 53249 | 29.9 | 1.77 | 1.08 | .69 |
| 28 | 7021 | 127 | EB16 | 760818 | 62816 | 11.5 | 1.90 | 1.80 | .10 |
| 29 | 7867 | 175 | EB70 | 761017 | 11634 | 6.3 | 3.50 | 3.67 | -.17 |
| 30 | 7874 | 179 | EB16 | 761017 | 132927 | 21.0 | 1.46 | .80 | .66 |
| 31 | 7896 | 118 | EB03 | 761019 | 22640 | 9.9 | 2.91 | 1.49 | 1.42 |
| 32 | 7924 | 146 | EB70 | 761021 | 15748 | 107.1 | 1.66 | 1.87 | -.21 |
| 33 | 7935 | 154 | EB70 | 761021 | 204806 | 19.3 | 3.51 | 1.69 | 1.82 |
| 34 | 7938 | 160 | EB43 | 761022 | 14326 | 28.8 | 2.56 | 1.69 | .87 |
| 35 | 7938 | 160 | EB70 | 761022 | 14324 | 63.0 | 2.56 | 1.64 | .92 |
| 36 | 7967 | 187 | EB19 | 761024 | 25109 | 28.9 | 2.91 | 1.81 | 1.10 |
| 37 | 8008 | 127 | EB16 | 761027 | 1755 | 2.9 | 2.74 | 2.08 | .66 |
| 38 | 8066 | 181 | EB70 | 761031 | 25130 | 23.8 | 8.20 | 8.08 | .12 |
| 39 | 8279 | 102 | EB71 | 761115 | 35912 | 23.1 | 2.26 | 1.90 | .36 |
| 40 | 8422 | 135 | EB03 | 761125 | 64441 | 17.9 | 4.33 | 2.93 | 1.40 |
| 41 | 8606 | 125 | EB71 | 761208 | 64213 | 33.0 | 1.87 | 1.88 | -.01 |
| 42 | 8649 | 159 | EB70 | 761211 | 75045 | 75.4 | 2.72 | 3.08 | -.36 |
| 43 | 8660 | 168 | EB70 | 761212 | 24102 | 10.4 | 6.39 | 6.63 | -.24 |
| 44 | 8848 | 156 | EB70 | 761225 | 92542 | 52.1 | 5.[illegible]6 | 4.59 | 1.27 |
| 45 | 8859 | 162 | EB70 | 761226 | 41559 | 33.5 | [illegible]82 | 3.96 | -.14 |
| 46 | 8861 | 165 | EB15 | 761226 | 71654 | 29.5 | 3.17 | 2.04 | 1.13 |
| 47 | 8877 | 107 | EB16 | 761227 | 103037 | 20.5 | 3.63 | 3.75 | -.12 |
| 48 | 8946 | 158 | EB41 | 770101 | 73217 | 20.3 | 4.03 | 2.85 | 1.18 |
| 49 | 8948 | 160 | EB21 | 770101 | 105817 | 27.3 | 2.71 | 1.60 | 1.11 |
| 50 | 9075 | 105 | EB04 | 770110 | 101829 | 23.8 | 4.30 | 3.69 | .61 |
| 51 | 9076 | 106 | EB03 | 770110 | 121042 | 27.2 | 3.66 | 3.29 | .37 |
| 52 | 9129 | 135 | EB03 | 770114 | 61859 | 28.1 | 3.86 | 3.65 | .21 |
| 53 | 9132 | 138 | EB71 | 770114 | 110007 | 15.7 | 2.25 | 1.53 | .72 |

TABLE 4.1. GEOS/BUOY COMPARISON RESULTS

| CASE | REV | UNIQ | BUOY | PCA DATE | PCA TIME | PCA KM | SWH (M) GEOS | SWH (M) BUOY | DIFF | |
|---|---|---|---|---|---|---|---|---|---|---|
| 54 | 9186 | 114 | EB70 | 770118 | 65859 | 15.5 | 5.21 | 5.97 | −.76 | |
| 55 | 9218 | 141 | EB19 | 770120 | 130204 | 30.1 | 4.60 | 3.87 | .73 | |
| 56 | 9253 | 167 | EB15 | 770123 | 4826 | 33.9 | 4.38 | 3.23 | 1.15 | |
| 57 | 9273 | 106 | EB41 | 770124 | 101539 | 26.3 | .87 | 1.75 | −.88 | |
| 58 | 9310 | 134 | EB41 | 770127 | 12758 | 17.1 | 3.35 | 2.56 | .79 | |
| 59 | 9355 | 170 | EB16 | 770130 | 54658 | 20.1 | 4.40 | 3.98 | .42 | |
| 60 | 9644 | 174 | EB43 | 770219 | 154519 | 7.7 | 6.18 | 5.77 | .41 | |
| 61 | 9799 | 136 | EB41 | 770302 | 143330 | 9.8 | 1.82 | 1.80 | .02 | |
| 62 | 9836 | 167 | EB41 | 770305 | 54548 | .0 | 3.23 | 3.12 | .11 | |
| 63 | 9998 | 132 | EB41 | 770316 | 160823 | 45.4 | 1.89 | .84 | 1.05 | |
| 64 | 10039 | 172 | EB70 | 770319 | 135945 | 6.8 | 1.66 | 1.37 | .29 | |
| 65 | 10057 | 187 | EB16 | 770320 | 201440 | 44.7 | 1.14 | 1.53 | −.39 | |
| 66 | 10080 | 115 | EB16 | 770322 | 113940 | 84.6 | 2.19 | 1.88 | .31 | |
| 67 | 10110 | 140 | EB03 | 770324 | 142750 | 36.7 | 2.87 | 1.93 | .94 | |
| 68 | 10110 | 140 | EB17 | 770324 | 142932 | 12.8 | 2.55 | 2.60 | −.05 | |
| 69 | 10128 | 153 | EB03 | 770325 | 204623 | 8.3 | 3.99 | 3.02 | .97 | |
| 70 | 10128 | 153 | EB16 | 770325 | 204131 | 92.5 | 2.18 | 1.72 | .46 | |
| 71 | 10157 | 174 | EB17 | 770327 | 215637 | 46.7 | 2.45 | 2.73 | −.28 | |
| 72 | 10163 | 103 | EB41 | 770328 | 82843 | 39.1 | .00 | .70 | −.70 | |
| 73 | 10166 | 105 | EB19 | 770328 | 132948 | 6.7 | 4.59 | 3.95 | .64 | |
| 74 | 10167 | 104 | EB70 | 770328 | 150747 | 35.2 | 2.23 | 2.19 | .04 | |
| 75 | 10208 | 134 | EB16 | 770331 | 124742 | 2.4 | 1.46 | 1.90 | −.44 | |
| 76 | 10227 | 148 | EB70 | 770401 | 204421 | 55.9 | .00 | 2.36 | −2.36 | ***Edited*** |
| 77 | 10240 | 157 | EB15 | 770402 | 183733 | 37.0 | 2.04 | 1.64 | .40 | |
| 78 | 10256 | 166 | EB16 | 770403 | 214933 | 9.3 | 2.31 | 1.80 | .51 | |
| 79 | 10305 | 134 | EB15 | 770407 | 92404 | 6.9 | 2.56 | 1.17 | 1.39 | |
| 80 | 10334 | 151 | EB71 | 770409 | 103742 | 50.7 | 2.26 | 1.10 | 1.16 | |
| 81 | 10366 | 106 | EB43 | 770411 | 164234 | 12.5 | 2.97 | 2.83 | .14 | |
| 82 | 10366 | 106 | EB70 | 770411 | 164238 | 10.6 | 2.97 | 3.00 | −.03 | |
| 83 | 10384 | 117 | EB16 | 770413 | 226734 | 77.6 | 5.75 | 3.87 | 1.88 | |
| 84 | 10433 | 146 | EB15 | 770416 | 103205 | 99.8 | 2.61 | 1.00 | 1.61 | |
| 85 | 10439 | 149 | EB15 | 770416 | 201225 | 24.6 | 2.64 | 1.13 | 1.51 | |
| 86 | 10533 | 159 | EB71 | 770423 | 121233 | 14.6 | .00 | .81 | −.81 | |
| 87 | 10535 | 163 | EB16 | 770423 | 163035 | 35.8 | 3.92 | 2.83 | 1.09 | |
| 88 | 10597 | 126 | EB19 | 770428 | 2034 | 27.9 | 1.13 | 1.30 | −.17 | |
| 89 | 10632 | 155 | EB15 | 770430 | 120655 | 38.2 | 1.06 | 1.30 | −.24 | |
| 90 | 10654 | 101 | EB03 | 770502 | 10406 | 2.5 | 3.33 | 3.19 | .14 | |
| 91 | 10654 | 101 | EB16 | 770502 | 5914 | 109.7 | 1.40 | 1.13 | .27 | |
| 92 | 10703 | 134 | EB01 | 770505 | 123241 | 33.7 | 1.17 | 1.34 | −.17 | |
| 93 | 10820 | 147 | EB19 | 770513 | 185531 | 46.4 | 2.69 | 3.19 | −.50 | |
| 94 | 10831 | 153 | EB15 | 770514 | 134146 | 24.6 | 1.13 | 1.11 | .02 | |
| 95 | 10959 | 108 | EB15 | 770523 | 144945 | 78.7 | 3.55 | 2.29 | 1.26 | |
| 96 | 10965 | 112 | EB15 | 770524 | 3005 | 45.7 | 3.55 | 2.62 | .93 | |
| 97 | 10979 | 123 | EB01 | 770525 | 1556 | 50.1 | 2.25 | 1.49 | .76 | |
| 98 | 11357 | 107 | EB15 | 770620 | 175921 | 46.0 | 1.89 | 1.40 | .49 | |
| 99 | 11505 | 135 | EB41 | 770701 | 43433 | 45.4 | 1.74 | .95 | .79 | |
| 100 | 11542 | 154 | EB41 | 770703 | 194650 | 36.3 | .00 | .84 | −.84 | |
| 101 | 11556 | 106 | EB01 | 770704 | 193306 | 17.3 | 1.18 | 1.05 | .13 | |
| 102 | 11633 | 148 | EB01 | 770710 | 54129 | 27.6 | 2.45 | 1.20 | 1.25 | |
| 103 | 11741 | 153 | EB41 | 770717 | 212135 | 20.6 | .49 | 1.00 | −.51 | |
| 104 | 11832 | 149 | EB01 | 770724 | 71614 | 35.4 | 1.14 | 1.72 | −.58 | |
| 105 | 11855 | 110 | EB04 | 770726 | 224853 | 12.9 | 1.19 | .60 | .59 | |
| 106 | 11883 | 130 | EB01 | 770727 | 221549 | 21.4 | 2.15 | 1.68 | .47 | |

**TABLE 4.1. GEOS/BUOY COMPARISON RESULTS (CONT.)**

| CASE | REV | UNIQ | BUOY | PCA | | | SWH (M) | | |
|---|---|---|---|---|---|---|---|---|---|
| | | | | DATE | TIME | KM | GEOS | BUOY | DIFF |
| 107 | 12028 | 171 | EB20 | 770807 | 41152 | 44.4 | 1.66 | .96 | .70 |
| 108 | 12031 | 174 | EB41 | 770807 | 85142 | 17.5 | 1.67 | 1.00 | .67 |
| 109 | 12068 | 121 | EB41 | 770810 | 417 | 13.6 | 1.27 | 1.00 | .27 |
| 110 | 12159 | 121 | EB01 | 770816 | 95839 | 7.6 | 2.37 | 1.03 | 1.34 |
| 111 | 12210 | 177 | EB15 | 770820 | 5915 | 39.9 | 2.99 | 1.30 | 1.69 |
| 112 | 12217 | 184 | EB71 | 770820 | 121901 | 46.9 | 1.80 | .50 | 1.30 |
| 113 | 12230 | 196 | EB41 | 770821 | 102929 | 42.3 | .61 | 1.00 | −.39 |
| 114 | 12395 | 150 | EB41 | 770902 | 24859 | 45.0 | .00 | .90 | −.90 |
| 115 | 12409 | 162 | EB01 | 770903 | 23314 | 6.7 | 1.67 | .69 | .98 |
| 116 | 12496 | 141 | EB01 | 770908 | 124137 | 37.2 | 2.04 | 1.00 | 1.04 |
| 117 | 12671 | 139 | EB15 | 770921 | 143029 | 21.6 | 2.18 | .92 | 1.26 |
| 118 | 12864 | 129 | EB15 | 771005 | 62452 | 38.2 | 2.07 | 1.37 | .70 |
| 119 | 12868 | 134 | EB17 | 771005 | 130512 | 3.0 | 1.05 | 1.43 | −.38 |
| 120 | 12870 | 137 | EB15 | 771005 | 160512 | 86.4 | .91 | .93 | −.02 |
| 121 | 12884 | 153 | EB41 | 771006 | 155205 | 30.9 | 1.62 | .86 | .76 |
| 122 | 12921 | 199 | EB41 | 771009 | 70421 | 20.6 | 1.89 | 1.44 | .45 |
| 123 | 12998 | 157 | EB15 | 771014 | 171307 | 13.7 | 3.30 | 2.70 | .60 |
| 124 | 13063 | 126 | EB15 | 771019 | 75933 | 27.3 | 1.63 | 1.03 | .60 |
| 125 | 13120 | 182 | EB41 | 771023 | 83902 | 39.1 | .00 | .93 | −.93 |
| 126 | 13197 | 151 | EB15 | 771028 | 184747 | 50.5 | .00 | 1.17 | −1.17 |

TABLE 4.1. GEOS/BUOY COMPARISON RESULTS (CONT.)

Using an edit criterion of three times the standard deviation of the differences between the altimeter and buoy determinations of significant waveheight, the standard deviation of the differences not edited (125 passes) is

$$S_D = 0.71 \text{ m} \tag{4.1}$$

The letter S is used to symbolize standard deviations of the sample population of 125 elements and must be differentiated from the symbol $\sigma$, which will be used to symbolize the standard deviation of the entire population.

With the assumption that the GEOS-3 estimates and the buoy measurements of significant waveheight are independent, then

$$\sigma_D^2 = \sigma_G^2 + \sigma_B^2 \tag{4.2}$$

where $\sigma_B$ is the standard deviation of the buoy significant waveheight measurements, $\sigma_G$ is the standard deviation of the altimeter significant waveheight estimates and $\sigma_D$ is the standard deviation of the difference between the GEOS-3 estimate and the buoy measurement of significant waveheight. The value of $S_D$ is an estimate of $\sigma_D$ and can be substituted into Equation (4.2) to yield

$$S_D^2 = \sigma_G^2 + \sigma_G^2 \tag{4.3}$$

Equation (4.3) could be used to solve for $\sigma_G$ if $\sigma_B$ was known. The NOAA Data Buoy Office estimates that $0.50 \leq \sigma_B \leq 1.00$ m

(Withee and Blassingame, 1976).

Examination of Equation (4.3) shows that as $\sigma_B$ is increased from 0.50 m to 1.00 m, $\sigma_G$ decreases. Therefore, the most conservative estimate for $\sigma_G$ is obtained when $\sigma_B = 0.50$ is used. Substituting this value and Equation (4.1) into Equation (4.3) yields

$$S_G = 0.50 \text{ m} \tag{4.4}$$

where the symbol S is again used to indicate that the standard deviation refers to the sample population.

The standard deviation of the entire population can be estimated to the 95% confidence limits by employing the chi-square distribution. These limits are given by

$$\frac{nS_G^2}{\chi^2_{.025}} \geq \sigma_G^2 \geq \frac{nS_G^2}{\chi^2_{.975}} \tag{4.5}$$

where n is the number of degrees of freedom (in this case n = 123). When $n > 30$, a normal approximation can be used and $\chi^2_\alpha$ can be determined from

$$\chi^2_\alpha = \frac{1}{2}(x_\alpha + [2n-1]^{1/2})^2 \tag{4.6}$$

where $x_\alpha$ is the $\alpha$-point of the cumulative normal distribution. From the normal probability function tables

$$F(x) = 0.025 \qquad x_{.025} = -1.96 \tag{4.7}$$

$$F(x) = 0.975 \qquad x_{.975} = +1.96 \tag{4.8}$$

Substituting Equations (4.7) and (4.8) into Equation (4.6) and using n = 123 yields

$$\chi^2_{.025} = 93.7 \tag{4.9}$$

$$\chi^2_{.975} = 155.1 \tag{4.10}$$

Substituting Equations (4.9) and (4.10) into Equation (4.5) yields

$$0.33 \geq \sigma_G^2 \geq 0.20 \text{ m} \tag{4.11}$$

and since $\sigma_G$ must be non-negative

$$0.57 \geq \sigma_G \geq 0.45 \text{ m} \tag{4.12}$$

Therefore, based upon the assumption of independence between the altimeter estimates and the buoy measurements of significant waveheights, the 3-sigma edit criteron, a value of $\sigma_B = 0.50$ m, and the sample population of 125 differences, there is a 95% probability that the value of $\sigma_G$ for the entire population of GEOS-3 passes lies between 0.45 m and 0.57 m.

The above values represent a conservative estimate under the assumptions given above. To illustrate, it can be shown that employing a 2 1/2-sigma edit criterion results in an estimate of 0.40 m for $\sigma_G$ with a 95% probability that the standard deviation

of the entire population of GEOS-3 passes lies between 0.36 m and 0.46 m. Similarly, the estimate of $\sigma_G$ would be lowered if the estimate of $\sigma_B$ was chosen to be larger than the minimum estimate published by NOAA. Based upon these results, the GEOS-3 design specification of $\pm$ 20% accuracy for 2.0 < SWH < 10 meters appears to be satisfied.

Table 4.2 lists the statistics of the comparisons of GEOS-3 estimates and buoy measurements for each of the buoys. Note that the results obtained for buoy EB15 are significantly worse than the results obtained for the other buoys. Due to this result, NOAA is currently investigating the accuracy of the significant waveheight measurements of buoy EB15.

## 4.2 Computation of the SWH Mean Difference

Using the same 3-sigma edit criterion for the difference between the GEOS-3 significant waveheight measurements that was described in Section 4.1, the mean difference of the 125 samples is

$$\bar{D} = 0.41 \text{ m} \qquad (4.13)$$

In Equation (4.13), the letter $\bar{D}$ is used to symbolize that the mean difference given is for the sample population. The mean difference for the entire population will be given the symbol $\mu_D$. Figure 4.1 illustrates that the differences are distributed normally about the mean of 0.41 m. It should be noted that the NOAA Data

| BUOY | BUOY TYPE | MEAN | SIGMA | #SAMPLES |
|---|---|---|---|---|
| EB01 | WSA | 0.47 | 0.72 | 10 |
| EB15 | WSA | 0.65 | 0.88 | 29 |
| EB41 | WSA | 0.30 | 0.80 | 27 |
| EB04 | WDA (NOMAD) | | | |
| EB13 | EEP (DISCUS) | 0.46 | 0.73 | 10 |
| EB71 | WDA (DISCUS) | | | |
| ALL ATLANTIC BUOYS | --- | 0.47 | 0.81 | 76 |
| ALL ATLANTIC BUOYS EXCEPT EB15 | --- | 0.32 | 0.76 | 47 |
| EB03 | WSA | 0.33 | 0.74 | 12 |
| EB16 | WSA | 0.44 | 0.67 | 11 |
| EB70 | WDA (DISCUS) | 0.20 | 0.72 | 13 |
| EB17 | WSA | | | |
| EB19 | WSA | | | |
| EB20 | WSA | 0.33 | 0.57 | 13 |
| EB21 | WSA | | | |
| EB43 | WSA | | | |
| ALL PACIFIC BUOYS | --- | 0.32 | 0.66 | 49 |
| ALL BUOYS | --- | 0.41 | 0.76 | 125 |
| ALL BUOYS EXCEPT EB15 | --- | 0.34 | 0.71 | 96 |

TABLE 4.2 STATISTICS OF $SWH_{GEOS} - SWH_{BUOY}$

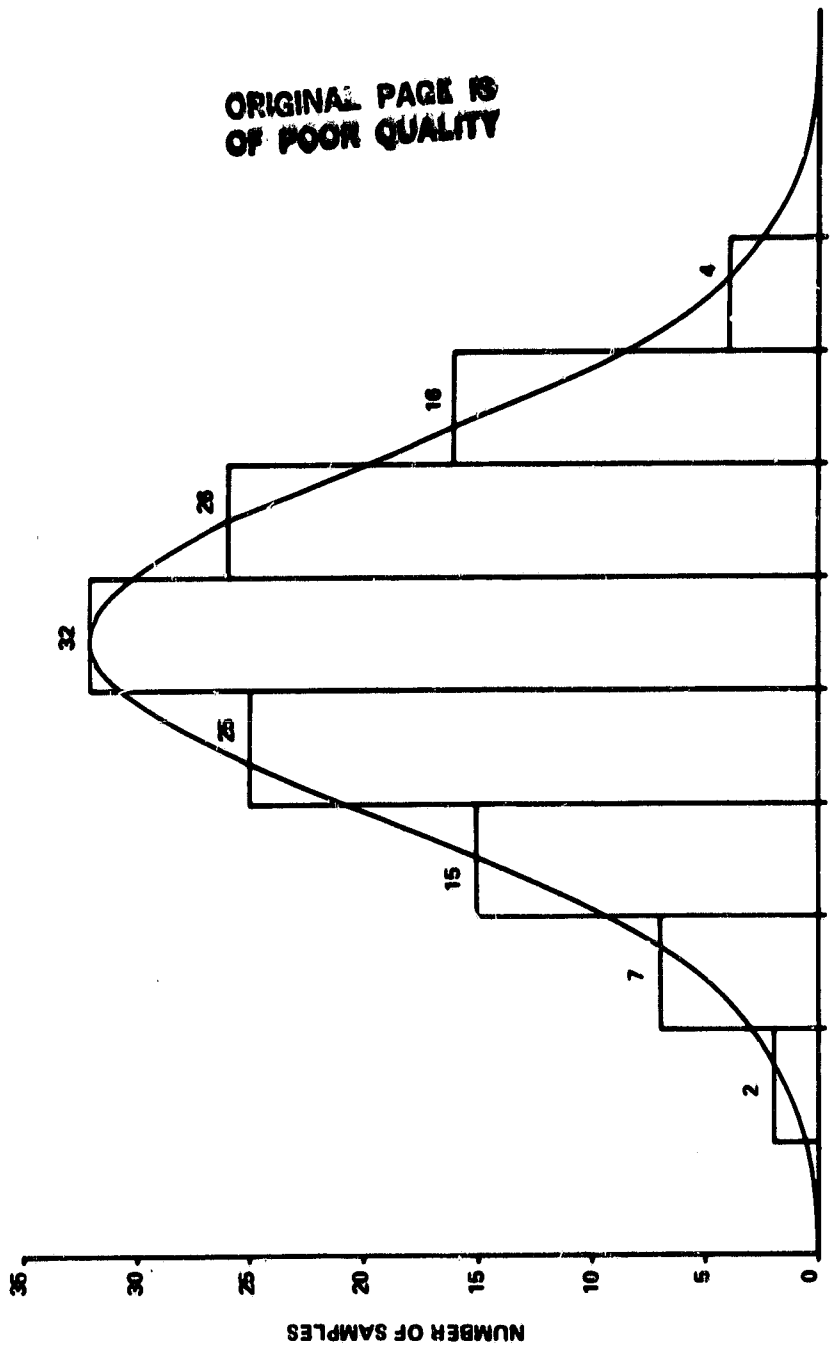


FIGURE 4.1. DISTRIBUTION OF SWH$_{GEOS}$ − SWH$_{BUOY}$

Buoy Office (Steele, 1980) estimates that they probably over-corrected for noise, especially for low sea state and that the over-correction would tend to make the buoys measure 15% low. This is consistent with the mean difference given in Equation (4.13).

The mean difference of the entire population can be computed to the 95% confidence limits by employing the t-distribution. These limits are

$$\bar{D} - \frac{t_{.975} S_D}{[n]^{1/2}} \leq \mu_D \leq D + \frac{t_{.975} S_D}{[n]^{1/2}} \qquad (4.14)$$

From the standard t-distribution tables,

$$t_{.975} = 1.980 \qquad (4.15)$$

for n = 123. Substituting Equations (4.1), (4.13) and (4.15) into Equation (4.14) yields

$$0.32 \leq \mu_D \leq 0.50 \text{ m} \qquad (4.16)$$

Therefore, based upon the assumption of independence between the altimeter estimates and the buoy measurements of significant waveheight, the 3-sigma edit criterion and the sample population of 125 differences, there is a 95% probability that the value of $\mu_D$ for the entire population of GEOS-3 passes lies between 0.32 m and 0.50 m.

As was the case with $\sigma_G$, the value of the mean differ-

ence for the population can be made to decrease by changing the edit criterion. It is not, however, a function of the estimated buoy standard deviation $\sigma_B$ . Although the magnitude of the mean difference cannot be precisely determined from this data set, that any mean difference is present is, in itself, an important result. Furthermore, as was pointed out earlier in this section, the mean difference could be entirely accounted for by the NDBO overcorrection for noise.

Two points should be cited here in connection with the mean difference. First, the altimeter significant waveheight estimate was calibrated by setting the smallest expected value of the significant waveheight algorithm to zero. This calibration is subject to error and could easily account for a small bias between the two estimates.

Second, the data which account for most of the mean difference are the data where significant waveheight is small. This is due to the previously mentioned algebraic sensitivity of the altimeter estimation algorithm for near-calm seas and to the fact that the magnitude of low sea states is often smaller than the precision of the buoys. This is readily seen by examining Table 4.1.

## 4.3 Linear Regression

Since the GEOS-3 significant waveheight estimate [illegible]

NOAA buoy significant waveheight measurement constitute two independent determinations of the same observable quantity, a linear regression analysis may be performed upon the two sets of data to determine their agreement. If both the altimeter estimate and the buoy measurement were perfect, a positive correlation with unity magnitude would be expected. The degree to which the actual correlation coefficient differs from unity is a measure of relative errors of the two estimates.

For a set of paired data points $(x_i, y_i, i=1,2,3,\ldots,N)$, the line which best fits the data (in the sense of least squares) is given

$$y = mx + b \tag{4.17}$$

where $m$ is the slope of the line and $b$ is the y-intercept of the line with $m$ and $b$ given by

$$m = \frac{\sum_{i=1}^{N} x_i y_i}{N\sigma_x^2} - \bar{x}\,\bar{y} \tag{4.18}$$

$$b = \bar{y} - m\bar{x} \tag{4.19}$$

where $\bar{x}$ and $\bar{y}$ are the mean values of $x_i$ and $y_i$, respectively. The correlation coefficient $\gamma$ is given by

$$\gamma = \frac{m\sigma_x}{\sigma_y} \tag{4.20}$$

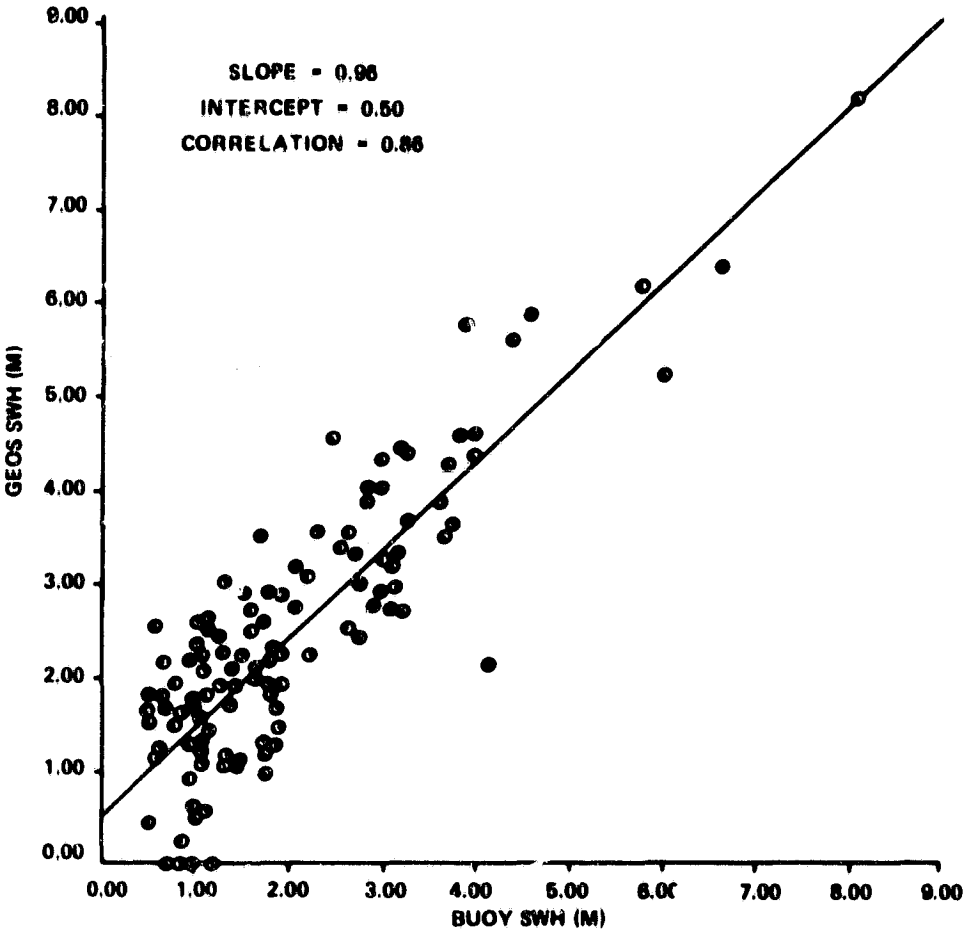


FIGURE 4.2. LINEAR REGRESSION WITH BUOY SWH AS INDEPENDENT VARIABLE

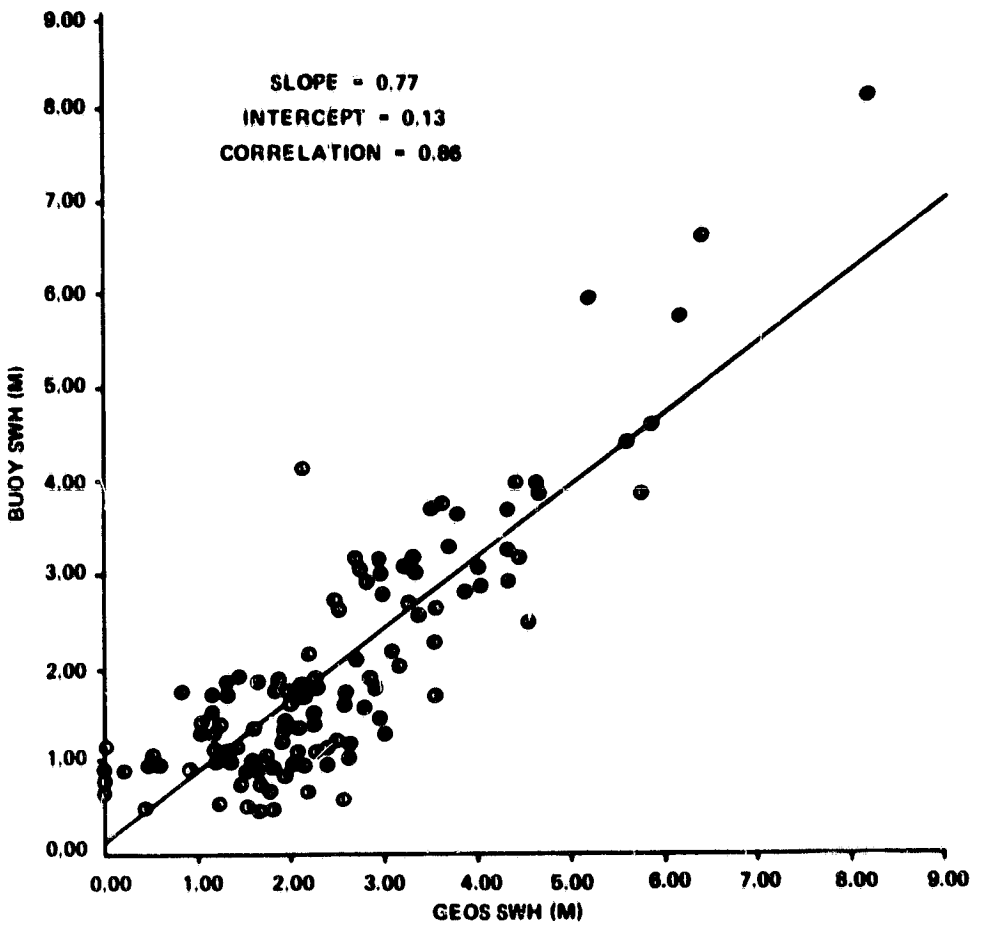


FIGURE 4.3. LINEAR REGRESSION WITH GEOS SWH AS INDEPENDENT VARIABLE

where $\sigma_x$ and $\sigma_y$ are given by

$$\sigma_x^2 = \frac{\sum_{i=1}^{N} x_i^2}{N} - \bar{x}^2 \qquad (4.21)$$

$$\sigma_y^2 = \frac{\sum_{i=1}^{N} y_i^2}{N} - \bar{y}^2 \qquad (4.22)$$

Additionally, the standard error of estimate, $S_E$, is computed from

$$S_E = \sigma_y [1 - \gamma^2]^{1/2} \qquad (4.23)$$

Figure 4.2 represents a linear regression analysis of the data presented in Table 4.1. The GEOS-3 significant waveheight estimate is the dependent variable, and the buoy significant waveheight measurement is the independent variable. Using the analysis presented above

$$m = 0.96 \qquad (4.24)$$

$$b = 0.50 \qquad (4.25)$$

$$\gamma = 0.86 \qquad (4.26)$$

$$S_E = 0.75 \qquad (4.27)$$

Similarly, Figure 4.3 represents a linear regression analysis of the data but with the altimeter significant waveheight estimate as the independent variable and the buoy significant waveheight measurement as the dependent variable. Under these conditions,

$$m = 0.77 \tag{4.28}$$

$$b = 0.13 \tag{4.29}$$

$$\gamma = 0.86 \tag{4.30}$$

$$S_E = 0.67 \tag{4.31}$$

The correlation coefficient given in Equations (4.26) and (4.30) indicate that the two data sets are significantly correlated, as would be expected. Although it is difficult to make any more than a qualitative assessment from the two linear regressions, it is important to remember that regression analysis assumes that the independent variable is without error. With this in mind and using the fact that the slope in Figure 4.2 is very close to unity and the slope in Figure 4.3 is slightly degraded, it might be inferred that the errors in the GEOS-3 significant waveheight estimates are slightly more prominent than the errors in the buoy significant waveheight measurements. Nevertheless, the important result of this analysis is the high correlation between the two data sets.

Figure 4.4 illustrates the difference between the altimeter estimate of significant waveheight and the buoy measurement of significant waveheight as a function of the distance from the point of closest approach to the buoy. Because the original data request made to the NOAA Data Buoy Office was based upon a 1/4 degree search area radius, there are more points with small PCA distance than with large PCA distance. Nevertheless, Figure 4.4 shows that the difference between the two estimates of significant waveheight is not a

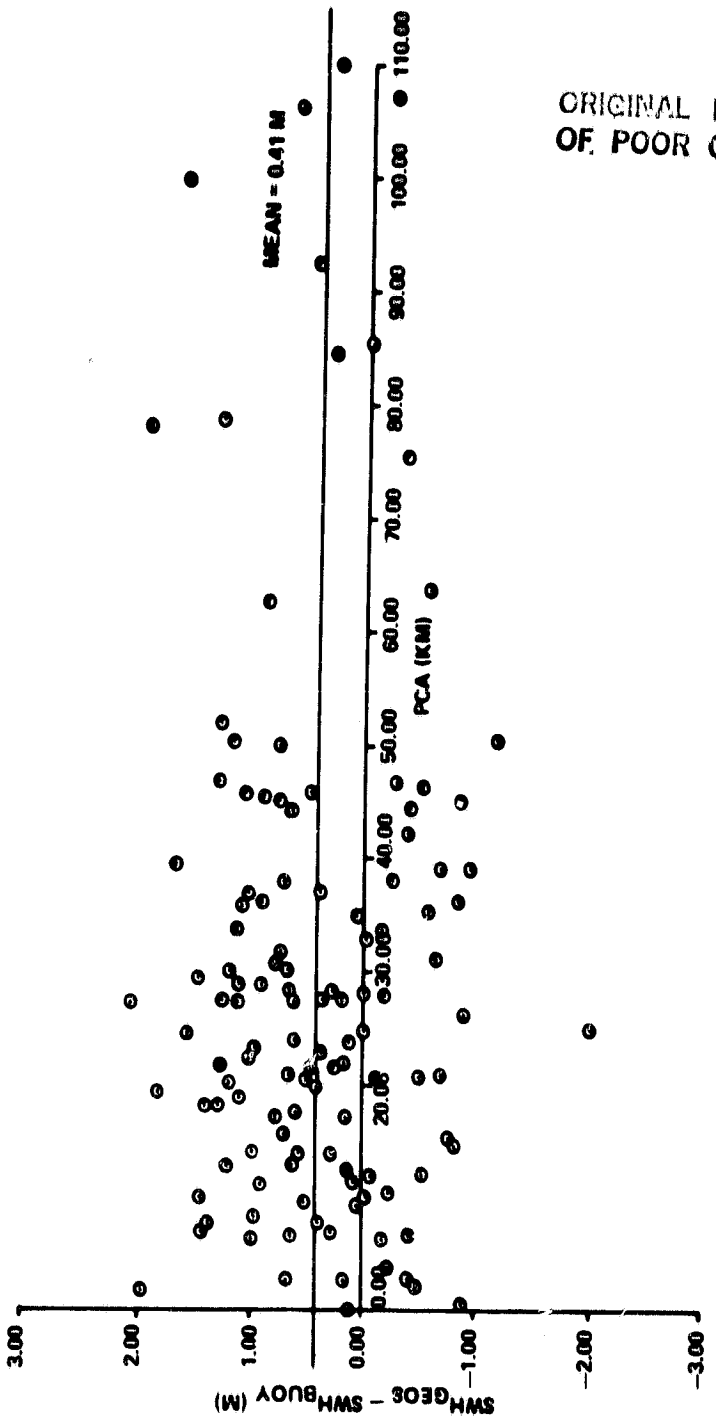


FIGURE 4.4. $SWH_{GEOS}-SWH_{BUOY}$ AS A FUNCTION OF PCA DISTANCE

function of PCA distance up to at least one equatorial degree (111 kilometers).

## 4.4 GOASEX Comparison

The Gulf of Alaska Seasat Experiment (GOASEX) was designed to aid in the determination of the accuracy of the Seasat geophysical parameters, including significant waveheight (Seasat Gulf of Alaska Workshop II Report, 1979). In that report, the significant waveheights from 17 ground track crossings of GEOS-3 and Seasat were compared and their statistics presented. For those 17 passes, the report found that the mean difference between the GEOS-3 real-time and the Seasat on-board estimates of significant waveheight was 59 cm. The GEOS-3 data used for that comparison was obtained from the GEOS-3 Near-Real-Time Data System (McMillan, 1978).

It should be noted that the GEOS-3 and Seasat data used in the comparison were not published in the report, but that only the statistics of that comparison were. For the purposes of verifying the results of that comparison, the data set was obtained from L. S. Fedor (1981) of the NOAA Environmental Research Laboratory, who served as chairman of both the GOASEX Altimeter Wind-Wave Panel and the GOASEX Sensor Intercomparison Panel. Examination of the data employed in the comparison led to the conclusion that the GEOS-3 data used had been improperly selected. The GEOS-3 project scientist, H. Ray Stanley (1981), concurred with that conclusion. The

proper GEOS-3 comparison data set is given in Table 4.3.

Analysis of the data in Table 4.3 yields a mean difference between the GEOS-3 real-time and the Seasat on-board determinations of significant waveheight of 24 cm, compared to a computed value of 59 cm published in the GOASEX report. (Note that the mean difference between the GEOS-3 estimate of significant waveheight and the Fedor Seasat estimate of significant waveheight is only 15 cm, compared to 51 cm published in the GOASEX report.) That report concluded that,

> The important point to note here is that all of the algorithms and the Seasat data seem to produce a lower value than the GEOS-3 estimates. This is consistent with other observations that the GEOS-3 waveheights tend to be slightly biased for the low waveheights encountered during this comparison, i.e., $1\ m \leq H\ 1/3 \leq 4\ m$.

The above statement implies that the GEOS-3 determination of significant waveheight was always smaller than the Seasat determination. As can be seen from Table 4.3, this is not the case.

Although the data set presented in Table 4.3 does indicate a mean bias between the GEOS-3 and Seasat significant waveheight estimates, the magnitude of that bias is considerably smaller than the bias reported in the GOASEX report. In fact, the bias is sufficiently small to be considered a confirmation of the accuracy of both determinations.

| DATE | SEASAT REV. | SEASAT TIME AT CROSSING | GEOS-3 REV. | GEOS-3 TIME AT CROSSING | LATITUDE AT CROSSING | LONGITUDE AT CROSSING | GEOS-3 SWH | SEASAT ONBOARD SWH | SEASAT FEDOR SWH |
|---|---|---|---|---|---|---|---|---|---|
| 780712 | 217 | 5:03:50 | 16824 | 3:33:24 | 55.62 | 214.42 | 1.99 | 1.90 | 1.98 |
| 780712 | 217 | 5:12:14 | 16825 | 6:47:25 | 28.47 | 194.20 | 2.74 | 2.84 | 2.39 |
| 780713 | 231 | 4:32:59 | 16838 | 3:17:51 | 54.58 | 222.02 | 2.47 | 1.90 | 1.89 |
| 780713 | 231 | 4:41:55 | 16839 | 6:31:24 | 25.54 | 201.61 | 2.52 | 2.57 | 2.24 |
| 780713 | 232 | 6:17:08 | 16839 | 6:37:18 | 43.47 | 186.84 | 2.18 | 1.20 | 1.44 |
| 780715 | 260 | 5:12:02 | 16867 | 4:28:29 | 52.11 | 211.91 | 2.12 | 1.26 | 1.34 |
| 780715 | 274 | 4:41:15 | 16881 | 4:12:51 | 50.79 | 219.45 | 2.02 | 1.71 | 1.76 |
| 780716 | 275 | 6:21:55 | 16882 | 5:54:36 | 50.68 | 194.26 | 0.91 | 1.01 | 1.47 |
| 780717 | 288 | 4:10:30 | 16895 | 3:57:14 | 49.38 | 226.97 | 2.58 | 1.39 | 1.67 |
| 780717 | 289 | 5:48:22 | 16895 | 4:00:39 | 57.83 | 211.38 | 2.18 | 1.00 | 1.11 |
| 780729 | 462 | 7:58:41 | 17067 | 7:44:31 | 53.03 | 186.17 | 1.67 | 1.52 | 1.67 |
| 780730 | 477 | 9:04:31 | 17080 | 5:52:55 | 63.36 | 185.55 | 0.70 | 1.30 | 1.49 |
| 780801 | 504 | 6:23:31 | 17108 | 5:19:26 | 57.70 | 218.42 | 1.75 | 1.27 | 1.75 |
| 780801 | 504 | 6:26:22 | 17109 | 6:57:39 | 49.01 | 208.78 | 2.22 | 1.82 | 1.91 |
| 780801 | 505 | 8:04:11 | 17109 | 7:01:08 | 57.60 | 193.19 | 1.03 | 1.04 | 1.29 |
| 780807 | 590 | 6:39:46 | 17194 | 7:09:35 | 51.00 | 213.52 | 3.45 | 3.71 | 3.19 |
| 780807 | 591 | 8:17:49 | 17194 | 7:12:51 | 58.75 | 197.75 | 0.00 | 0.97 | 1.27 |

Mean of GEOS - SEASAT (Onboard) = 24 cm
Mean of GEOS - SEASAT (Fedor) = 15 cm

Table 4.3 GEOS-3/SEASAT Comparison Statistics for Sub-Track Crossings

# CHAPTER 5

# GLOBAL ATLAS OF SWH DATA

## 5.1 Description of the SWH Global Atlas

During the GEOS-3 mission, altimeter data spanning 1500 hours were received and processed at Wallops Flight Center. Approximately 93% of the received data was intensive mode and, therefore, suitable for the calculation of significant waveheight. This large data set, representing approximately 8,000 GEOS-3 data segments, was used in its entirety in the generation of the significant waveheight global atlas which follows. All 8,000 intensive mode GEOS-3 passes were processed by a computer program which used the significant waveheight estimation algorithm and smoothing technique presented in Chapter 2. That program ran continuously for several months in order to accomplish this task. (It should be noted that less than 40% of the GEOS-3 data set was high data rate intensive mode data and, therefore, suitable for processing by the algorithms that use IRS data.)

Due to the vast size of the data set, it was necessary to partition the oceans into subdivisions where the statistics of the estimated significant waveheight could be accumulated, rather than the individual data points themselves. The size chosen for the sub-

divisions was a $1^{o}x1^{o}$ square. This was the smallest feasible partition size consistent with the storage capabilities of the computer software and the contouring limitations of the plot hardware.

The significant waveheight statistics for each of the $1^{o}$ x $1^{o}$ partitions were retained for a range of values:

1. SWH < 1.5 m
2. SWH < 2.5 m
3. SWH > 3.5 m
4. SWH > 6.0 m

These partition levels were suggested by the U. S. Navy Marine Climatic Atlas of the World (U. S. Navy, 1974). By using the same partition levels that were used in that publication, the results of the GEOS-3 estimates of significant waveheight could be compared with yet another independent source of significant waveheight data.

Upon examination of the statistics for the $1^{o}x1^{o}$ subdivisions, it was found that the number of data points per square varied widely from a high of several thousand in the GEOS-3 calibration area (bounded by Wallops Island, Bermuda, Merritt Island and Grand Turk) to a low of several dozen in the extreme latitudes of the southern Indian Ocean. The data sparseness in certain remote regions combined with the fact that the statistics of a $1^{o}x1^{o}$ subdi-

vision which contained only a few GEOS-3 data passes could be corrupted by a single pass of data taken during inclement weather conditions, suggested that the $1^{\circ}x1^{\circ}$ subdivisions should be smoothed. This was accomplished by combining the results of the $1^{\circ}x1^{\circ}$ subdivisions into larger subdivisions.

Several smoothing sizes were examined, including $3^{\circ}x3^{\circ}$, $5^{\circ}x5^{\circ}$, $7^{\circ}x7^{\circ}$ and $9^{\circ}x9^{\circ}$. In each of these cases, all the $1^{\circ}x1^{\circ}$ subdivisions in the smoothing area were averaged without weighting. After inspection of the smoothed results, the $7^{\circ}x7^{\circ}$ smoothing area was chosen since it removed the spurious points without eliminating the fine detail near coastal zones. Accordingly, the contour levels which follow for a given latitude and longitude, $\bar{\phi}$ and $\bar{\lambda}$, respectively, contain data within the $7^{\circ}x7^{\circ}$ square given by

$$\phi - 3\ 1/2 \leq \bar{\phi} \leq \phi + 3\ 1/2 \tag{5.1}$$

$$\lambda - 3\ 1/2 \leq \bar{\lambda} \leq \lambda + 3\ 1/2 \tag{5.2}$$

In addition to the four significant waveheight partition levels defined above, it was necessary to represent the temporal trends of the significant waveheight data. Therefore, the contour maps which follow are segmented in time as follows:

1. December through February

2. March through May



C-2

3. June through August

4. September through November

5. Entire GEOS-3 mission (April, 1975, to December, 1978)

The first four divisions correspond to the four seasons and show global trends in the significant waveheight data on an annual basis. All contour maps contain isopleths of 0-10%, 11-30%, 31-50%, 51-70%, 71-90% and 91-100%.

The GEOS-3 significant waveheight global atlas is presented in Vol. II, Figures A.1 to A.20. It must be pointed out that the atlas presented here is "global" in the sense that data have been compiled from nearly all parts of the world. However, there are certain areas of the atlas which contain no contour designation. These areas are due to gaps in the data or to holes in the telemetry coverage for that particular season. Additionally, since the inclination of GEOS-3 was 115°, no data were obtained outside the region $-65^{\circ} < \phi < +65^{\circ}$.

## 5.2 Comparison with the Navy Climatic Atlas

The comparison between the GEOS-3 derived significant waveheight contour maps and the U. S. Navy Climatic Atlas (U. S. Navy, 1974) contour maps is presented here. In particular, the differences between the two sources of significant waveheight for

the northern Atlantic Ocean will be analyzed because both sources are derived from a larger data set in that region and, therefore, are presumably more accurate in that region.

Each of the northern Atlantic Ocean contour maps was compared with the significant waveheight contour maps published in the U. S. Navy atlas. That atlas contains contour maps for each month rather than each season so that a direct comparison is difficult. The analysis was accomplished by examining the U. S. Navy contour map for the middle month in the seasonal GEOS-3 contour map and noting any significant differences between the first and last month and the middle month. For example, the GEOS-3 contour maps for March through May (Vol. II, Fig. A.5 through A.8) were compared with the U. S. Navy Climatic Atlas contour maps for April, and any significant differences between the March and April and the April and May contour maps in the U. S. Navy publication were noted.

To illustrate the method by which the two atlases were compared, examine Figure 5.1, which is a reproduction of one of the contour maps from the U. S. Navy atlas. Unfortunately, the U. S. Navy contour maps were drawn in different colors, which were not able to be reproduced in this investigation. However, from examination of Figure 5.1 in the region lying within latitudes $10^{o}$ to $20^{o}$ North and longitudes $60^{o}$ to $70^{o}$ West, it is apparent that the U. S. Navy atlas estimates that significant waveheight is less than 1.5 meters 50% to 60% of the time in the month of January. The December

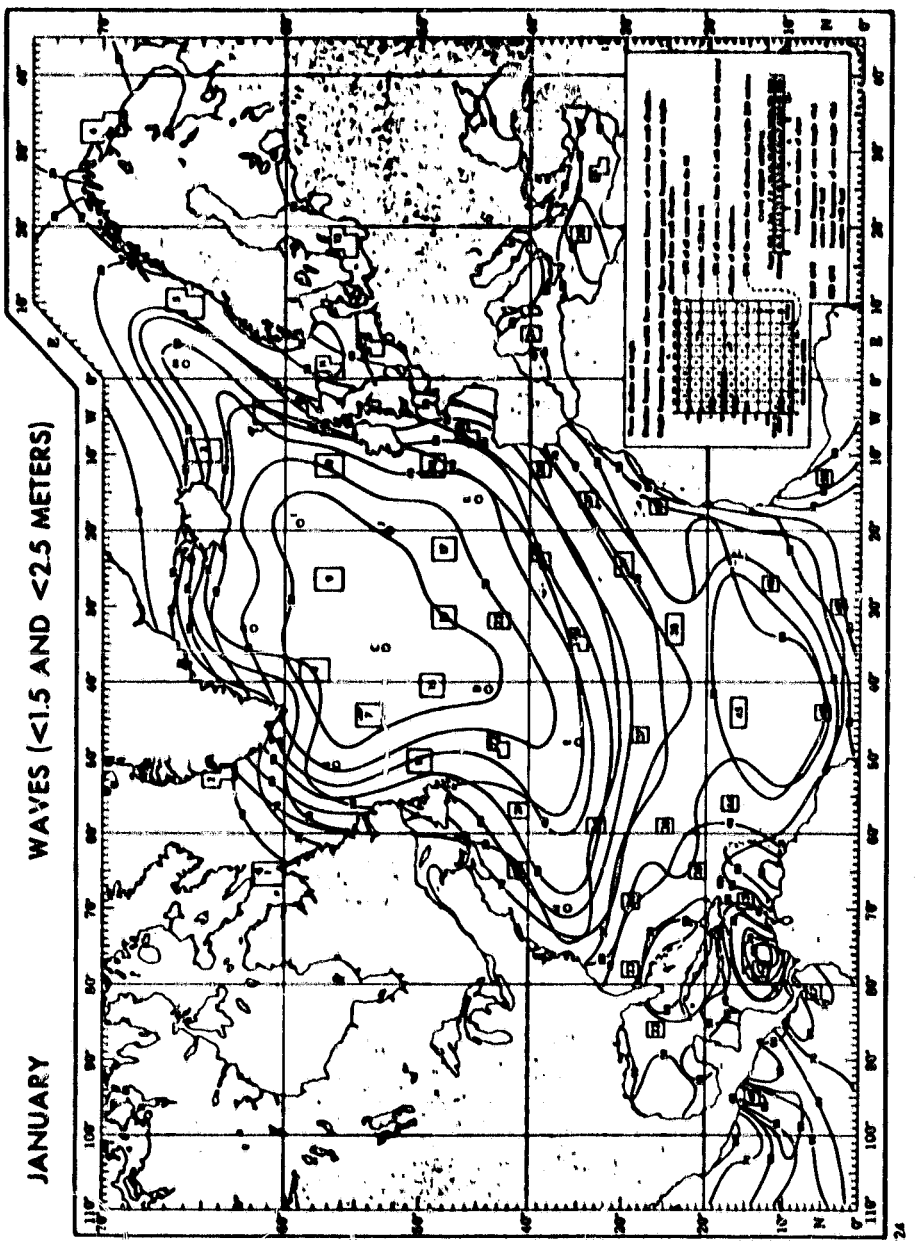


FIGURE 5.1. U. S. NAVY ATLAS CONTOUR MAP OF SWH < 1.5 AND SWH < 2.5 FOR JANUARY

and February contour maps in the U. S. Navy atlas are similar for this area. Volumn II, Fig. A.1, however, indicates that the altimeter estimates of significant waveheight in this region were less than 1.5 meters only 10% to 30% of the time.

5.2.1 December through February Comparison

The GEOS-3 significant waveheight contour maps for the months of December through February (Vol. II, Fig. A.1 through A.4) were compared with the corresponding U. S. Navy Climatic Atlas contours in the northern Atlantic Ocean, and the results of that comparison are as follows:

1. For significant waveheight less than 1.5 meters, the GEOS-3 contours show a lower percentage of data in the latitudes less than $30^{o}$ than do the U. S. Navy contours. The GEOS-3 estimates in the South Atlantic Bight indicate 10% to 30% of the data is less than 1.5 meters, while the Navy data indicates 30% to 50%. In the southern portion midway between the South American and African continents, the Navy data indicates 30% of the significant waveheight measurements are less than 1.5 meters, while the GEOS-3 data, though sparse, estimates that percentage at less than 10%.

2. For significant waveheight less than 2.5 meters, the Navy atlas again estimates a higher percentage of data near North America

than do the GEOS-3 estimates. In the South Atlantic Bight, the GEOS-3 data indicates 50% to 70% of the significant waveheight estimates are less than 2.5 meters. The Navy atlas estimates 80% to 90% of the waves are less than 2.5 meters in that region. The Gulf of Mexico and the Caribbean Sea contour maps agree satisfactorily.

3. For the contour maps of significant waveheight greater than 3.5 meters, the GEOS-3 estimates indicate a higher percentage of values above a latitude of $40^{\circ}$. The GEOS-3 estimates indicate that a large region of the northern Atlantic Ocean has significant waveheight greater than 3.5 meters for 70% to 90% of the time during these months. The Navy atlas estimates that percentage to be 50% to 60%. Similarly, the GEOS-3 contours indicate a region in the South Atlantic Bight and another region in the Gulf of Mexico where over 10% of the significant waveheight data is greater than 3.5 meters. The Navy atlas shows no such area.

4. The GEOS-3 contours of significant waveheight greater than 6.0 meters indicate a higher percentage of data in the extreme northern latitudes for these months than does the Navy atlas. The GEOS-3 contours show a large area where SWH exceeds 6.0 meters 30% to 50% of the time. The Navy atlas indicates SWH exceeding 6.0 meters only 15% of the time in that region.

Summarizing the November through February data, there are fewer calm sea state estimates for GEOS-3 than for the Navy data. Conversely, there are more high sea state estimates for GEOS-3 than appear in the U. S. Navy Climatic Atlas.

5.2.2 March through May Comparison

The results of the comparison in the northern Atlantic Ocean for the months of March through May (Vol. II, Fig. A.5 through A.8) are:

1. For significant waveheight less than 1.5 meters, the GEOS-3 data showed a much higher percentage of data in the mid northern latitudes, while finding a significantly smaller percentage of data in the southernmost latitudes of the northern Atlantic Ocean. The western coast of the African continent showed considerable discrepancy, with the GEOS-3 data indicating most of the data to be within the 10% to 30% range, while the Navy atlas found 60%, 70% and even 80% of the data to be less than 1.5 meters in some portions of that area. Both sources agreed rather well in the Caribbean, but the GEOS-3 data showed the percentage of significant waveheight data in the central Gulf of Mexico region to be 30% to 50% while the Navy atlas indicated 60% to 70%.

2. For significant waveheight less than 2.5 meters, the GEOS-3

data in the middle to northernmost latitudes indicated that SWH was less than 2.5 meters 10% to 30% of the time. The Navy atlas estimated that SWH was less than 2.5 meters 40% to 60% of the time in that region.

3. The GEOS-3 data indicated a large area in the extreme northern latitudes where over 50% and even over 70% of the data was greater than 3.5 meters. The Navy atlas showed only 30% of the data to be greater than 3.5 meters, except for March when 40% of the data exceeded 3.5 meters. All other portions of the northern Atlantic Ocean agreed rather well.

4. For significant waveheight greater than 6.0 meters, the Navy atlas showed about 5% in the northern extremities whereas the GEOS-3 contour map indicated a large area of 10% to 30%. No significant amounts of data were found to be greater than 6.0 meters in the southern part of the region for either source.

Summarizing the March through May data, the GEOS-3 estimates of significant waveheight indicate a higher percentage of high waves and a lower percentage of low waves in the mid to northern latitudes of the region. The southern latitudes of the region agree rather well. In the Caribbean and the Gulf of Mexico, the GEOS-3 estimates are considerably less calm than the results from the U. S. Navy Climatic Atlas.

### 5.2.3 June through August Comparison

The results of the comparison in the northern Atlantic Ocean for the months June through August (Vol. II, Fig. A.9 to A.12) are:

1. For significant waveheight less than 1.5 meters, the Navy atlas showed contour levels of 20% to 50% north of latitude 45°, while the GEOS-3 results indicated that percentage was in the range of 10% to 30%. Of even more significance was the South Atlantic Bight region. For this area, the GEOS-3 results indicated 30% to 50% of the data was less than 1.5 meters, while the Navy atlas indicated 70% to 80% was less than 1.5 meters. The Navy atlas also showed a higher percentage of calm seas in the Gulf of Mexico. Here, the Navy estimates that 70% to 80% of the significant waveheight estimates are less than 1.5 meters, while the GEOS-3 results indicate that percentage should be 50% to 70%.

2. For significant waveheight less than 2.5 meters, the two sources agree rather well in the mid-latitudes. In the extreme northern latitudes the GEOS-3 estimates indicate an area where 30% to 50% of the data is less than 2.5 meters, while the Navy contours show that portion of the area contains 70% to 80% of the significant waveheight measurements less than 2.5 meters. Similarly, in the South Atlantic Bight region, the Navy contours indicate over 90% of the data is less than 2.5 meters,

while the GEOS-3 data estimates 70% to 90% of the data to be in that range.

3. The GEOS-3 contours and the U. S. Navy contours agree well for the percentage of data greater than 3.5 meters and greater than 6.0 meters during these months.

Summarizing the June through August data, the percentage of GEOS-3 estimates of significant waveheight are lower than the percentage of Navy estimates of significant waveheight for low to calm seas during these months. The high seas contour levels are similar.

5.2.4 September through November Comparison

The results of the comparison in the northern Atlantic Ocean for the months of September through November (Vol. II, Fig. A.13 to A.16) are:

1. For significant waveheight less than 1.5 meters, the two sources compare rather favorably with the exception of the mid latitudes and the extreme northern latitudes. In the mid latitudes, the Navy estimates that 30% to 60% of the data is less than 1.5 meters, while the GEOS-3 data indicates that most of the offshore contours in this area are 10% to 30%. In the extreme northern latitudes, the GEOS-3 contours indicate less

than 10% of the data is less than 1.5 meters, while the Navy atlas indicates 10% to 30% of the data is less than 1.5 meters.

2. The GEOS-3 and Navy contour maps for significant waveheight less than 2.5 meters agree well in most areas. There is, however, a significant difference in the extreme northern latitudes. The U. S. Navy Climatic Atlas estimates as high as 80% of the data in this region to be less than 2.5 meters, while the GEOS-3 estimates indicate only 10% to 30% of the data has values of significant waveheight less than 2.5 meters.

3. The GEOS-3 contours of significant waveheight indicate that 50% to 70% of the data in the extreme northern latitudes was estimated to be greater than 3.5 meters. The U. S. Navy contours in the same region indicate only 30% to 40% of the data to be greater than 3.5 meters. The remainder of the Northern Atlantic Ocean contours of GEOS-3 data agreed well with the Navy contours. Additionally, the contours of significant waveheight greater than 6.0 meters agreed well throughout the entire area.

Summarizing the September through November data, the GEOS-3 estimates indicate a much lower percentage of high seas in the extreme northern latitudes than did the Navy atlas. The GEOS-3 data also indicated fewer calm seas off the U. S. coast than did the U. S. Navy Climatic Atlas.

## 5.3 Discussion of the Contour Comparisons

From the information presented in Sections 5.2.1 through 5.2.4, one overriding point is clear: there are significant differences between the U. S. Navy Climatic Atlas and the GEOS-3 significant waveheight atlas. This is an extremely important result which could have significant impact on such areas as ship routing and design of offshore construction. These GEOS-3 results have potential for providing an overall improvement in significant waveheight atlases, especially when combined with other sources to provide data for the poorly determined GEOS-3 regions.

The major differences between the two contour atlases can be summarized as follows:

1. The GEOS-3 contours indicate a significantly smaller percentage of calm seas in the lower latitudes.

2. The GEOS-3 contours in the extreme northern latitudes indicate a significantly higher percentage of high sea states.

3. The Navy contours indicate a higher percentage of significant waveheight measurements in the range of 2.5 to 3.5 meters.

It should be pointed out that since the GEOS-3 estimate has been proven to be accurate by comparison with buoy and Seasat data, the Navy contour maps should at least be scrutinized care-

fully. The differences between the two atlases could arise because of the error sources in each (sparse measurements in various regions, instrument errors, errors caused by human measurements, etc.) or because the GEOS-3 contour estimates are made up of only four years of significant waveheight data, whereas the Navy data has been compiled over decades.

C. L. Parsons, a NASA meteorologist at Wallops Flight Center who has published several papers on the GEOS-3 significant waveheight estimate, believes (1978) that these differences are not unexpected. The U. S. Navy data used in the extreme latitudes are quite sparse, especially during the winter months. Additionally, the Navy atlas, in its preface, states:

> Waveheights reported by most transient ships tend to be underestimated in comparison to those recorded by Ocean Weather Stations and dictated by the synoptic situation.

This is consistent with the conclusions stated earlier in this section that the U. S. Navy contour maps indicate a higher percentage of low sea states and a lower percentage of high sea states than do the GEOS-3 contour maps.

In Parsons (July, 1979), it is demonstrated that the GEOS-3 significant waveheight measurements agree better with wave recorder data than do measurements made by a human observer. Parsons (September, 1979) also points out that ships avoid high sea state areas where possible and shows storm tracks where GEOS-3 meas-

urements agreed well with ship measurements, but indicated that very few ship measurements were available within the most violent areas of the storms.

These factors, combined with the fact that all of the Navy data in the extreme latitudes come from human estimates made onboard transient ships, suggests that the GEOS-3 estimate would be higher in these regions. Parsons also believes (1978) that the GEOS-3 estimates contain fewer calm seas near the coastal regions of North America because of the numerical problems encountered by the altimeter estimation algorithm in regions of calm seas (see Section 2.5). H. Ray Stanley, the GEOS-3 project scientist, concurs in both of these conclusions.

# CHAPTER 6

## CONCLUSIONS AND RECOMMENDATIONS

An algorithm has been derived for computing ocean significant waveheight from the altimeter measurements of the GEOS-3 satellite. The altimeter-derived estimates appear to be accurate to about 50 cm, based upon a comparison of 125 statistically representative passes of GEOS-3 altimeter data with independent measurements of significant waveheight made by NOAA Data Buoy Office buoys. The algorithm appears to be valid for a variety of ocean conditions, since the GEOS-3 significant waveheight estimates and the buoy significant waveheight measurements agree quite well for both low and high sea states.

Analysis of the altimeter estimates and the buoy measurements of significant waveheight indicates that a mean bias of about 41 cm exists between the two determinations with the GEOS-3 estimates being higher. This is consistent with a 15% buoy overcorrection for noise. The bias could easily be eliminated by adjustment of the calm sea risetime parameter in the altimeter significant waveheight algorithm. However, because such a small difference is insignificant for all known applications and because a large amount of GEOS-3 data has been distributed with the calm sea risetime coef-

ficient used in this investigation, no changes were made to the algorithm used in the reduction and distribution of the data.

Linear regression analysis performed upon the GEOS-3 significant waveheight estimates and the NOAA buoy significant waveheight measurements indicate a high degree of correlation. Furthermore, the standard error of estimate was essentially unchanged when the GEOS-3 estimate was changed from the dependent variable to the independent variable. This analysis indicates that the relative accuracies of the altimeter estimates and the buoy measurements of significant waveheight are about the same.

The results presented in Chapter 4 clearly demonstrate the accuracy and the reliability of the SWH estimation algorithm derived in this investigation. Additionally, the design specification of $\pm$ 20% accuracy for 2.0 < SWH < 10 meters was met. Furthermore, because estimates can be computed in near-real-time, sigrificant waveheight measurements produced from satellite altimetry could have significant impact on ship routing, search and rescue operation, meteorological research, recreational activities and numerous other areas where quick and reliable sea state information is desired.

Although the correlation between the two determinations of significant waveheight has been demonstrated, additional investigation could lead to more specific information about the relationship of the GEOS-3 estimates to the buoy measurements. Since the origi-

nal set of buoy data ordered from the NOAA Data Buoy Office was based upon a 1/4 degree search area around the buoy and since it has been demonstrated that the search area could be made larger than one degree, the number of comparisons could be greatly enlarged from 125 if the buoy data search area was enlarged.

If a much larger set of buoy data was available, the relative accuracy of the altimeter estimates to the buoy measurements of significant waveheight could be studied more extensively. In particular, the buoy data could be separated by buoy type. In this way, not only could a more powerful statement be made about the accuracy of the GEOS-3 significant waveheight estimates, but the relative accuracies of the different types of buoys could be more accurately determined.

A data set consisting of 17 ground track crossings of GEOS-3 and Seasat was analyzed in an attempt to verify the GOASEX conclusion that there existed a mean bias between the two determinations of 59 cm. That analysis concluded that the mean bias was 24 cm.

A global atlas of significant waveheight contours was presented. This atlas, which contained 1500 hours of GEOS-3 data, took several months of computer time to compile. Contour maps were presented for the months December to February, March to May, June to August and September to November. Additionally, contour maps for

the composite of the entire GEOS-3 mission were presented.

The GEOS-3 contour maps were compared with the contour maps in the U. S. Navy Climatic Atlas and significant differences were discovered. That these two atlases differed substantially is an important result in itself and indicates the need for future study. In general, the GEOS-3 estimates of significant waveheight showed a higher percentage of high sea states and a lower percentage of low sea states than did the Navy estimates.

The obvious practicality of significant waveheight estimates made on a global, near-real-time basis from space is currently offset by the facts that only GEOS-3 and Seasat were equipped to make such estimates and that, due to onboard power constraints, the GEOS-3 altimeter was turned on and off at scheduled times. Since the on/off schedule was determined several weeks in advance, it was often difficult to obtain significant waveheight estimates at the time and place they were needed. Additionally, it is evident that a single satellite with altimeter measurements only at nadir will not supply the capability to produce real-time estimates of significant waveheight with global coverage. These shortcomings are yet further arguments for a series of satellites, equipped with altimeters which operate continuously. Such a series of satellites would provide global estimates of significant waveheight to the scientific, military and industrial communities.

# BIBLIOGRAPHY


Abramowitz, M. and I. A. Segun, Handbook of Mathematical Functions, Dover Publications, Inc., New York, New York, 1968.

Apel, J., Private communication to H. R. Stanley on sea state correlation distance, 1975.

Austin, H., Private communication on the use of historical SWH data for the prediction of structural stress, December, 1979.

Brown, G. S., "The Average Impulse Response of a Rough Surface and Its Applications," IEEE Trans. Antennas and Propagation, AP-25 (1), 1977.

Brown, G. S. and L. S. Miller, "Final Report for Task D Under Engineering Studies Related to the GEOS-C Radar Altimeter," NASA CR-137462, 1974.

Draper, N. R. and H. Smith, Applied Regression Analysis, John Wiley and Sons, Inc., New York, New York, 1975.

Fedor, L. S. and D. E. Barrick, "Measurements of Ocean Wave Heights With Satellite Radar Altimeters," EOS Trans. AGU, Vol. 59, 1978.

Fedor, L. S., T. W. Godbey, J. F. R. Gower, R. Guptill, G. S. Hayne, C. L. Rusenach and E. J. Walsh, "Satellite Altimeter Measurements of Sea State - An Algorithm Comparison," Journal of Geophysical Research, Vol. 84, No. B8, July, 1979.

Fedor, L. S., Private communication on the comparison of GEOS-3 and Seasat significant waveheight estimates during the Gulf of Alaska Seasat Experiment (GOASEX), February, 1981.

GEOS-C Mission Plan, NASA, TK-6340-001, Wallops Island, Virginia, 1974.

Gower, J. F. R., "Measurements of Ocean Surface Wave Height Using GEOS-3 Satellite Radar Altimeter Data," Remote Sensing Environment, Vol. 8, No. 4, December, 1979.

Hadsell, P. R., "Buoy Data Archiving Systems," Project Monitoring Branch, National Oceanographic Data Center, 1974.

Hammond, D. L., R. A. Mennella and E. J. Walsh, "Short Pulse Radar Used to Measure Sea Surface Wind Speed and SWH," IEEE Trans. of Antennas and Propagation, Vol. AP-25, No. 1, January, 1977.

Hayne, G. S. "Ocean Significant Waveheight Estimates from GEOS-3: Details of the Method," Annual Meeting of the American Geophysical Union, San Francisco, California, December, 1976.

Hayne, G. S., "Initial Development of a Method of Significant Waveheight Estimation for GEOS-3," NASA CR-141425, 1977.

Hayne, G. S., Private communication on the problems associated with the Godbey SWH estimation algorithm, November, 1980.

Hofmeister, E. L., B. N. Kenney, T. W. Godbey and R. J. Berg, "Data User's Handbook and Design Error Analysis, GEOS-C Radar Altimeter, Vol. 1," General Electric Co., May, 1976.

Hofmeister, E. L. and B. N. Keeney, "Comparison of GEOS-3 Radar Altimeter On-Orbit Performance with Ground Test Performance," Spring Meeting of the American Geophysical Union, Washington, D. C., June, 1977.

Huang, N. E. and S. R. Long, "An Experimental Study of the Surface Elevation Probability Distribution and Statistics of Wind-Generated Waves," J. Fluid Mechanics, Vol. 101, in press.

IEEE Journal of Oceanic Engineering, Vol. OE-5, No. 2, April, 1980.

Jackson, F. C., "The Reflection of Impulses from a Nonlinear Random Sea," GSFC X-946-79-10, March, 1979.

Leitao, C. D. and C. L. Purdy, "Wallops GEOS-C Altimeter Preprocessing Report," NASA TM X-69357, May, 1975.

Lerch, F. J., R. P. Belott, S. M. Klosko and E. M. Lithowski, "Laser Reference Orbits and Altimeter Validation for GEOS-3," Marine Geodesy Symposium, Miami, Florida, September, 1978.

McMillan, J. D., "GEOS-3 Altimeter Preprocessing Documentation and Analyses," NASA Contract NAS6-2639, November, 1975.

McMillan, J. D. and N. A. Roy, "A Comparison of GEOS-3 H-1/3 Data with National Buoy Data," GEOS-3 Final Investigators' Meeting, New Orleans, Louisiana, November, 1977.

McMillan, J. D., "GEOS-3 Near-Real-Time Significant Waveheight and Wind Speed Data System," NASA Wallops Flight Center (unnumbered), March, 1978.

McMillan, J. D., D. W. Hancock and R. G. Forsythe, "NOSS Altimeter Algorithm Freeze Report," in press, October, 1980.

McMillan, J. D., Technical memorandum to G. Brown and H. R. Stanley on the largest computed pointing angle error for GEOS-3, November, 1980.

McMillan, J. D., "Catalog of Sea State and Wind Speed in the South Atlantic Bight," NASA CR-156872, December, 1980.

Neumann, G. and W. J. Pierson, Principles of Physical Oceanography, Prentice-Hall, Inc., Englewood Cliffs, New Jersey, 1966.

Parsons, C. L., "The Measurement of Significant Waveheight in Near-Real-Time Using the GEOS-3 Radar Altimeter," Annual Meeting of the American Geophysical Union, San Francisco, California, December, 1976.

Parsons, C. L., "An Assessment of GEOS-3 Significant Waveheight Measurements," National Ocean Survey Ocean Wave Climate Symposium, Washington, D. C., July, 1977.

Parsons, C. L., Private communication on the differences between GEOS-3 and Navy SWH contour maps, November, 1978.

Parsons, C. L., "GEOS-3 Waveheight Measurements: An Assessment During High Sea State Conditions in the North Atlantic," Journal of Geophysical Research, Vol. 84, No. B8, July, 1979.

Parsons, C. L., "On the Remote Detection of Swell by Satellite Radar Altimeter," Monthly Weather Review, Vol. 107, No. 9, September, 1979.

Remond, F. X., "Ocean Spectrum Measurement with Analog Filters," Proceedings of the 22nd International Instrumentation Symposium, San Diego, California, May, 1976.

Rufenach, C. L. and W. R. Alpers, "Measurement of Ocean Wave Heights Using the GEOS-3 Altimeter," Journal of Geophysical Research, Vol. 84, No. B8, July, 1979.

Seasat Gulf of Alaska Workshop II Report, JPL 622-107, October, 1979.

Stanley, H. R., "The GEOS-3 Project," Journal of Geophysical Research, Vol. 84, No. B8, July, 1979.

Stanley, H. R., Private communication on the effects of AGC fluctuation and associated SWH estimation error sources, November. 1980.

Stanley, H. R. and R. E. Dwyer, "NASA Wallops Flight Center GEOS-3 Altimeter Data Processing Report," NASA RP-1066, November, 1980.

Stanley, H. R., Private communication on the comparison of GEOS-3 and Seasat significant waveheight estimates during the Gulf of Alaska Seasat Experiment (GOASEX), February, 1981.

Steele, K., J. M. Hall and F. X. Remond, "Routine Measurements of Heave Displacement Spectra from Large Discuss Buoys in the Deep Ocean," Proceedings of the First Combined IEEE Conference on Engineering in the Ocean Environment and the Annual Meeting of the Marine Technology Society (OCEAN 75), September, 1975.

Steele, K., A. Trampus, P. Wolfgram and B. Graham, "An Operational High Resolution Wave Data Analyzer System for Buoys," Proceedings of the Second Annual Combined Conference Sponsored by the Marine Technology Society and the IEEE (Ocean 76), 1976.

Steele, K. and A. Johnson, "NDBO Wave Measurements," Office of Ocean Engineering, NOAA Data Buoy Office, 1977.

Steele, K., Private communication on the accuracy of buoy significant waveheight measurements, November, 1980.

U. S. Navy Marine Climatic Atlas of the World, Vol. 1, U. S. Navy, NAVAIR 50-1C-528, 1974.

Walsh, E. J., "Analysis of Experimental NRL Radar Altimeter Data," Radio Science, Vol. 9, Nos. 8 and 9, August-September, 1974.

Walsh, E. J., "Analysis of GEOS-3 Altimeter Data and Extraction of Ocean Waveheight and Dominant Wavelength," NASA TM-73281, March, 1979.

Walsh, E. J., "Extraction of Ocean Wave Height and Dominant Wavelength from GEOS-3 Altimeter Data," Journal of Geophysical Research, Vol. 84, No. B8, July, 1979.

Withee, G. W. and W. C. Blasingame, "Environmental Data Quality Estimates for Ocean Data Buoys," Proceedings of the Second Annual Combined Conference Sponsored by the Marine Technology and the IEEE (Oceans 76), 1976.

# APPENDIX A

# GLOBAL ATLAS OF GEOS-3 SIGNIFICANT WAVEHEIGHT DATA

| FIGURE | | PAGE |
|---|---|---|
| A.1 | December Through February - Percent Significant Waveheight < 1.5 Meters | 1 |
| A.2 | December Through February - Percent Significant Waveheight < 2.5 Meters | 2 |
| A.3 | December Through February - Percent Significant Waveheight > 3.5 Meters | 3 |
| A.4 | December Through February - Percent Significant Waveheight >6.0 Meters | 4 |
| A.5 | March Through May - Percent Significant Waveheight < 1.5 Meters | 5 |
| A.6 | March Through May - Percent Significant Waveheight < 2.5 Meters | 6 |
| A.7 | March Through May - Percent Significant Waveheight > 3.5 Meters | 7 |
| A.8 | March Through May - Percent Significant Waveheight > 6.0 Meters | 8 |
| A.9 | June Through August - Percent Significant Waveheight < 1.5 Meters | 9 |
| A.10 | June Through August - Percent Significant Waveheight < 2.5 Meters | 10 |
| A.11 | June Through August - Percent Significant Waveheight > 3.5 Meters | 11 |
| A.12 | June Through August - Percent Significant Waveheight > 6.0 Meters | 12 |
| A.13 | September Through November - Percent Significant Waveheight < 1.5 Meters | 13 |
| A.14 | September Through November - Percent Significant Waveheight < 2.5 Meters | 14 |
| A.15 | September Through November - Percent Significant Waveheight > 3.5 Meters | 15 |
| A.16 | September Through November - Percent Significant Waveheight > 6.0 Meters | 16 |

FIGURE PAGE

A.17 Entire Mission - Percent Significant Waveheight < 1.5 Meters . . . . . 17

A.18 Entire Mission - Percent Significant Waveheight < 2.5 Meters . . . . . 18

A.19 Entire Mission - Percent Significant Waveheight > 3.5 Meters . . . . . 19

A.20 Entire Mission - Percent Significant Waveheight > 6.0 Meters . . . . . 20

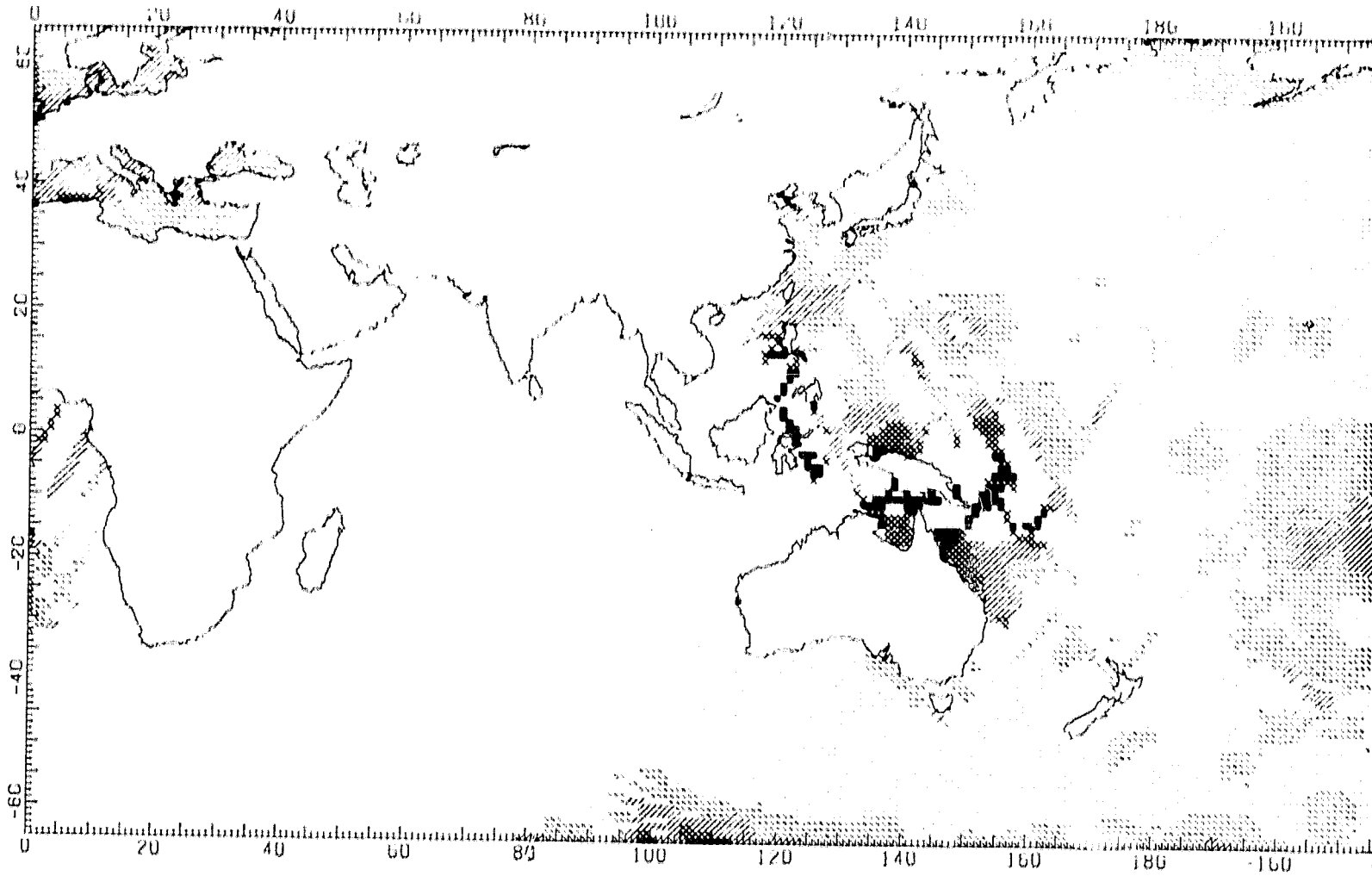

FOLDOUT FRAME J

ORIGINAL PAGE IS
OF POOR QUALITY

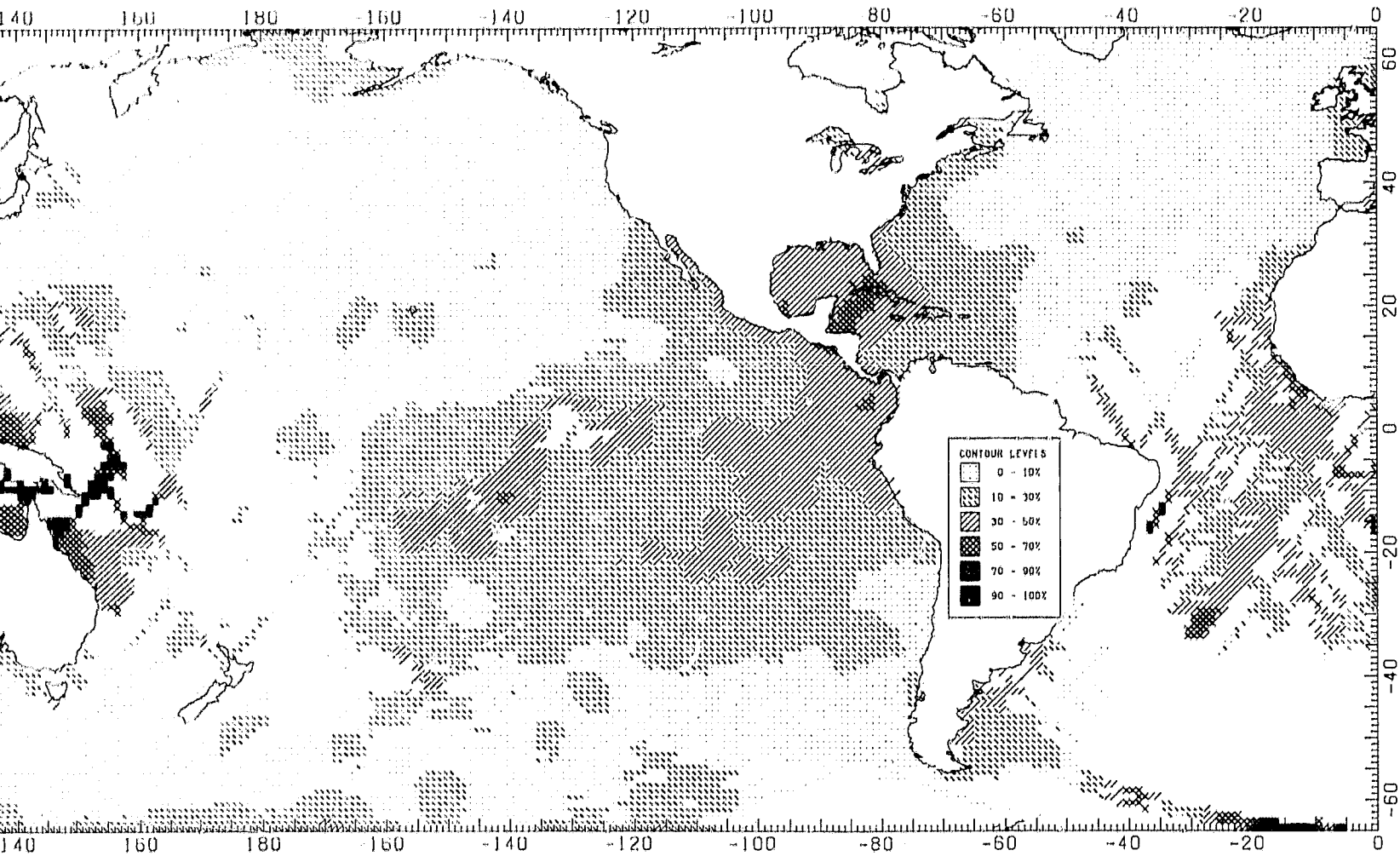


A.1 December Through February - Percent Significant Waveheight < 1.5 Meters

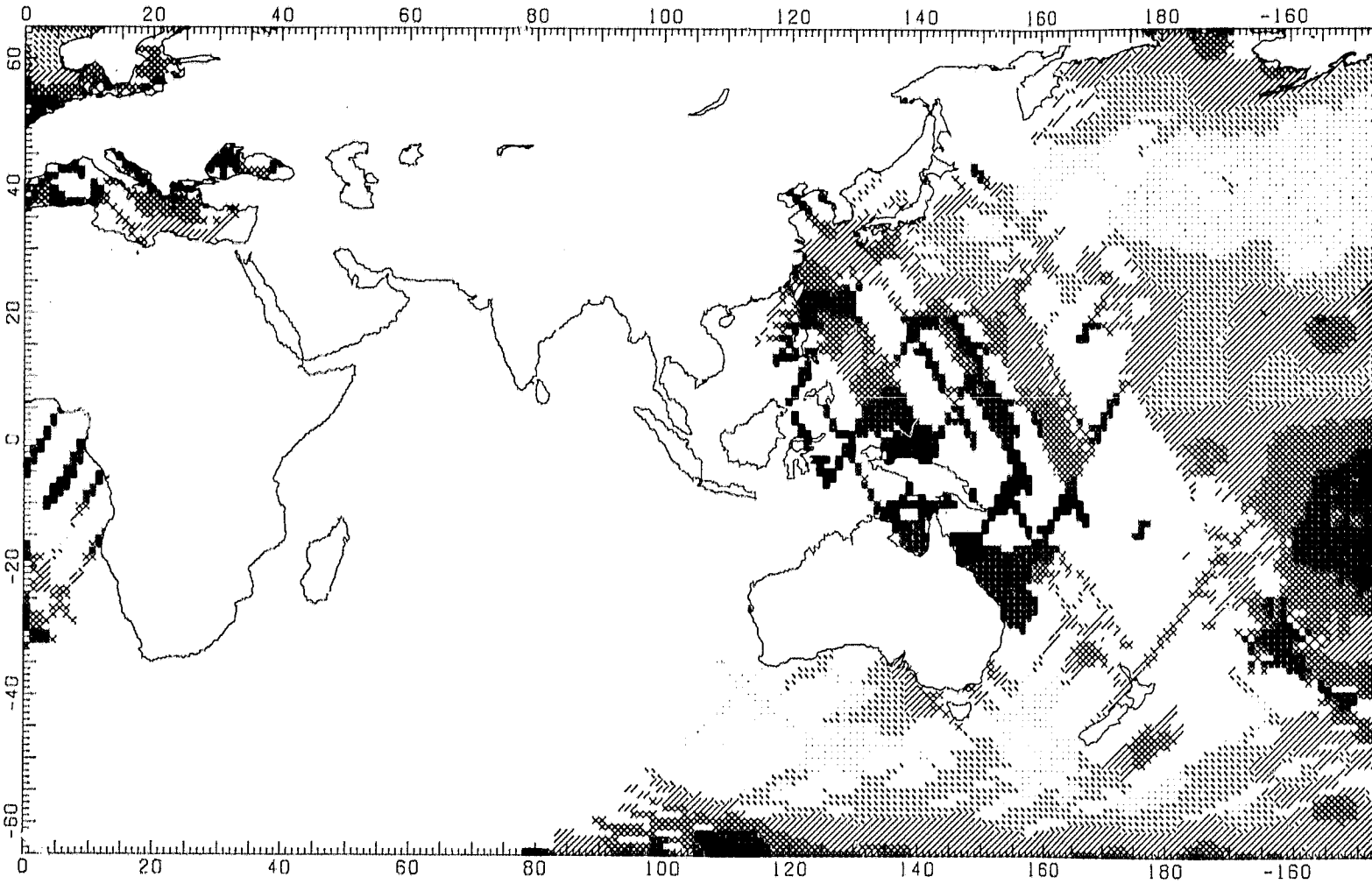

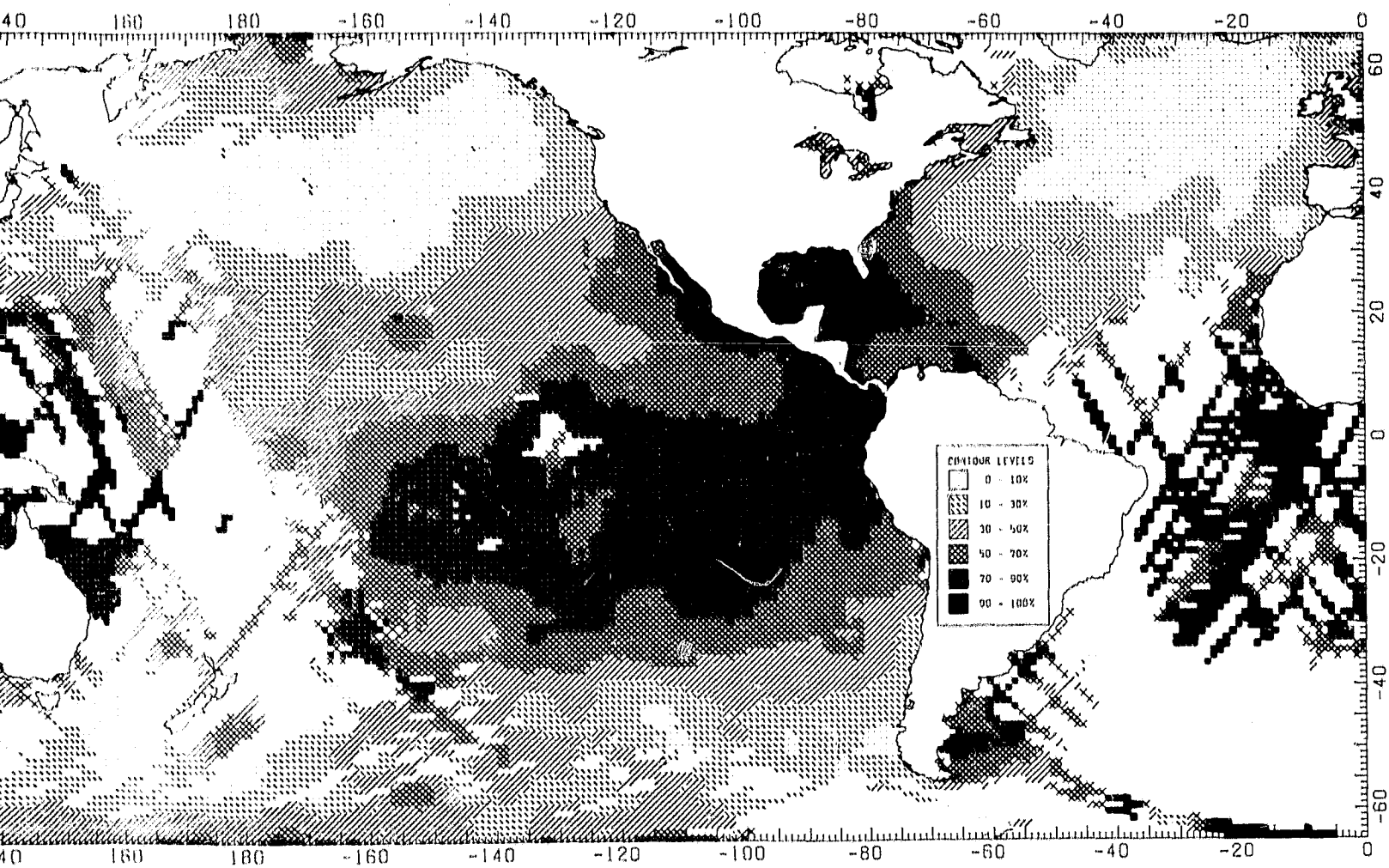




2

A.2 December Through February - Percent Significant Waveheight < 2.5 Meters

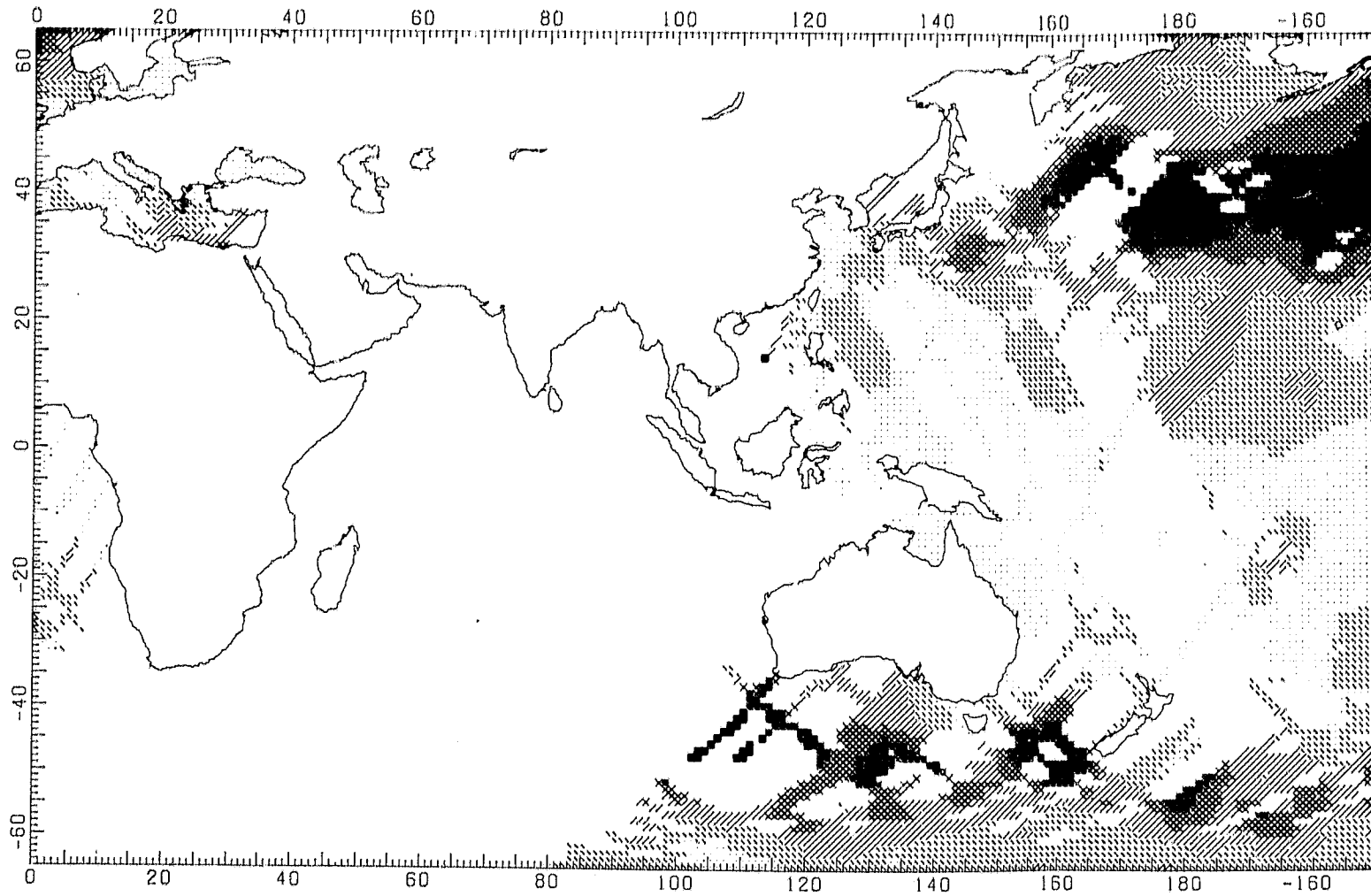


FOLDOUT FRAME

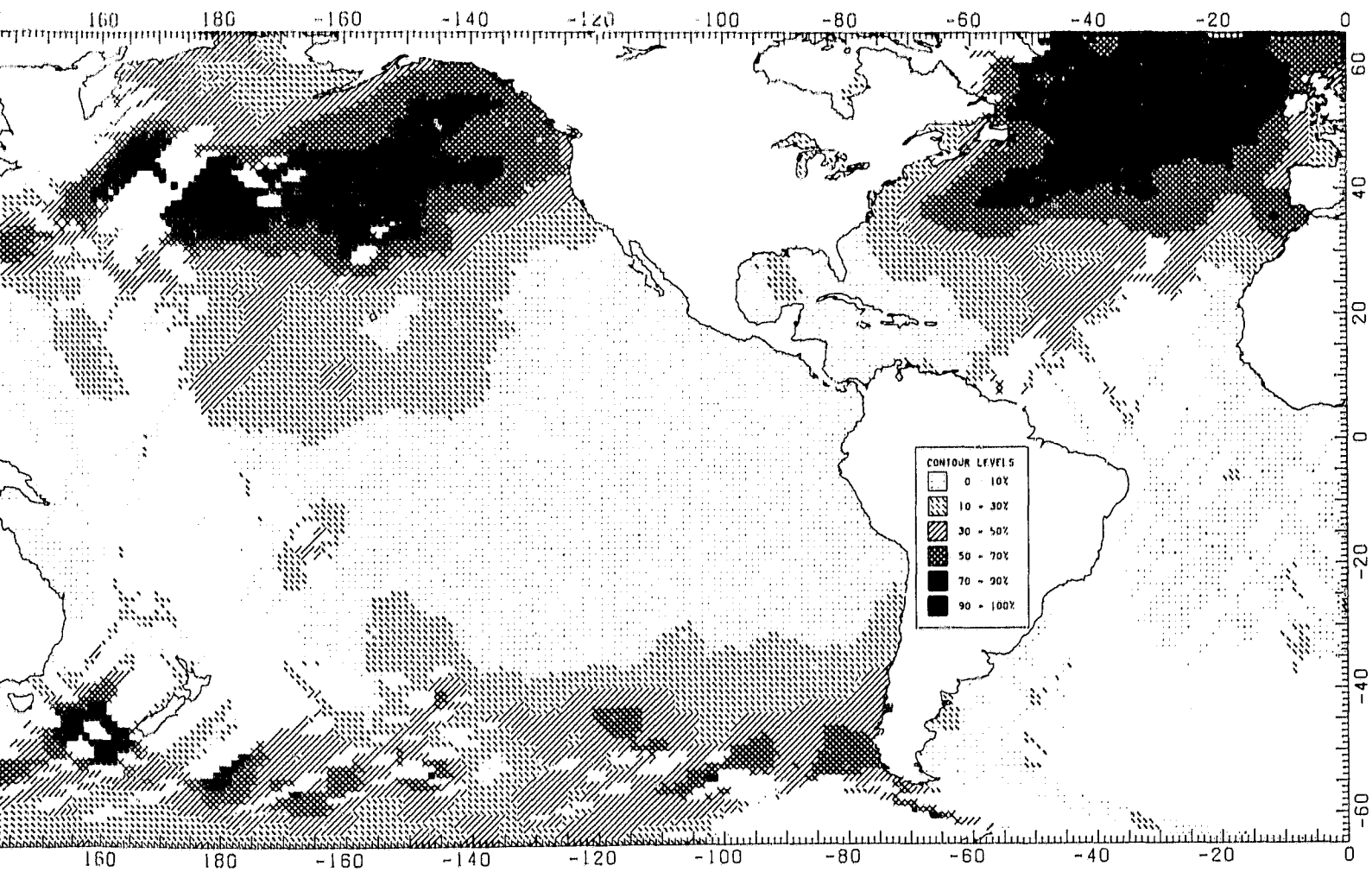


FOLDOUT FRAME 2

ORIGINAL PAGE IS
OF POOR QUALITY

A.3 December Through February - Percent Significant Waveheight > 3.5 Meters

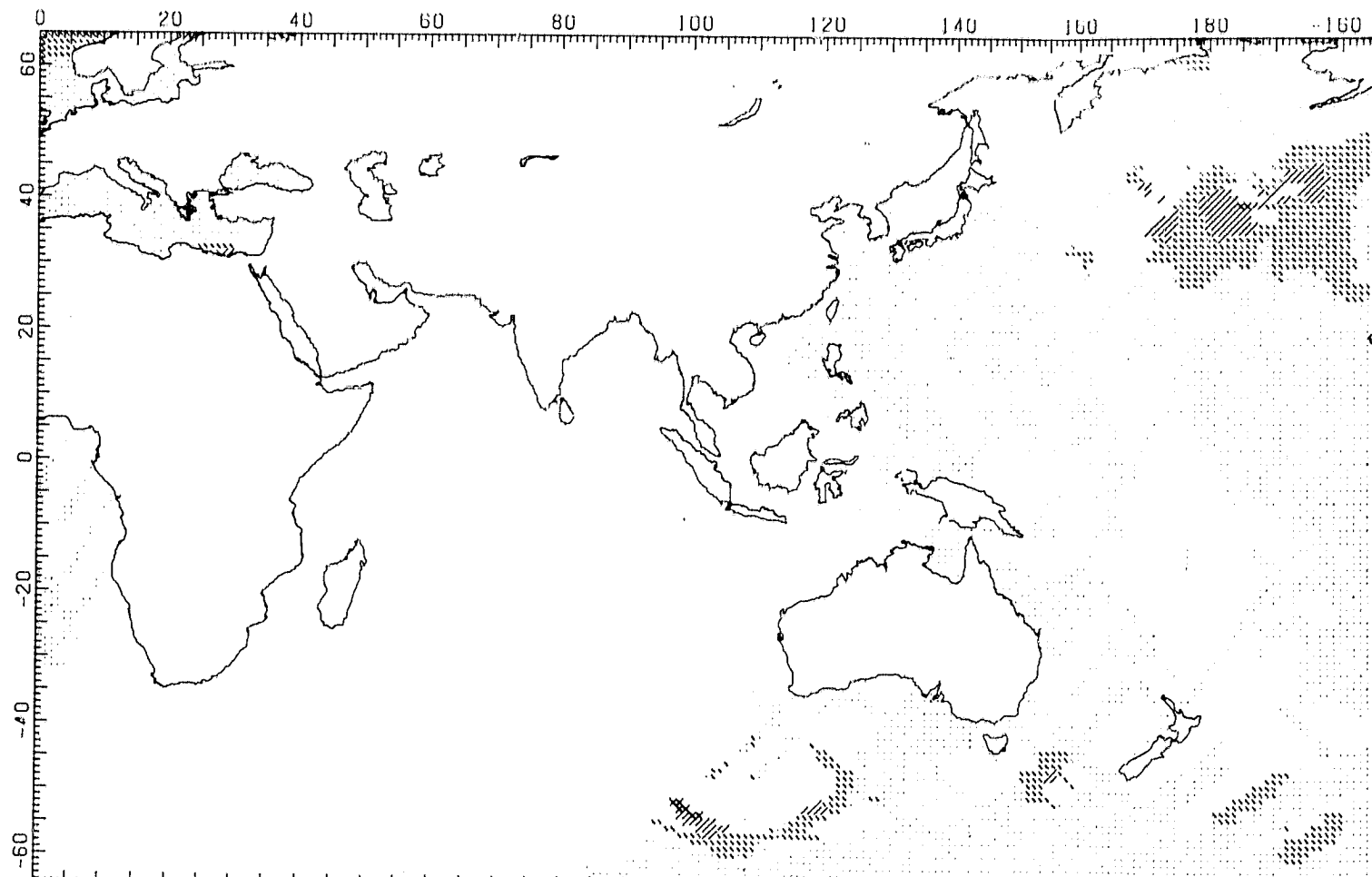

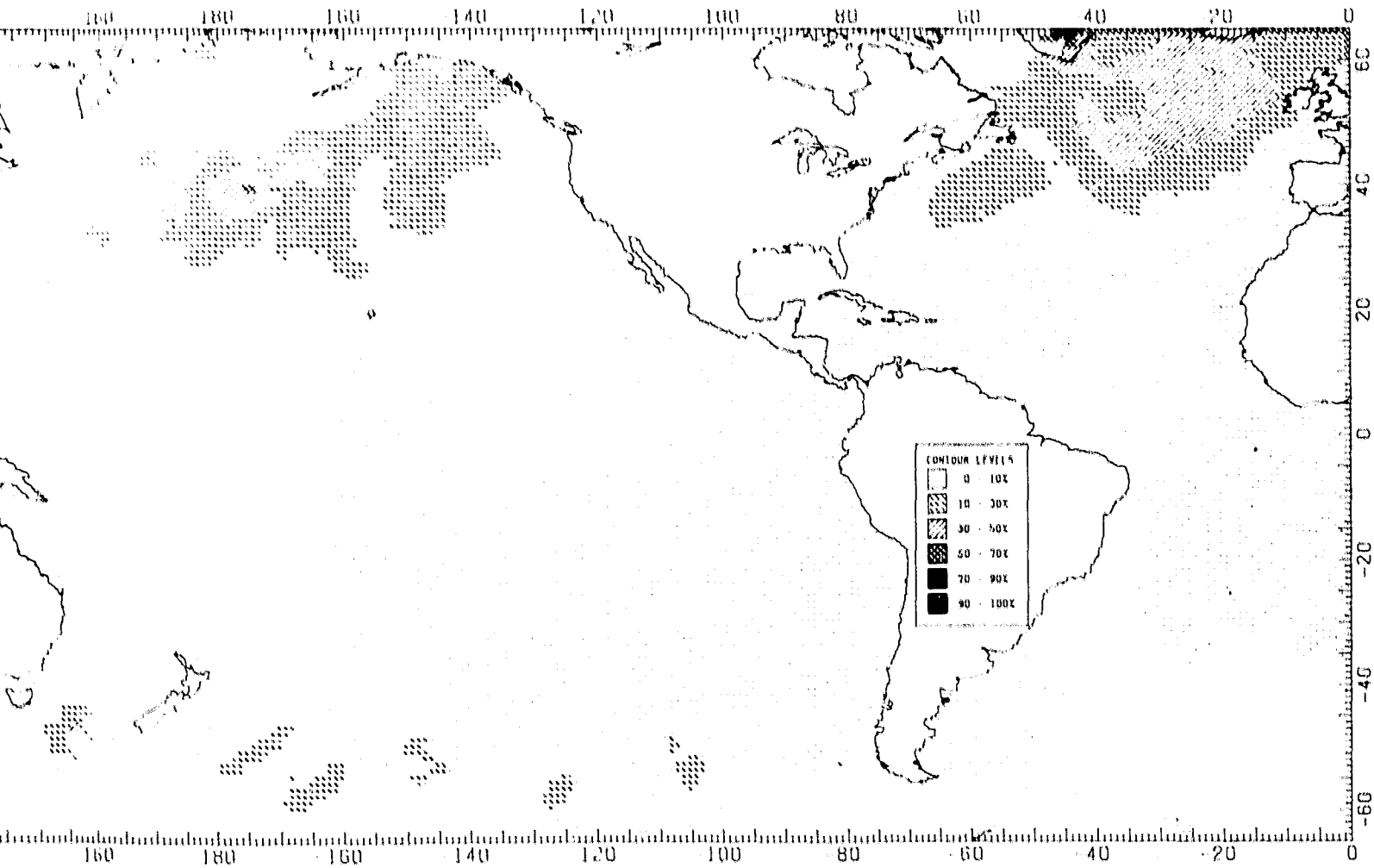


ORIGINAL PAGE IS
OF POOR QUALITY

FOLDOUT FRAME 9

A.4 December Through February - Percent Significant Waveheight > 6.0 Meters

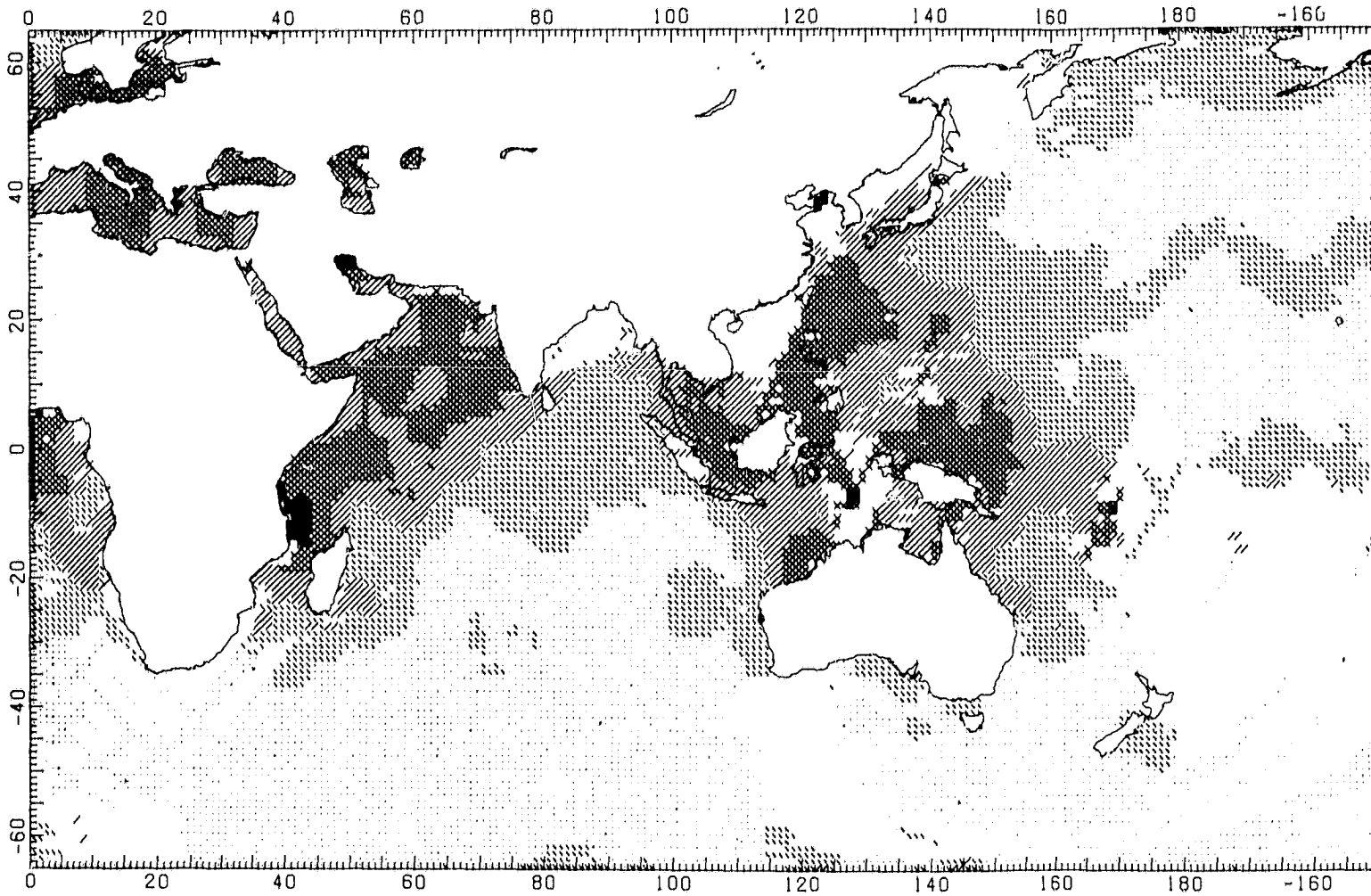




OF POOR QUALITY

FOLDOUT FRAME

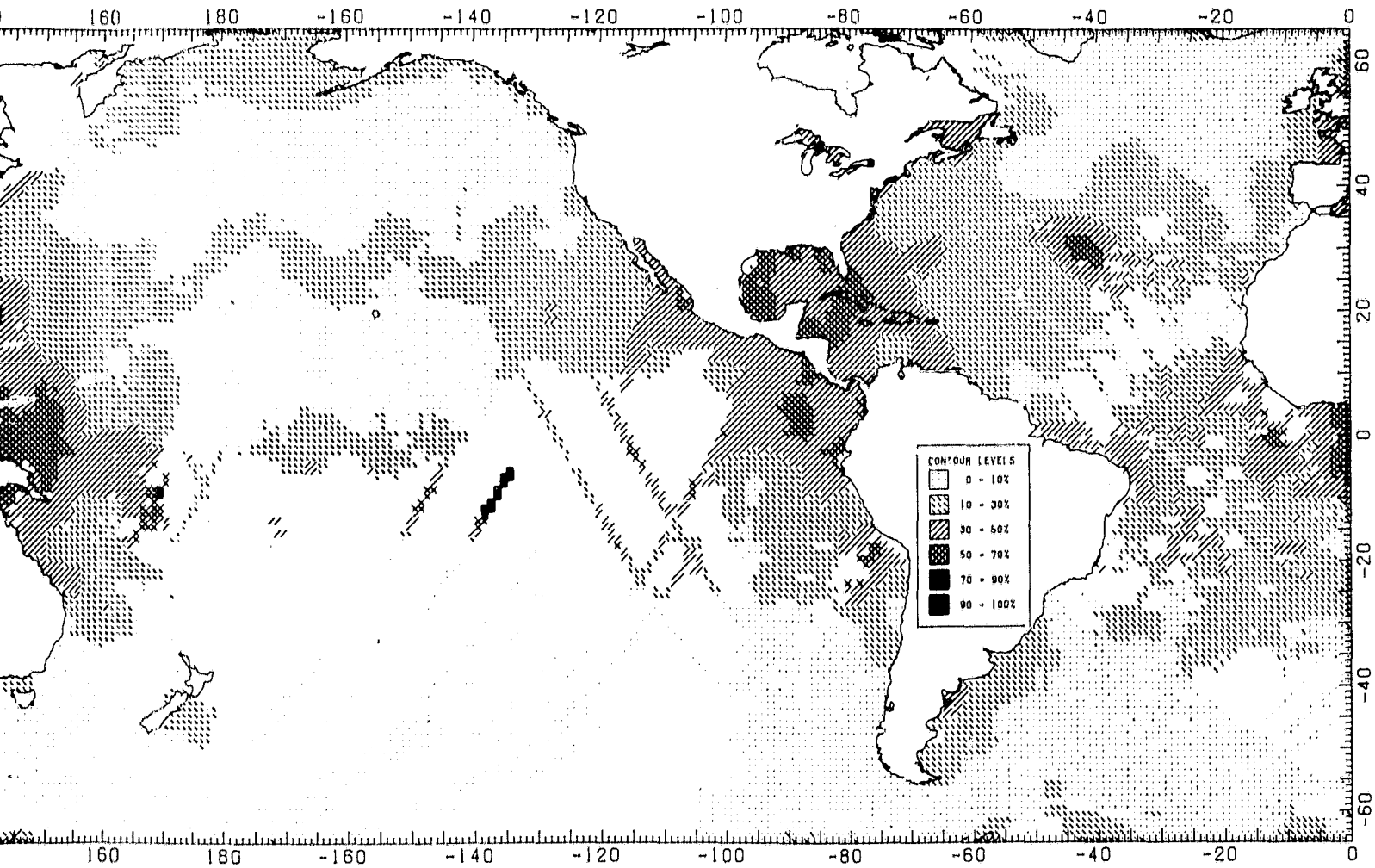






A.5 March Through May - Percent Significant Waveheight < 1.5 Meters

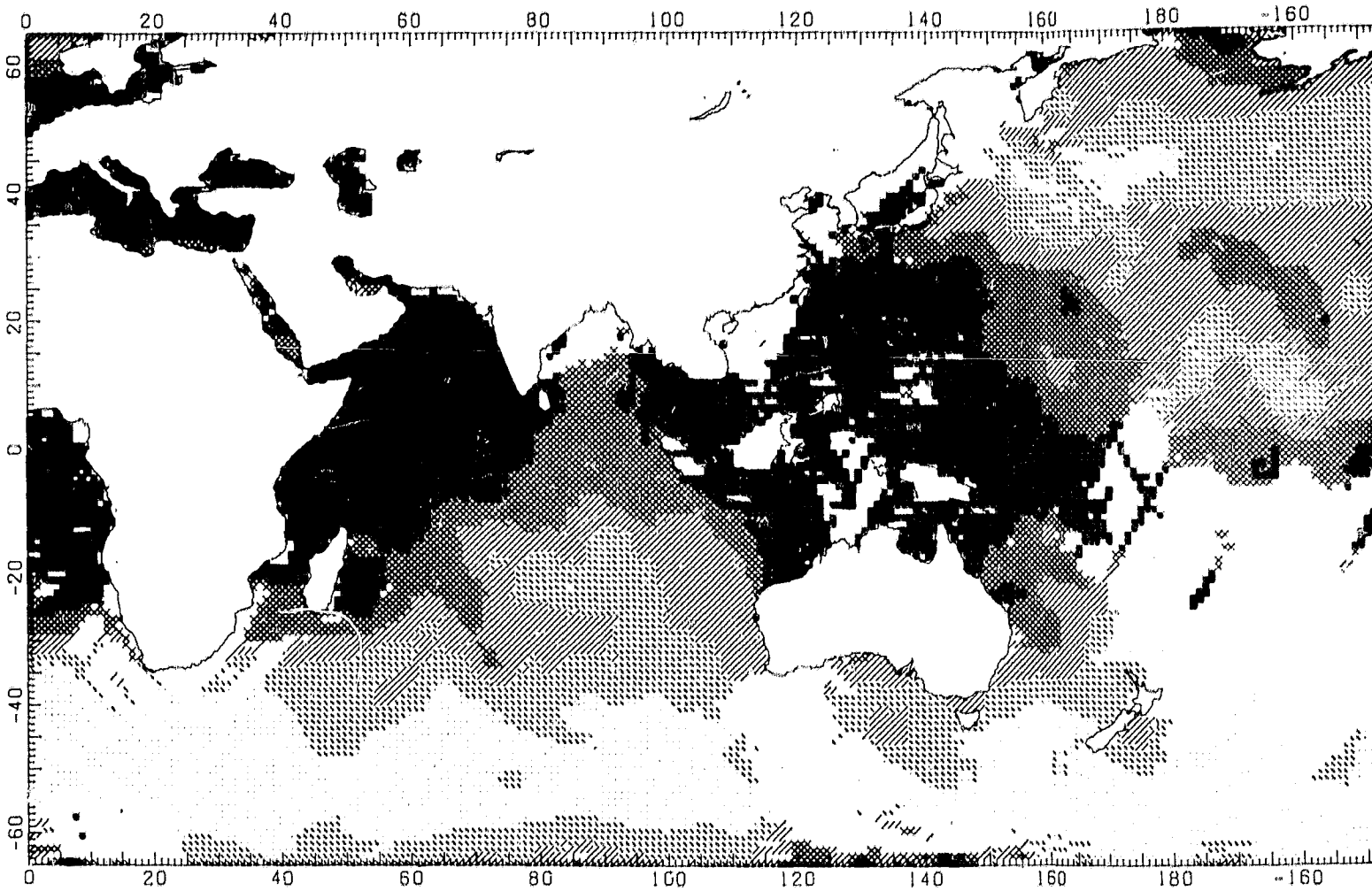

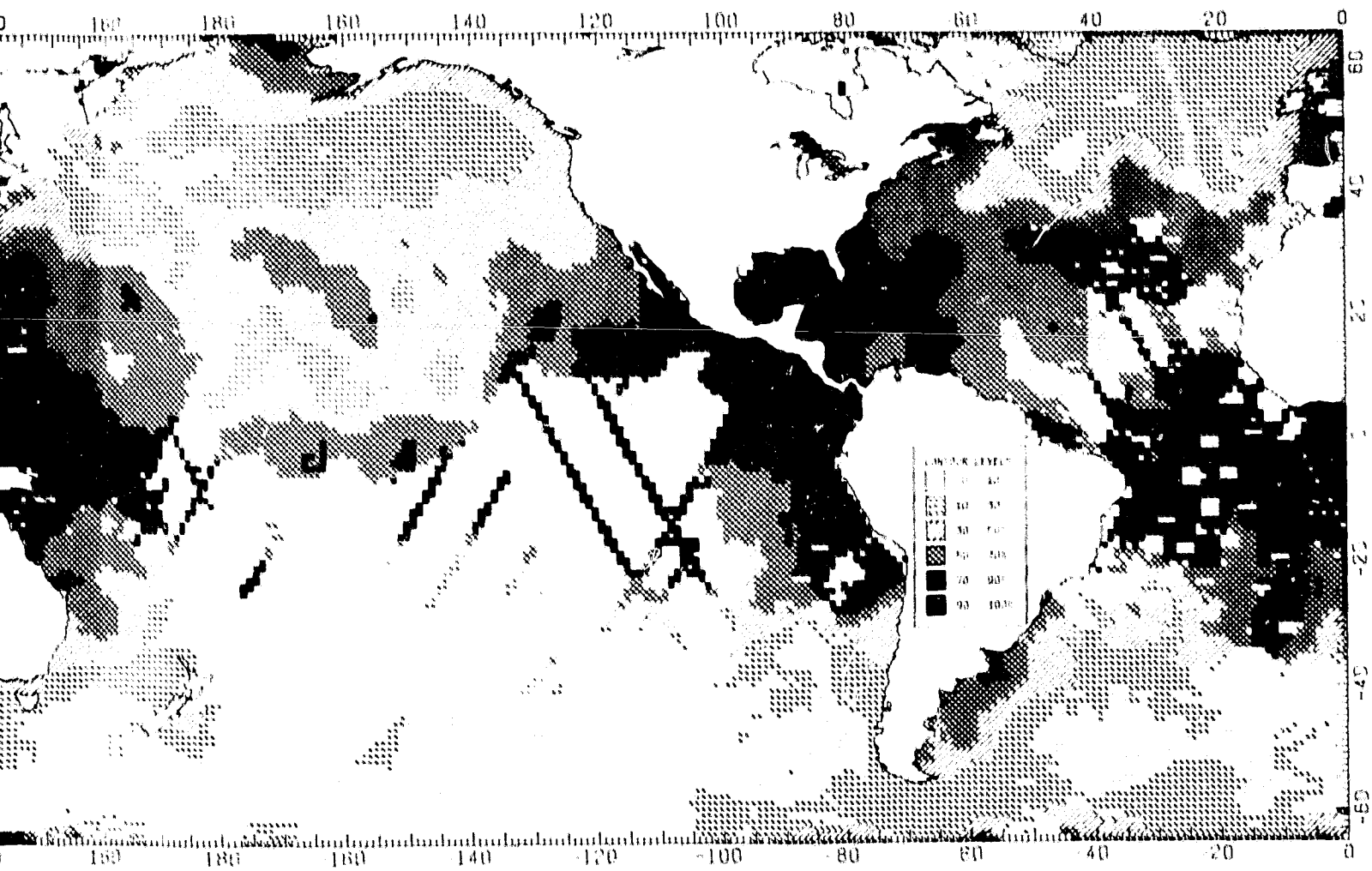


FOLDOUT FRAME 2

A.6 March Through May - Percent Significant Waveheight < 2.5 Meters

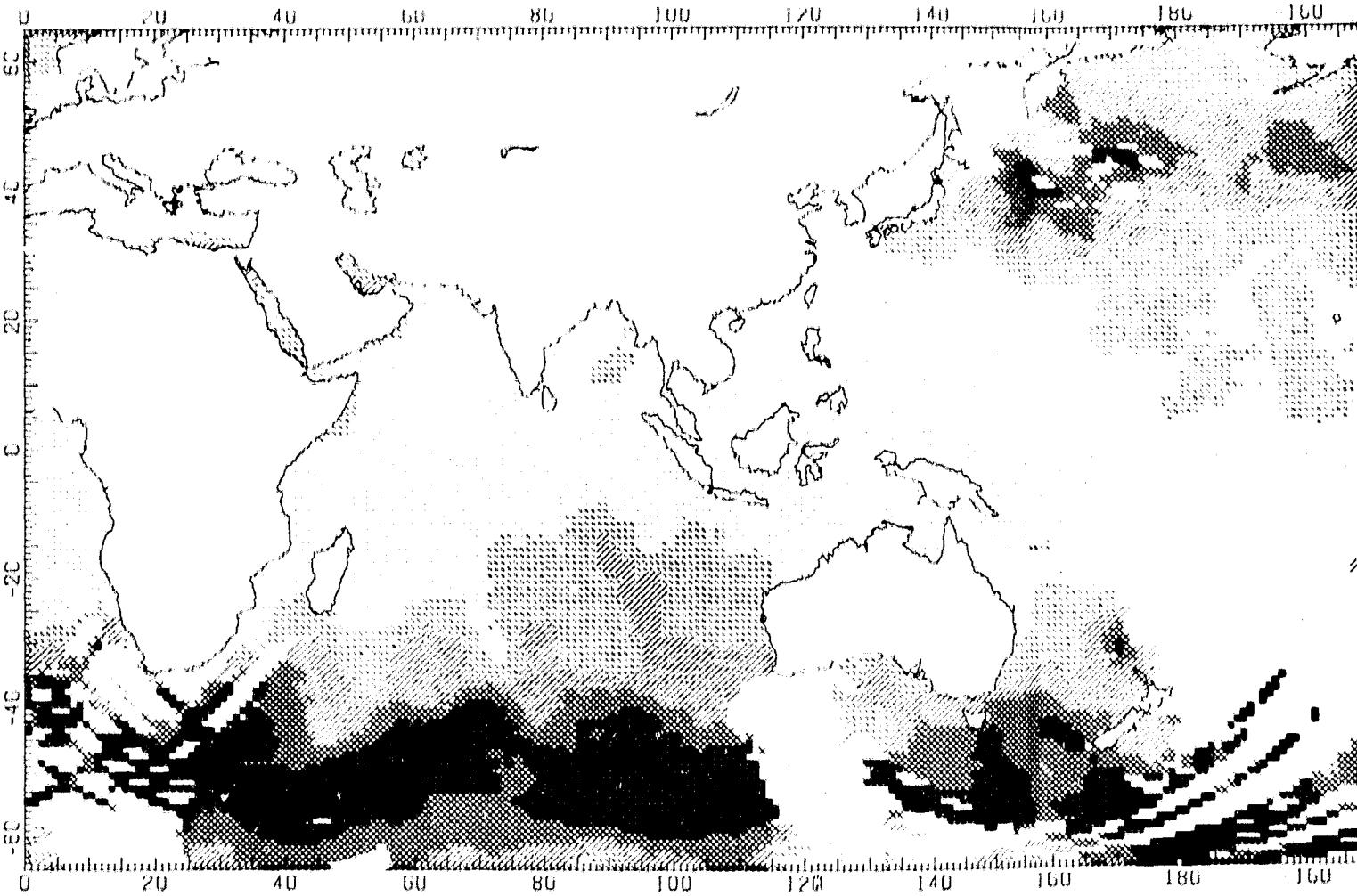


FOLDOUT FRAME

ORIGINAL PAGE IS
OF POOR QUALITY

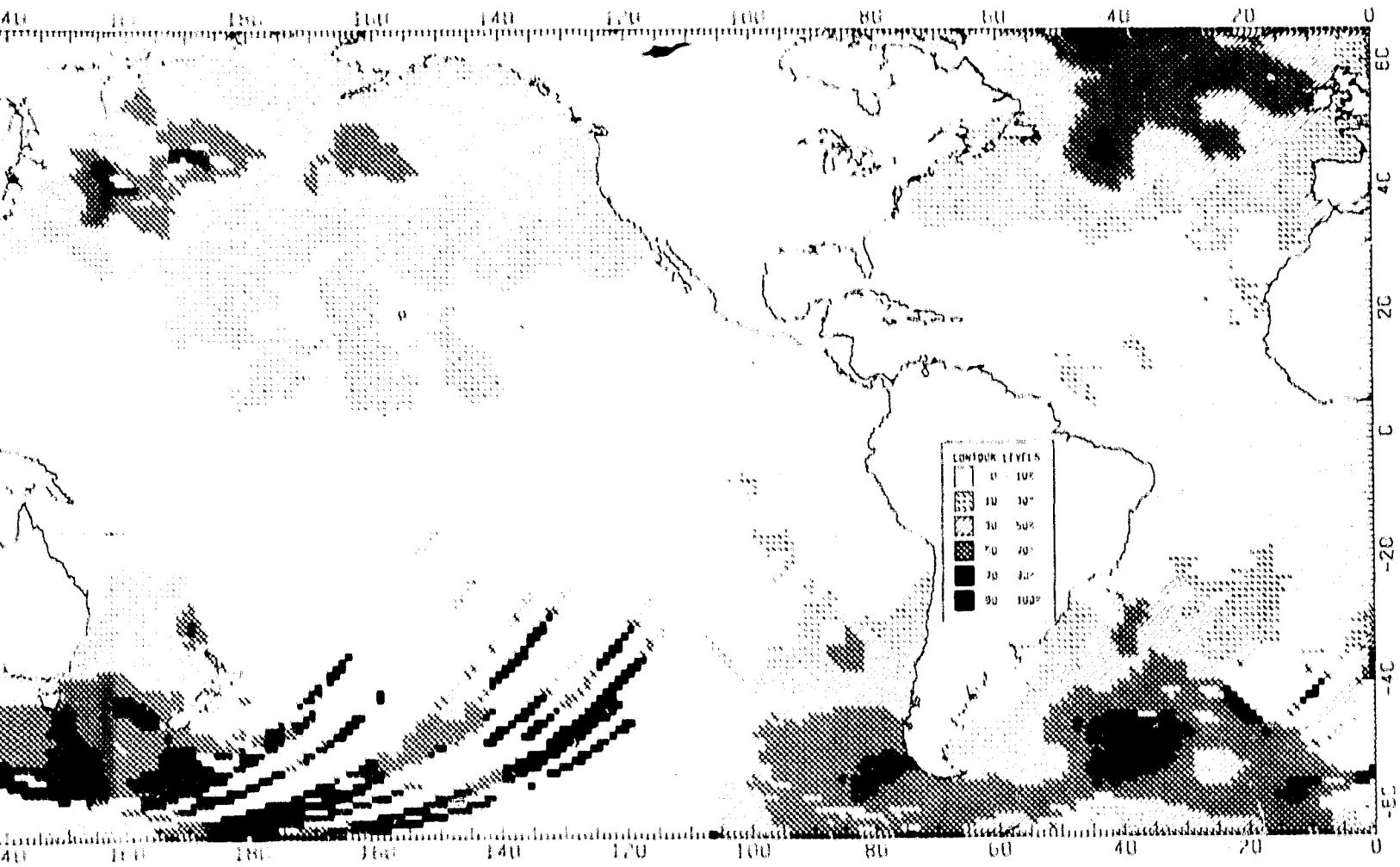




FOLDOUT FRAME 2

A.7 March Through May - Percent Significant Waveheight > 3.5 Meters

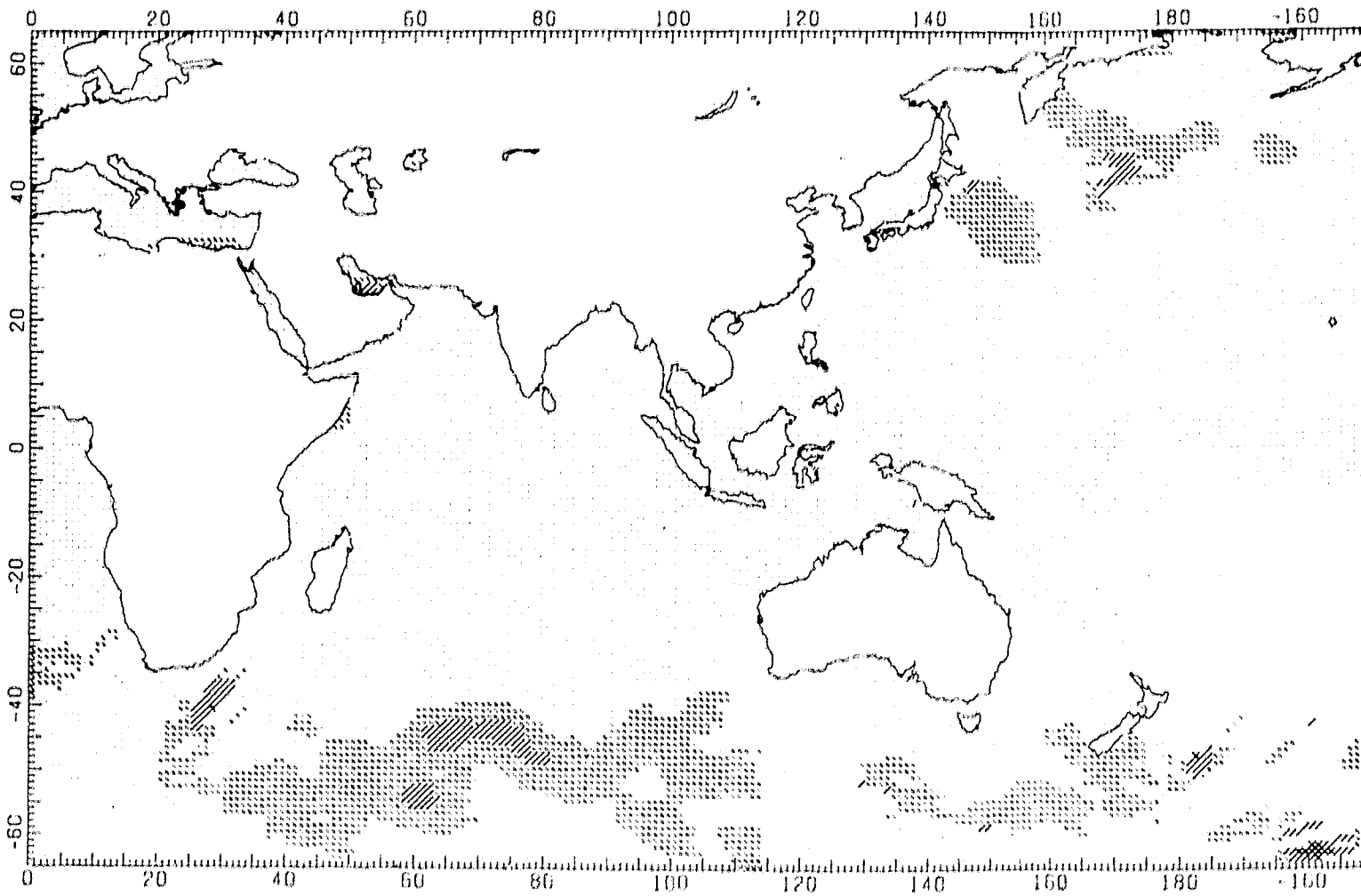




FOLDOUT FRAME

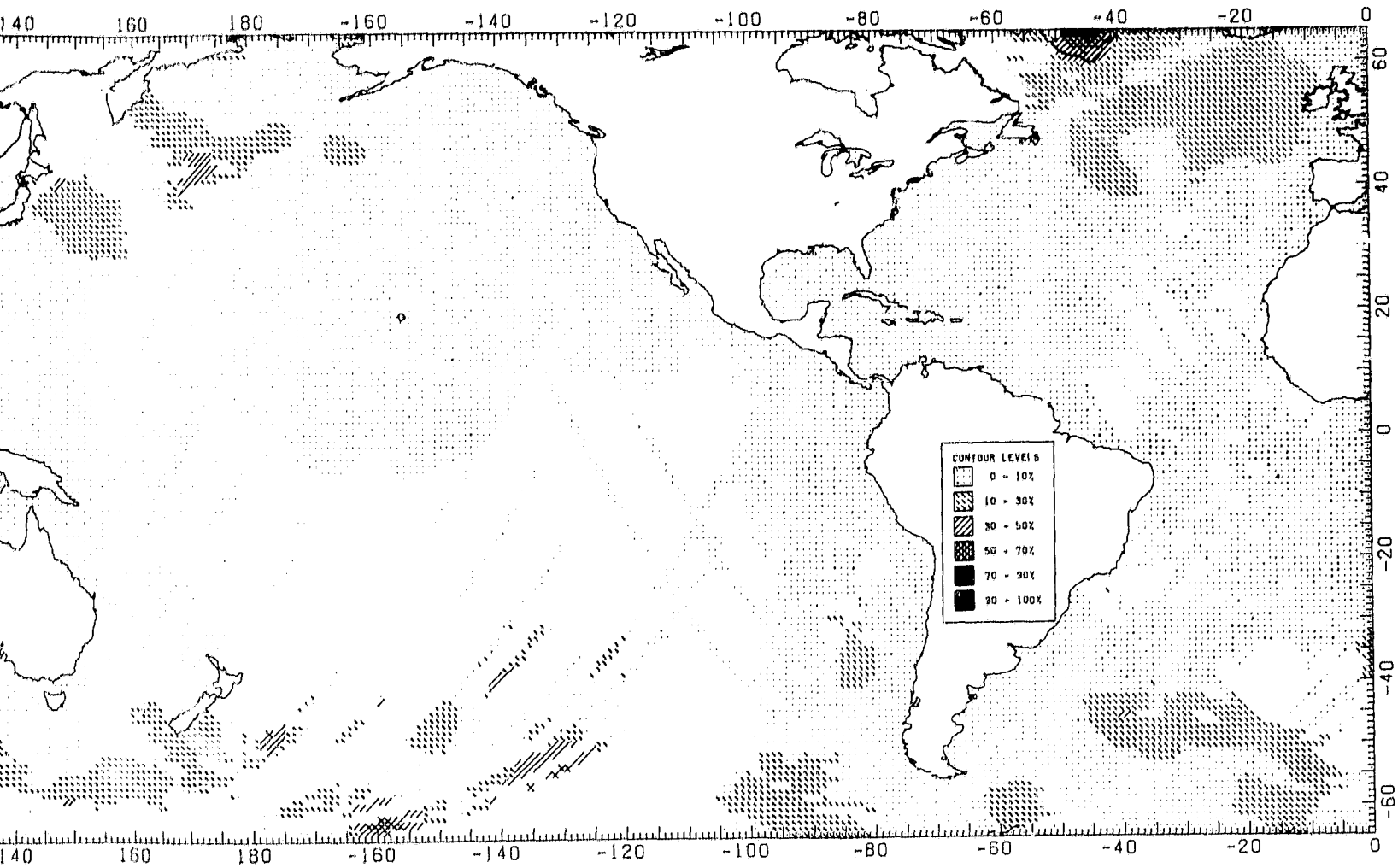




A.8 March Through May - Percent Significant Waveheight > 6.0 Meters

FOLDOUT FRAME 2

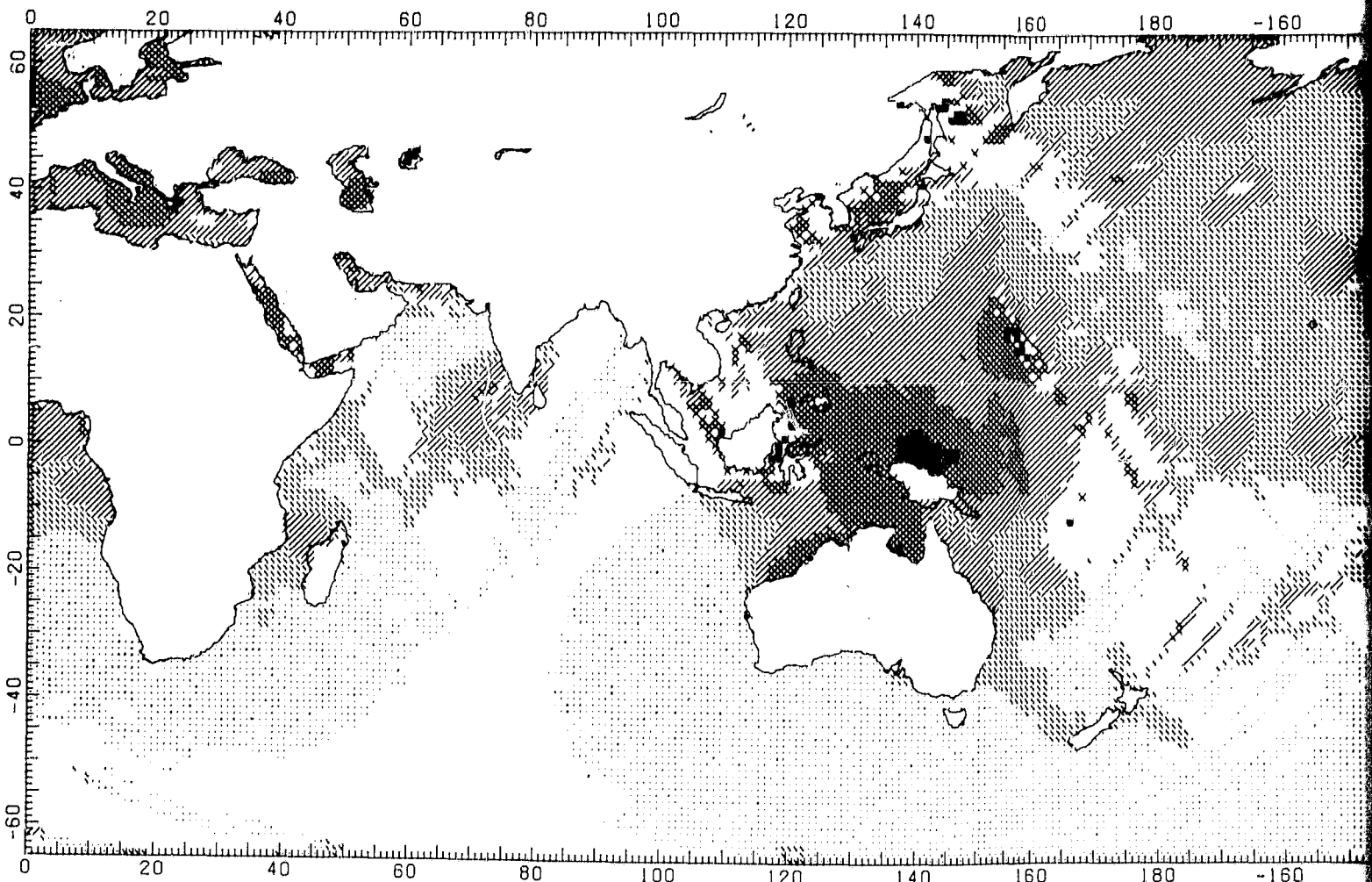

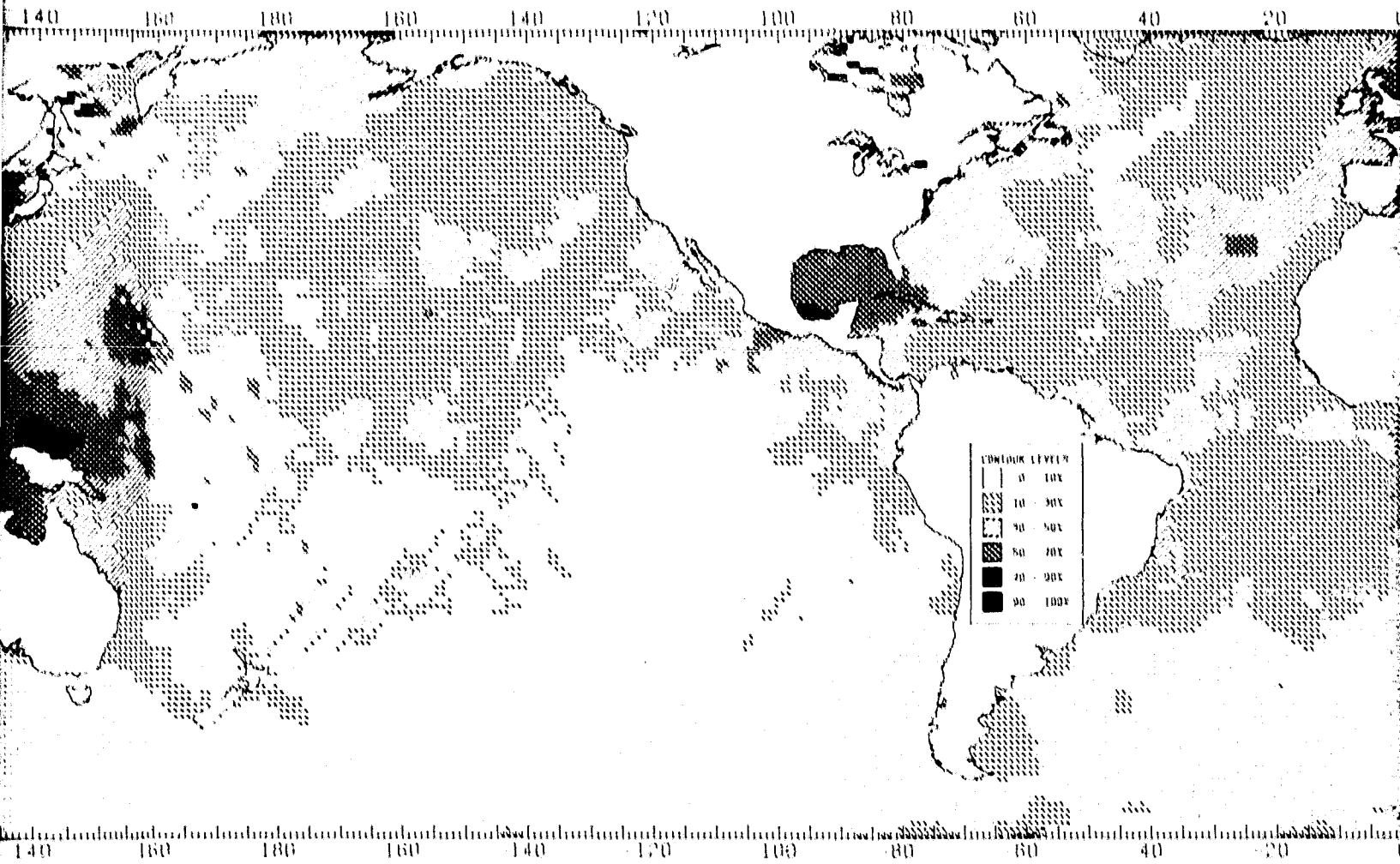




A.9 June Through August - Percent Significant Waveheight < 1.5 Meters

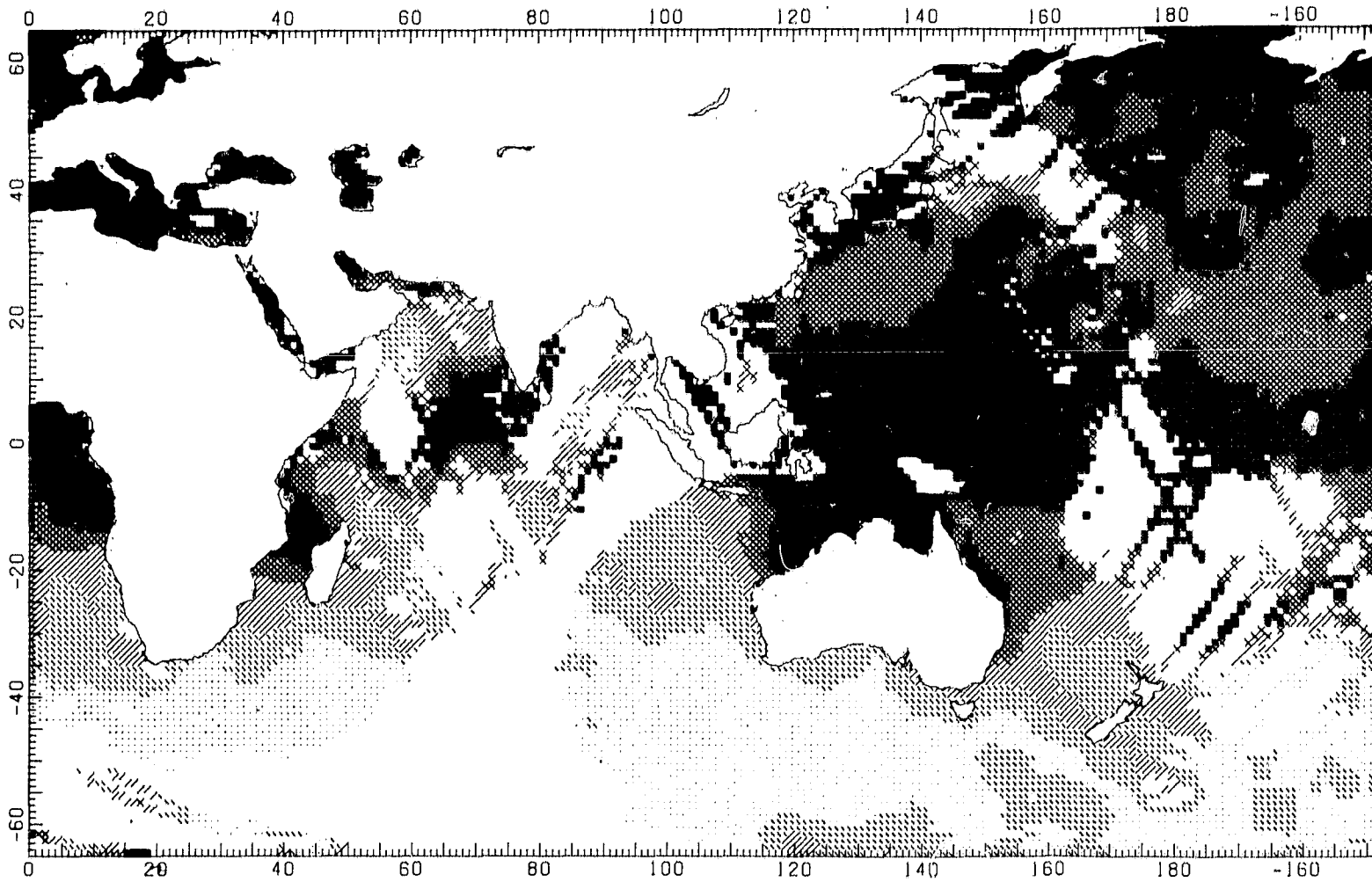

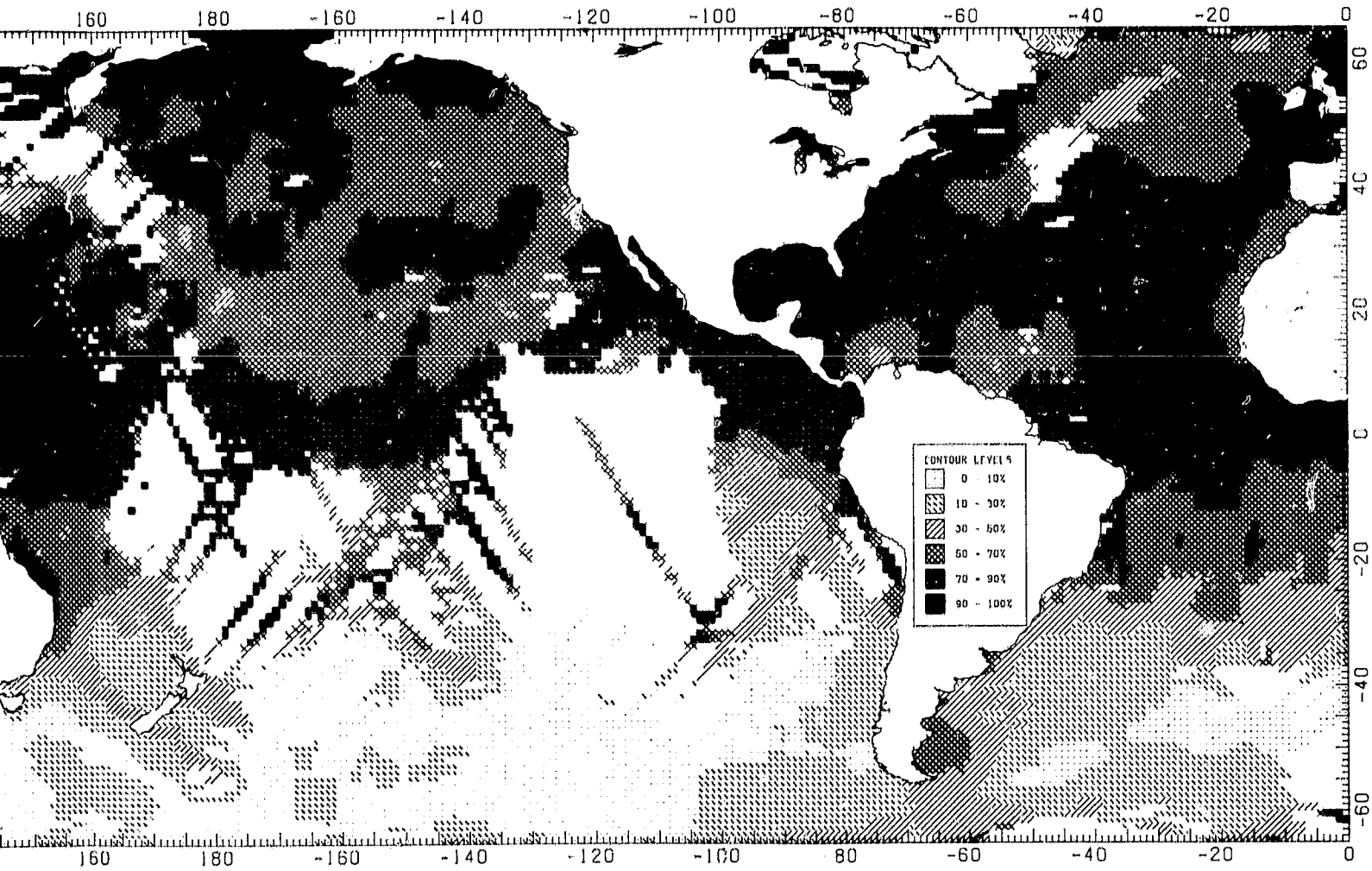




A.10 June Through August - Percent Significant Waveheight < 2.5 Meters

FOLDOUT FRAME 1

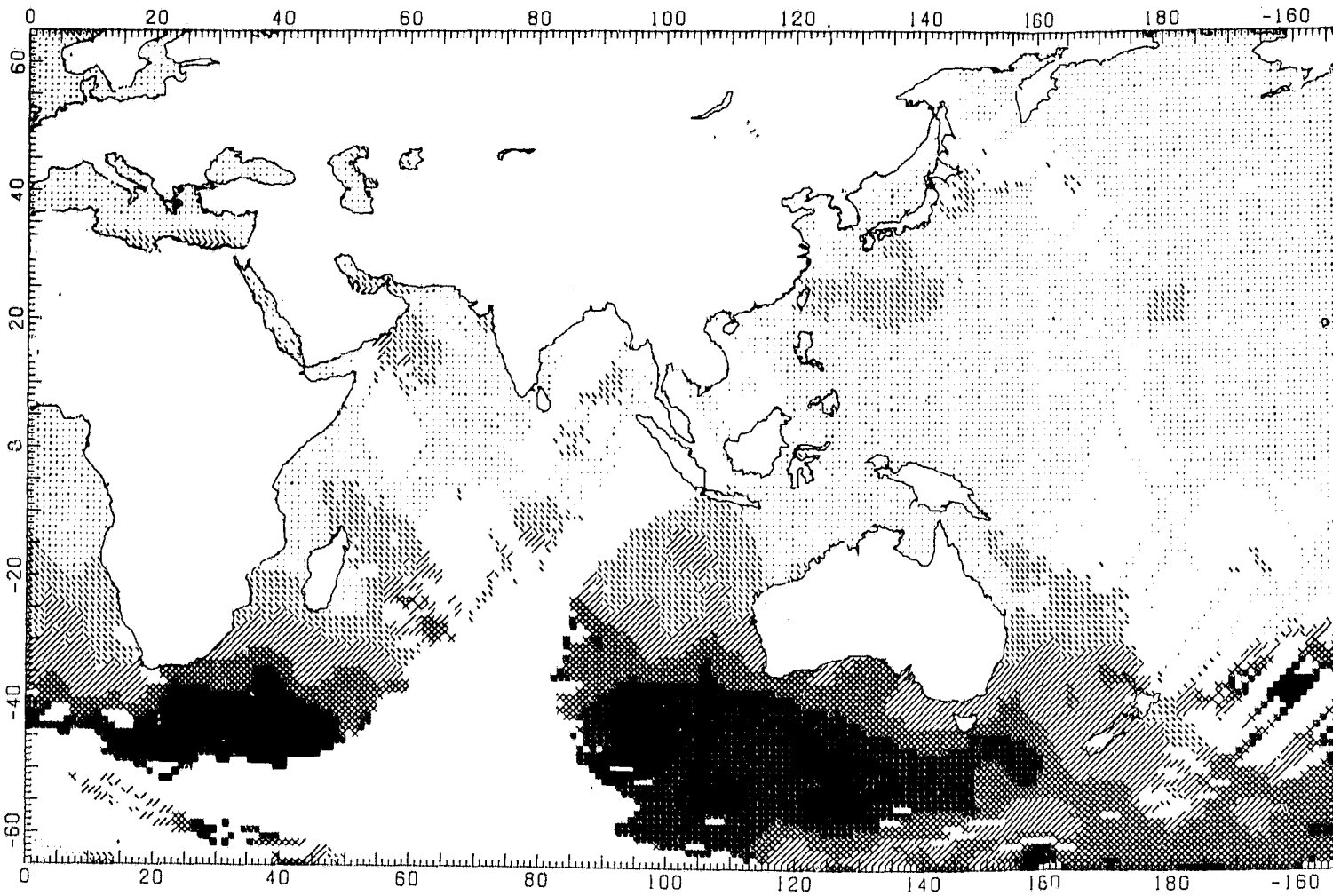

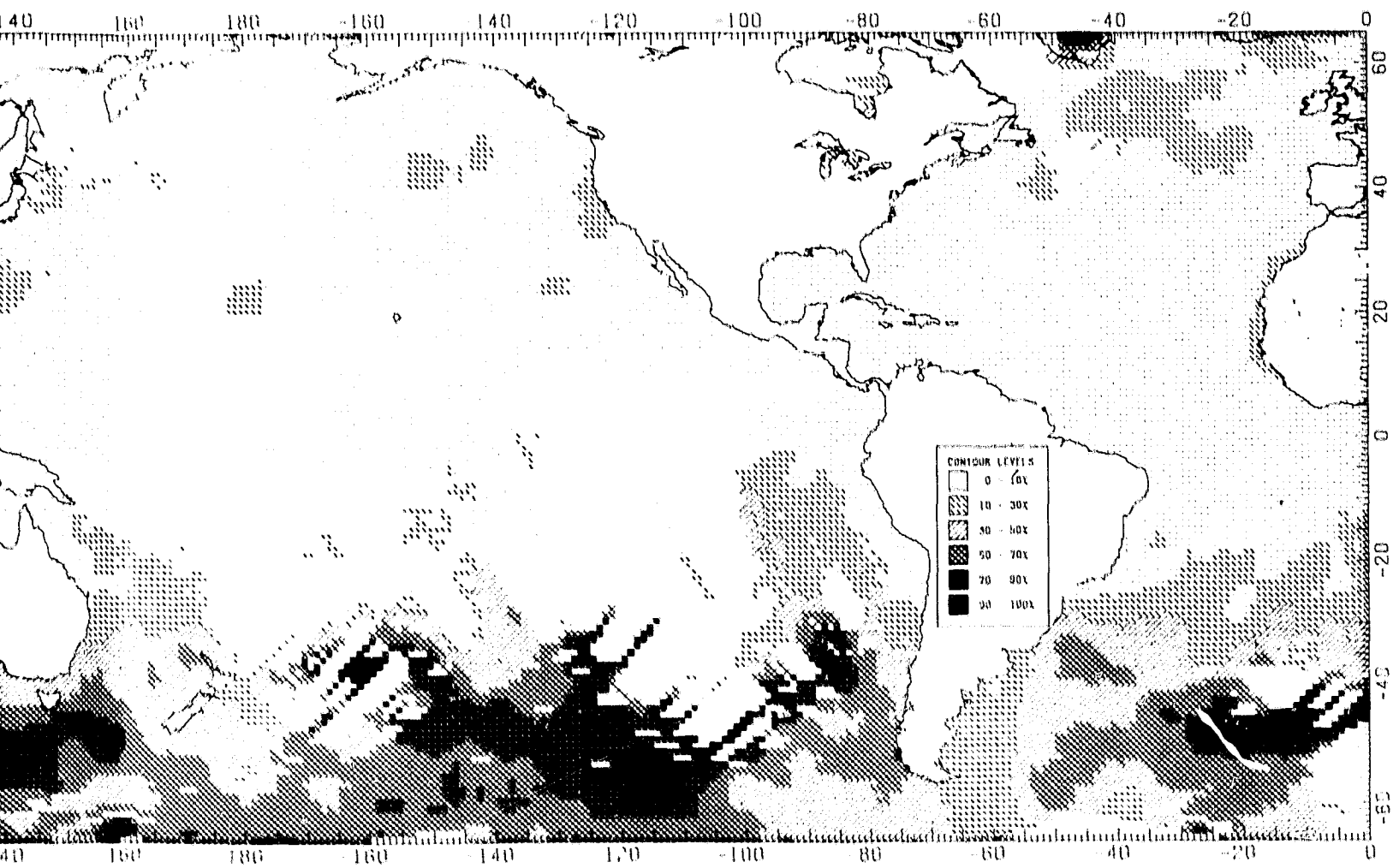


FOLDOUT FRAME 2

A.11 June Through August - Percent Significant Waveheight > 3.5 Meters

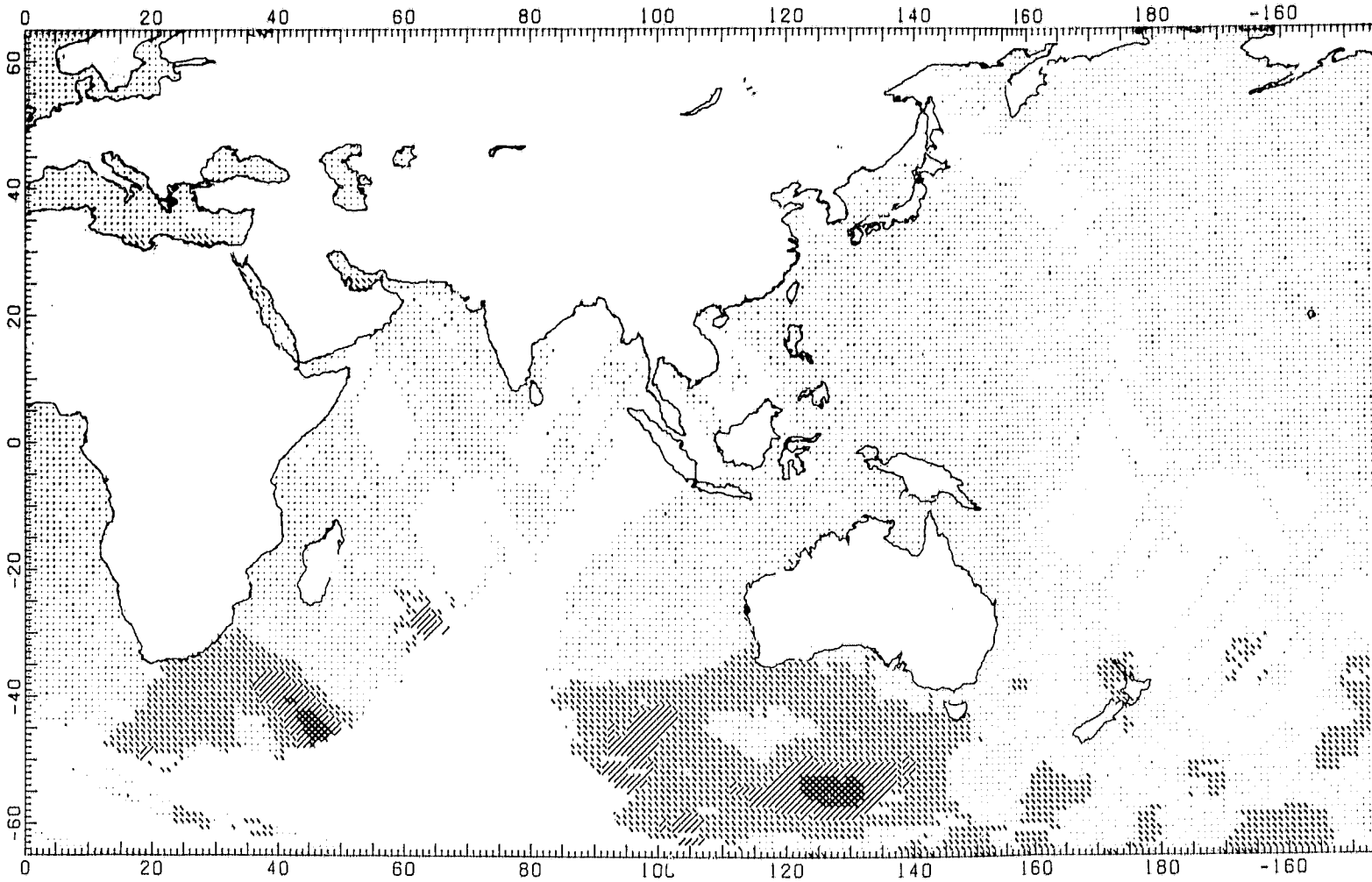


FOLDOUT



DOUT FRAME

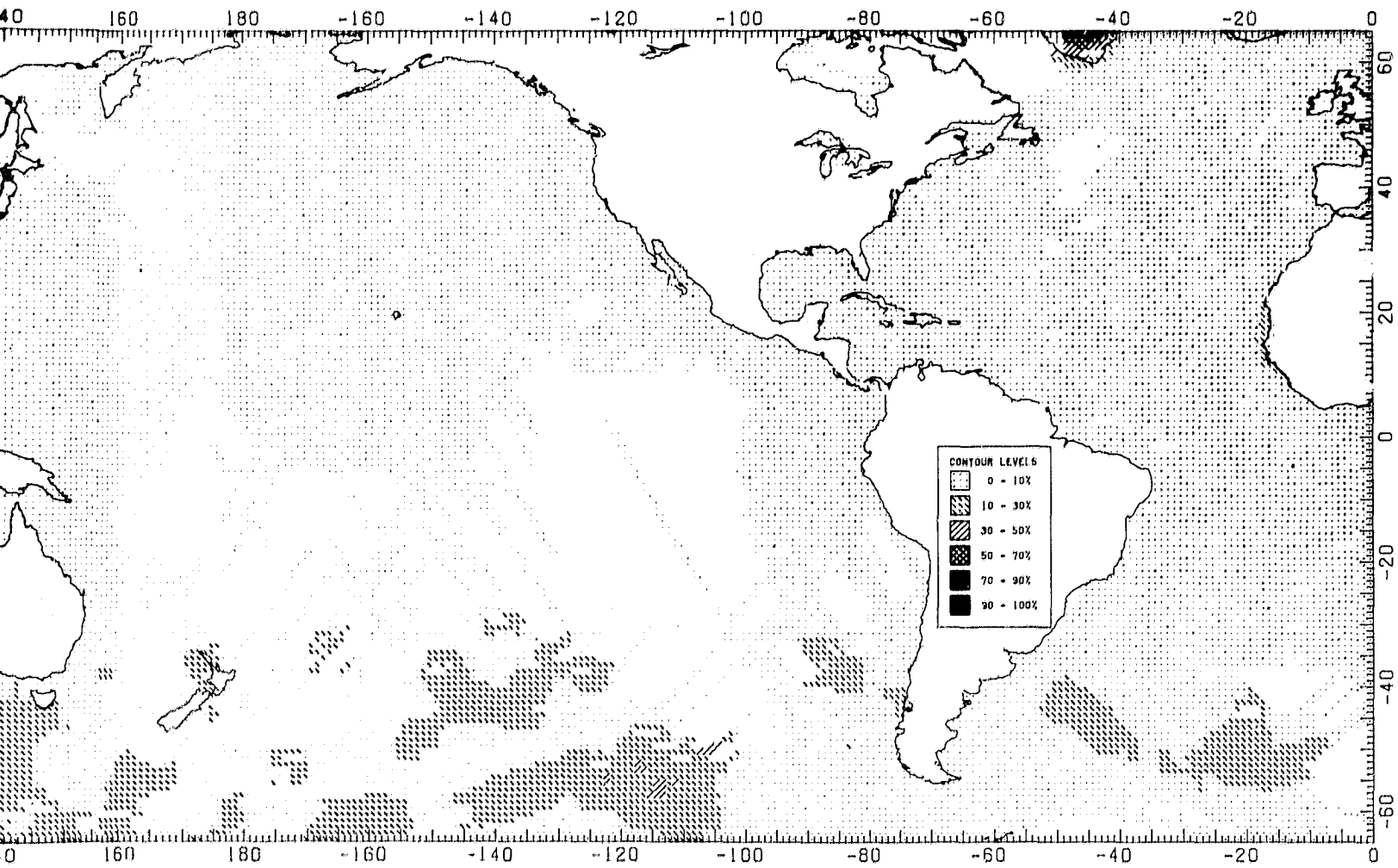






FOLDOUT FRAME

A.12 June Through August - Percent Significant Waveheight > 6.0 Meters

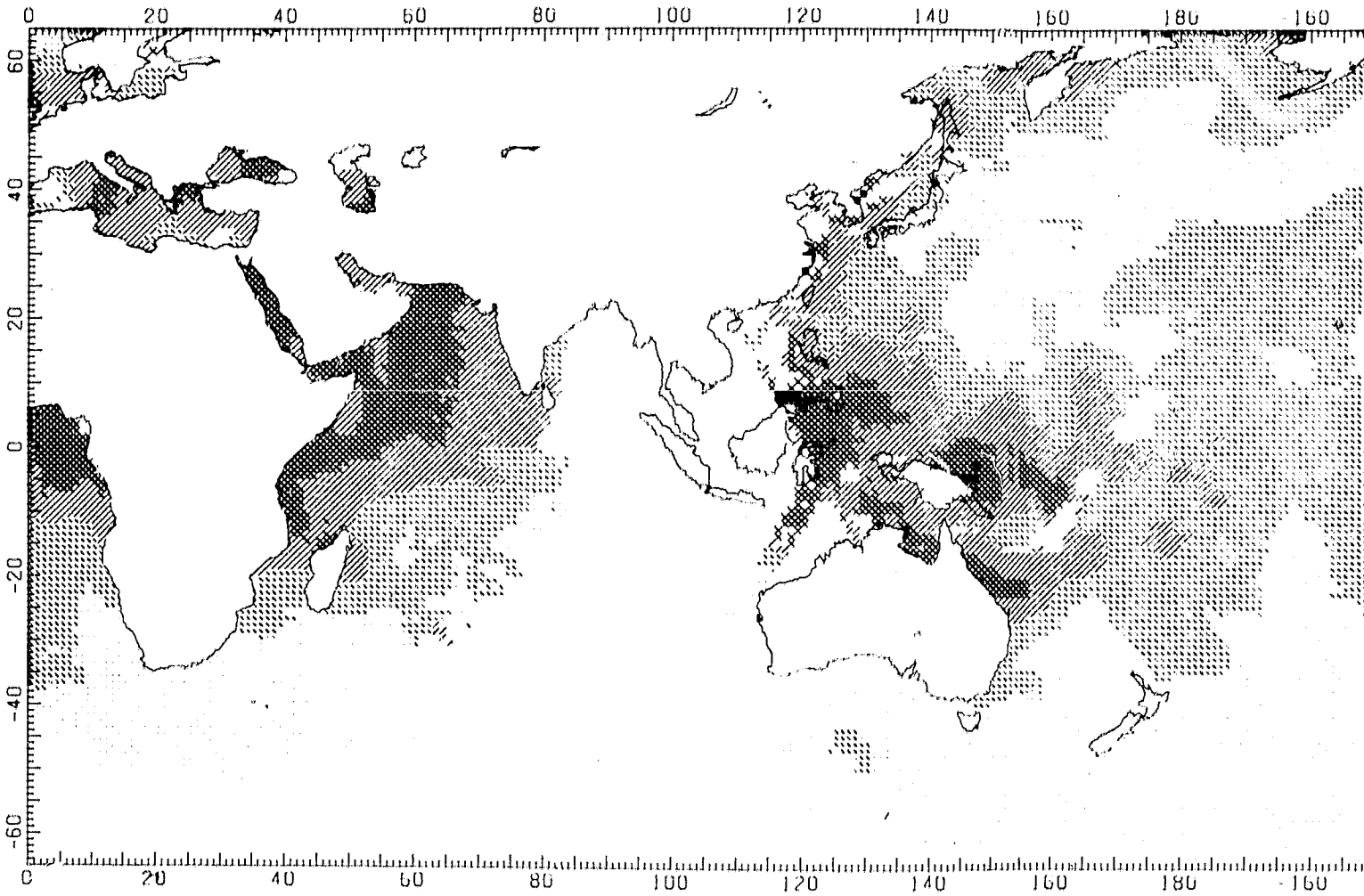

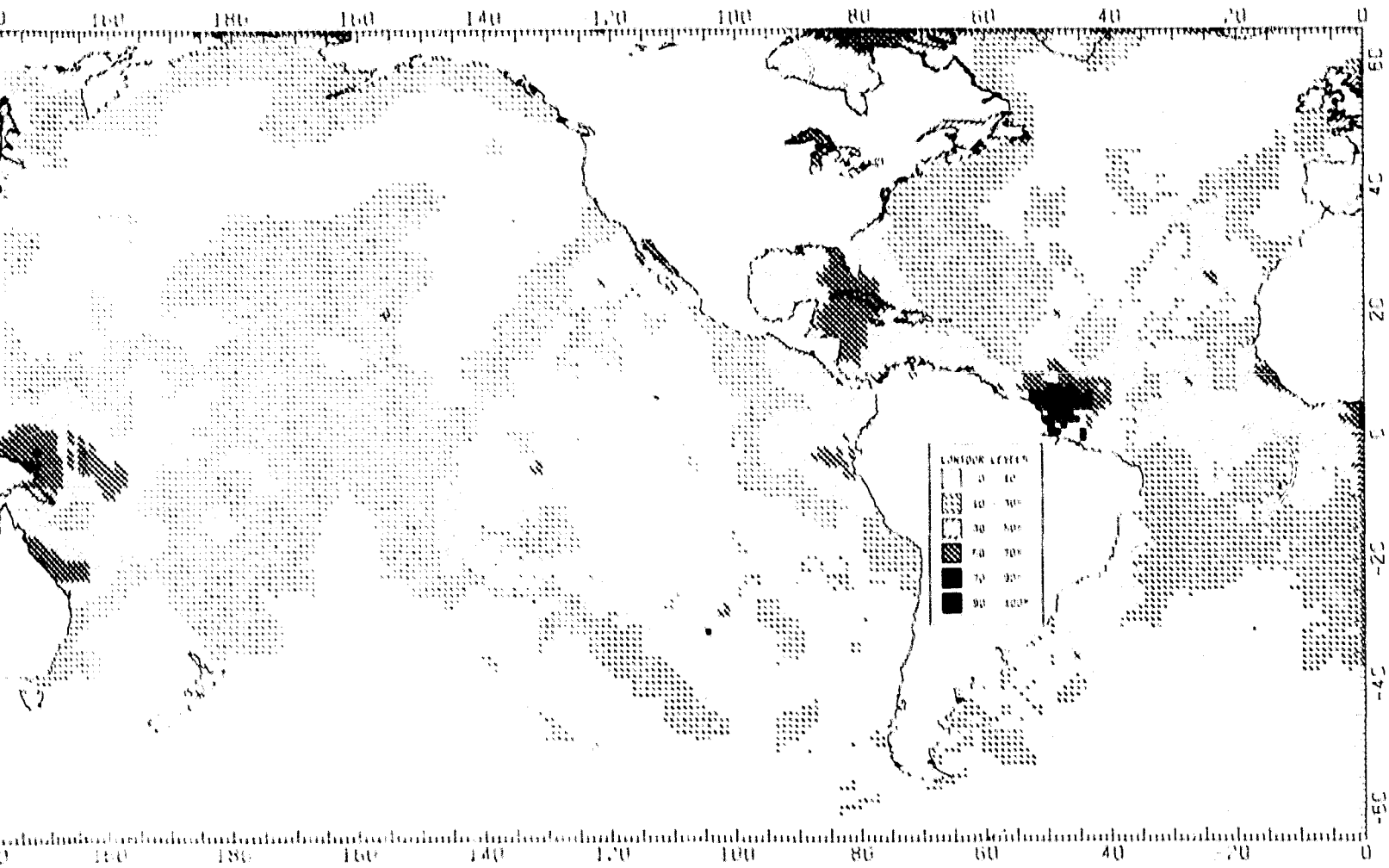


FOLDOUT FRAME 9

ORIGINAL PAGE IS
OF POOR QUALITY

A.13 September Through November - Percent Significant Waveheight < 1.5 Meters

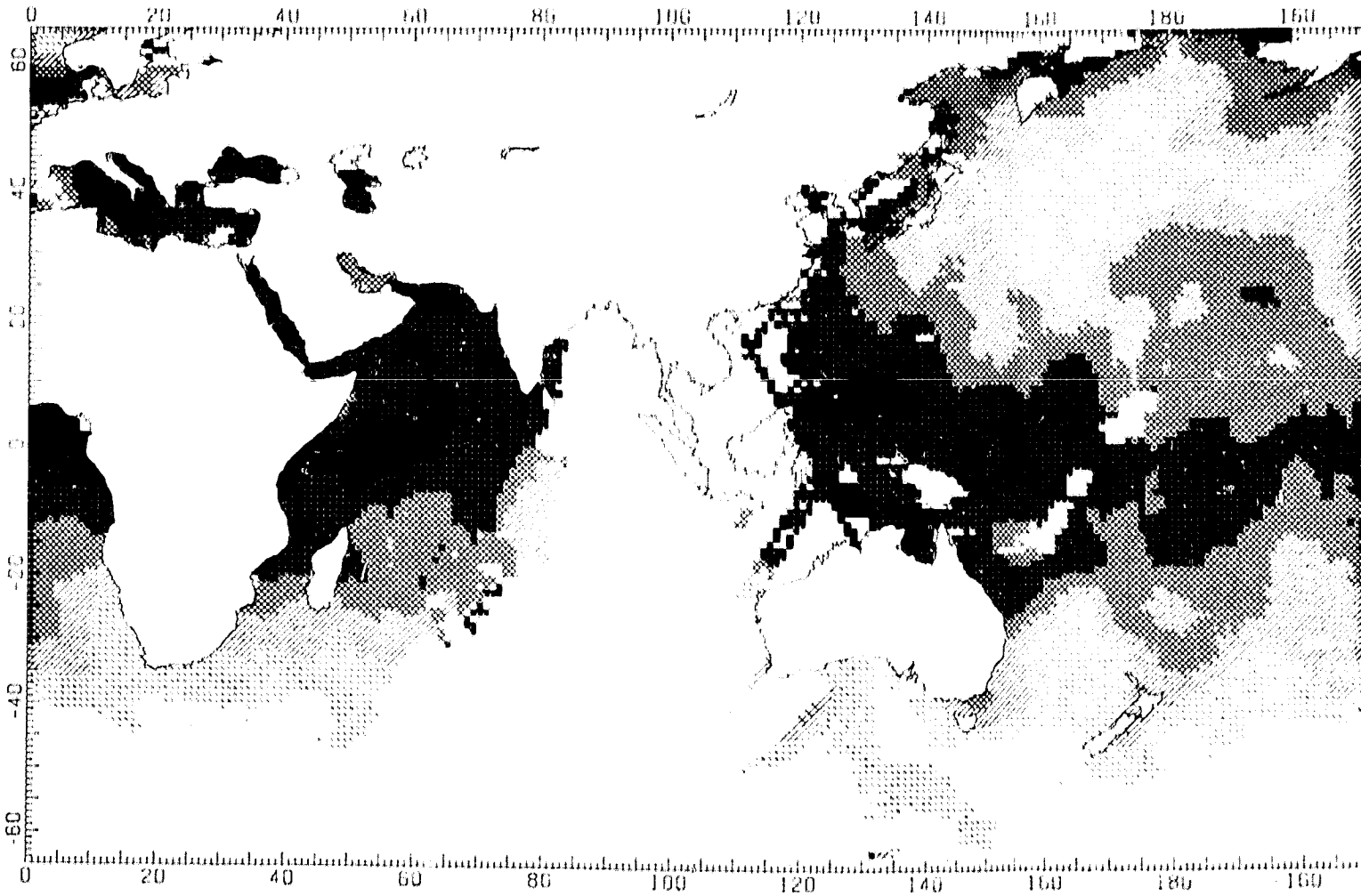




FOLDOUT FRAME

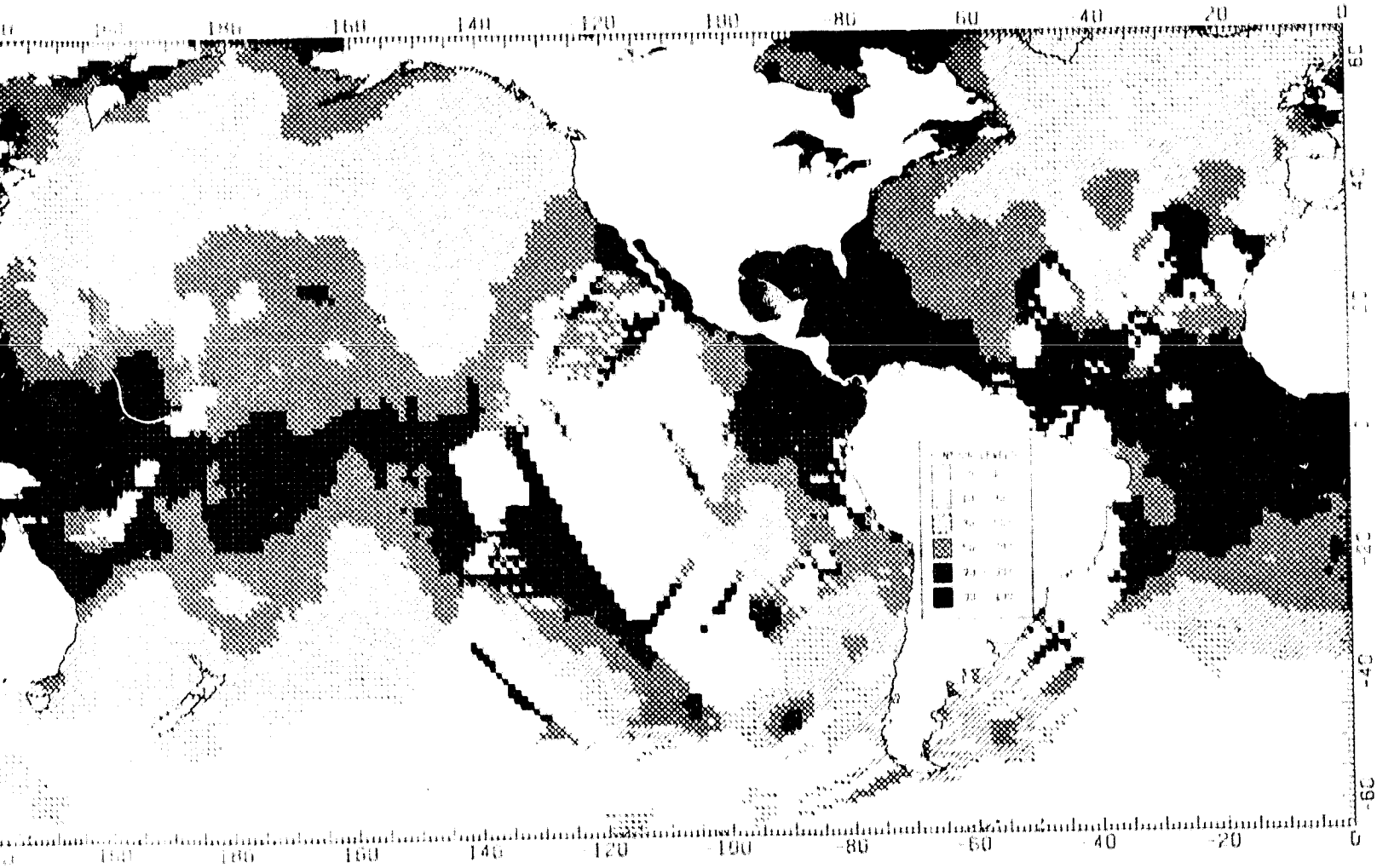

A.14 September Through November - Percent Significant Waveheight < 2.5 Meters

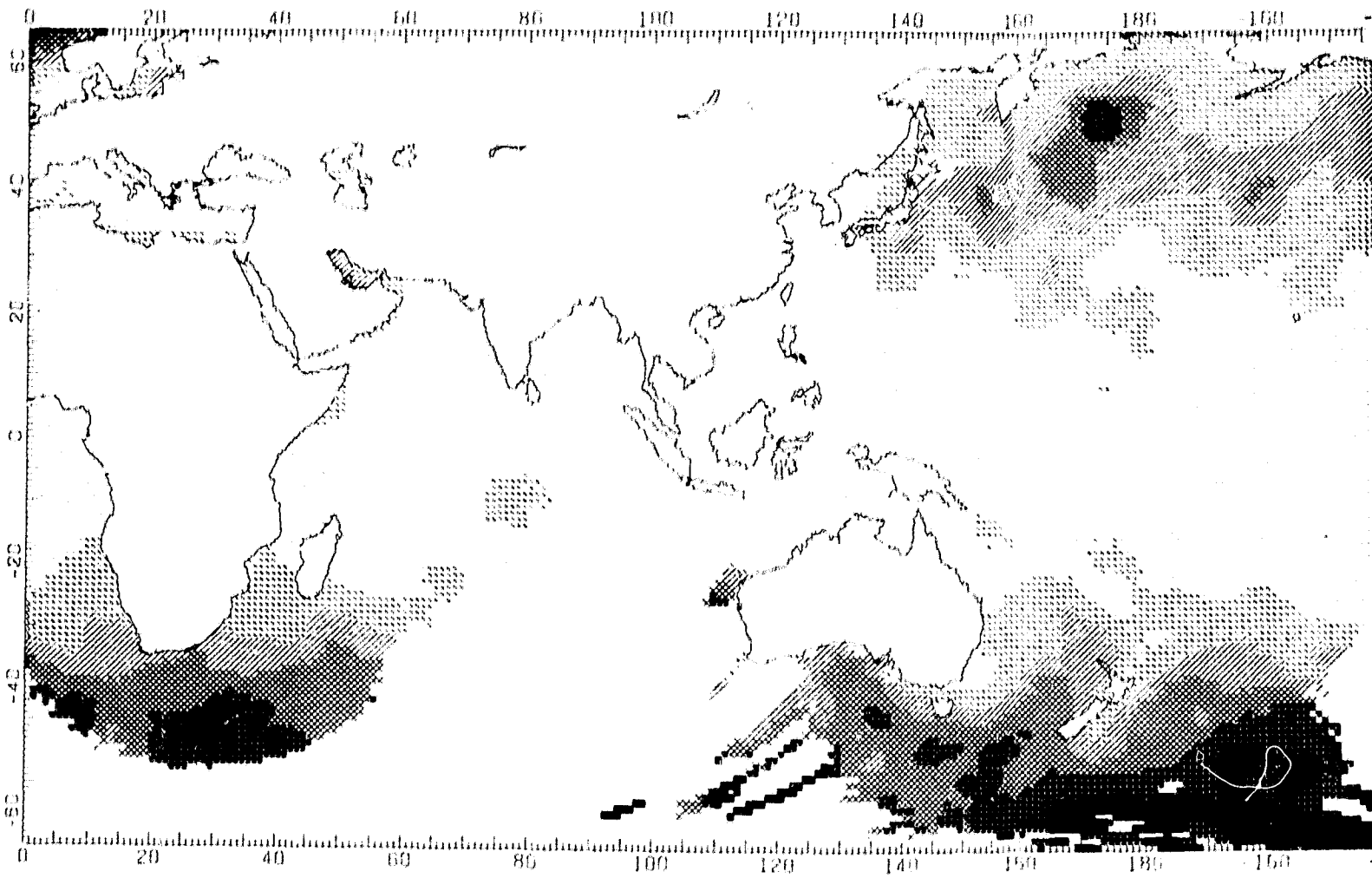




FOLDOUT FRAME

FOLD

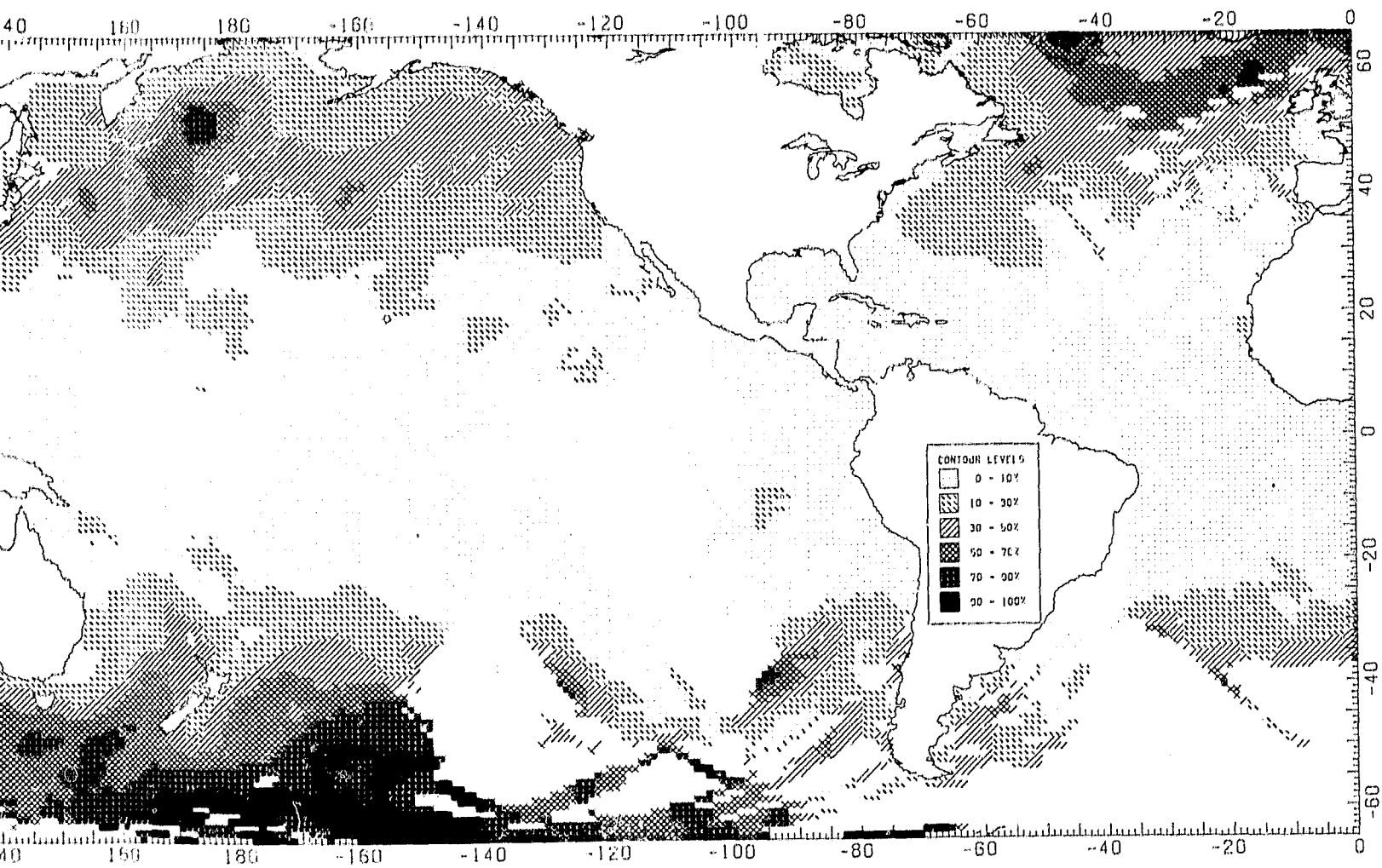




FOLDOUT FRAME 2

A.15 September Through November - Percent Significant Waveheight > 3.5 Meters

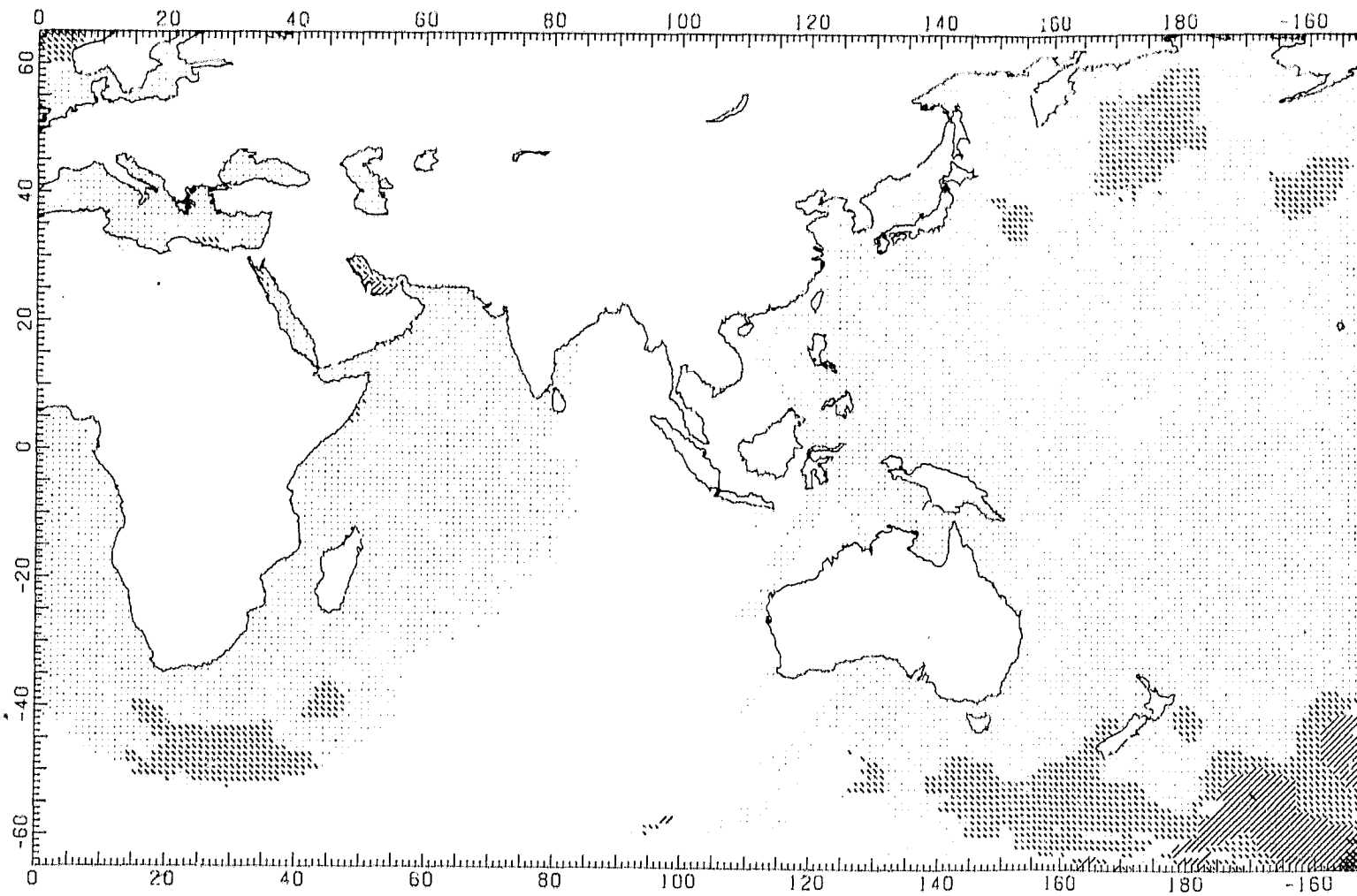


FOLDOUT FRAME

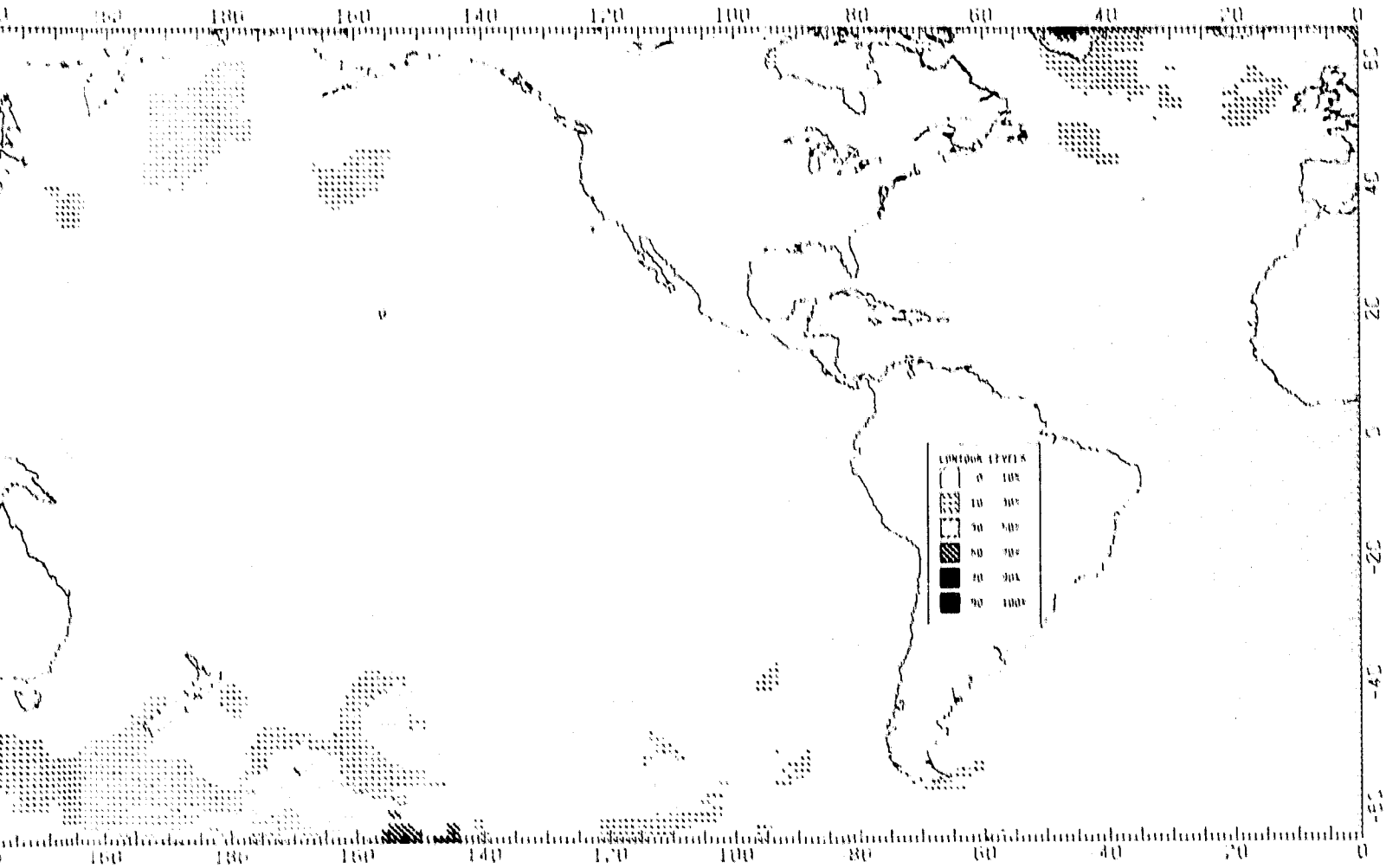

FOLDOUT FRAME 4

A .16 September Through November - Percent Significant Waveheight > 6.0 Meters

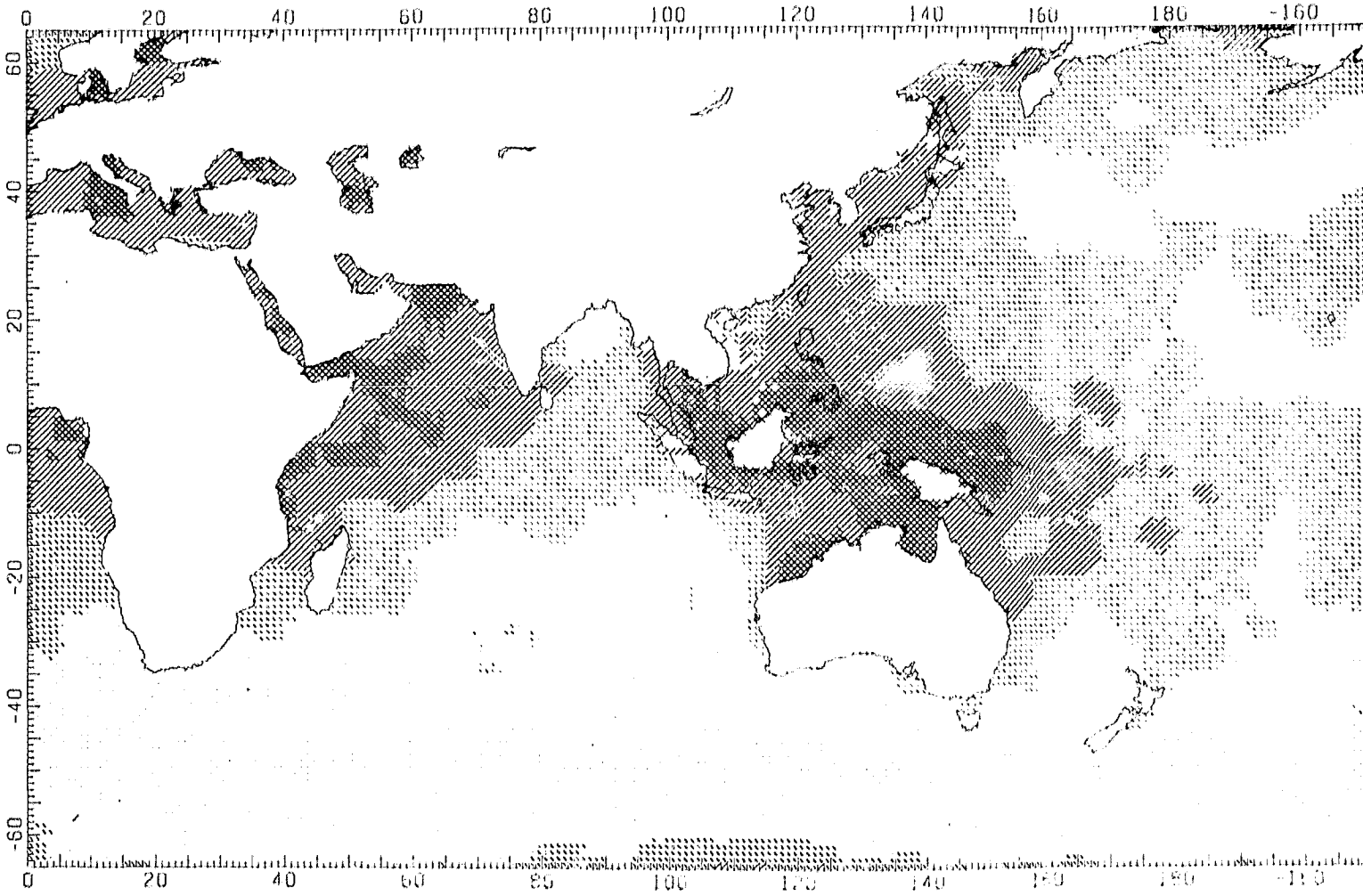




FOLDOUT FRAME

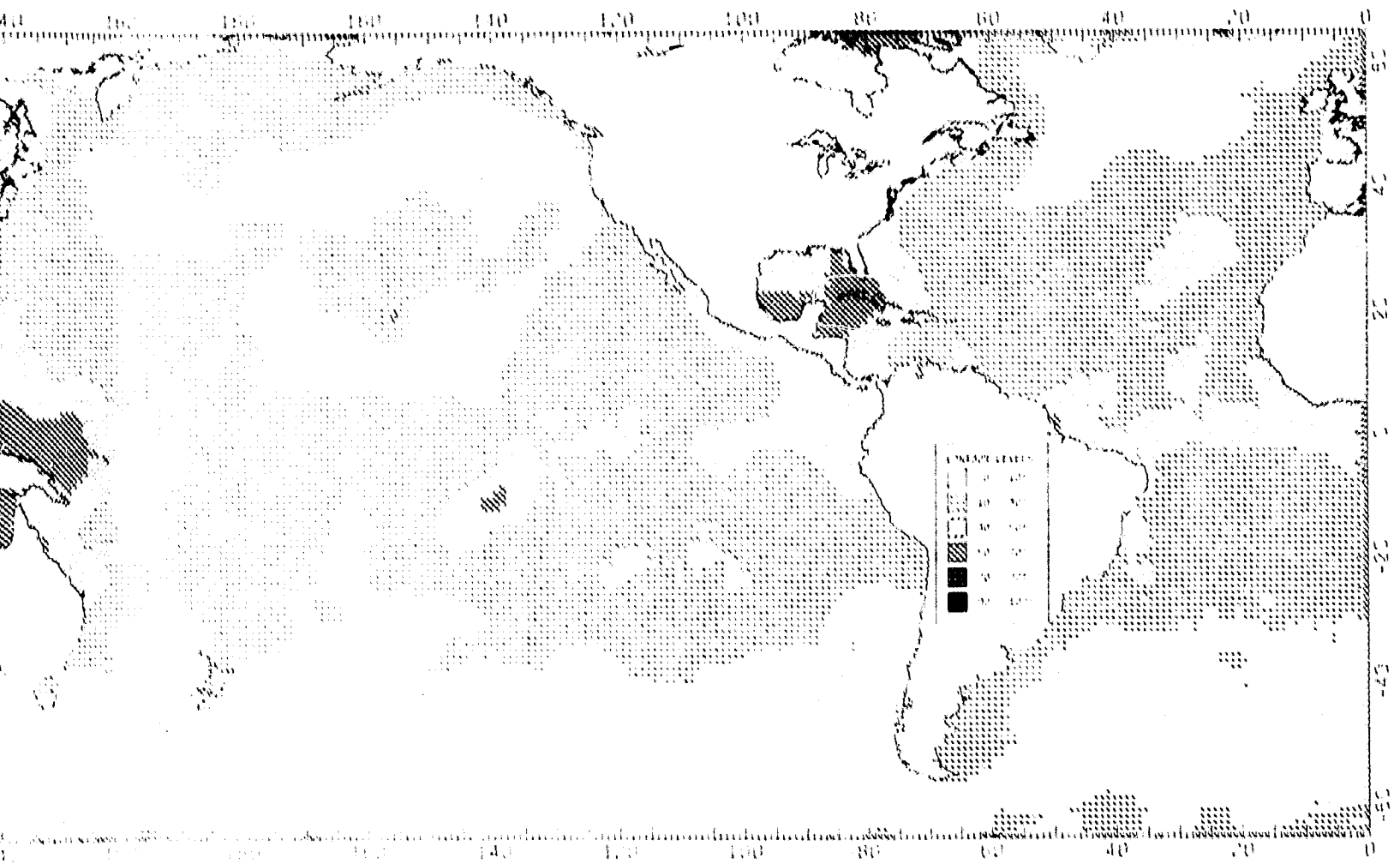

FOLDOUT FRAME 7

A.17 Entire Mission - Percent Significant Waveheight < 1.5 Meters

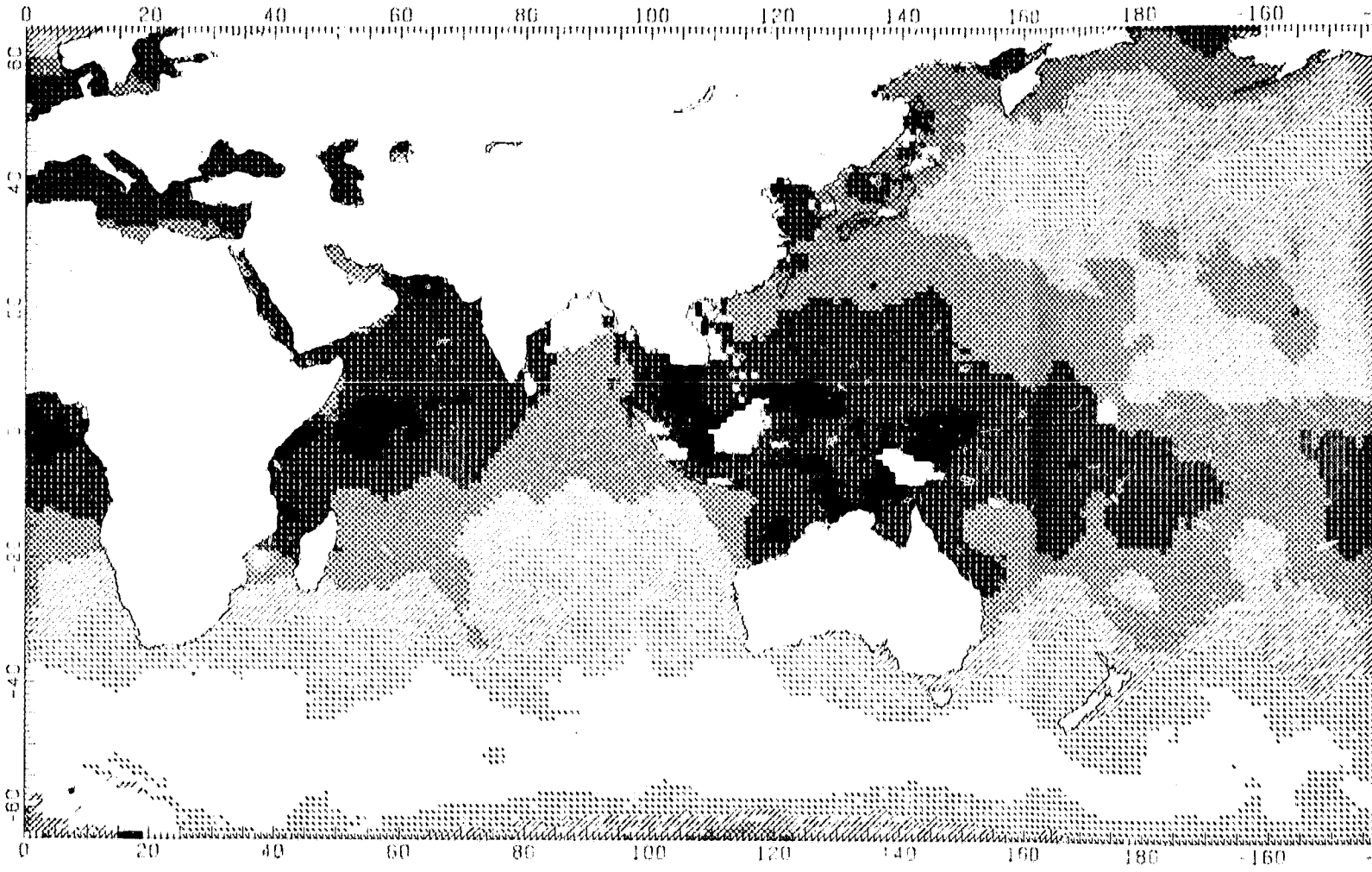


FOLDOUT FRAME

ORIGINAL PAGE IS

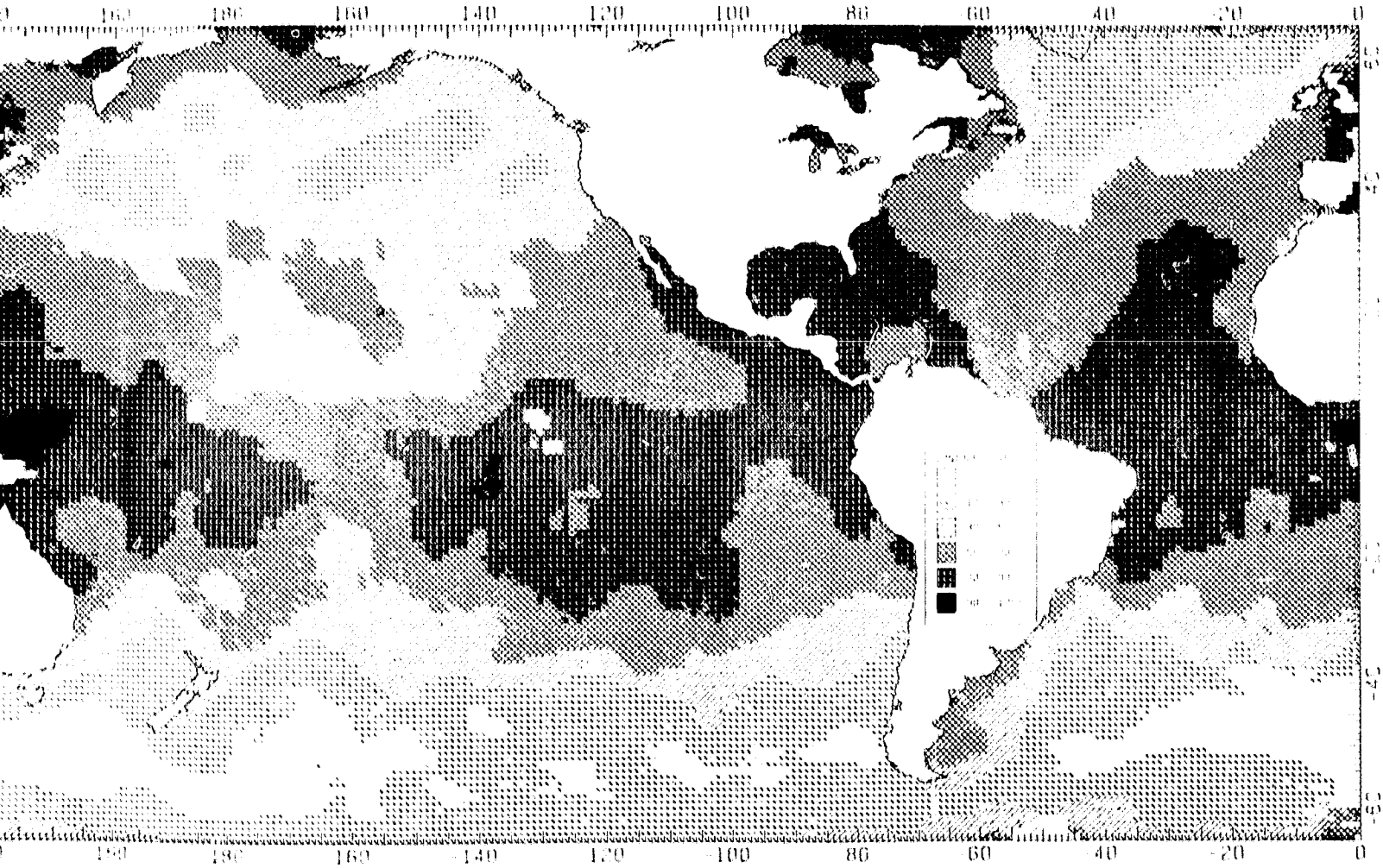


FOLDOUT FRAME

ORIGINAL PAGE IS
OF POOR QUALITY

A.18 Entire Mission - Percent Significant Waveheight < 2.5 Meters

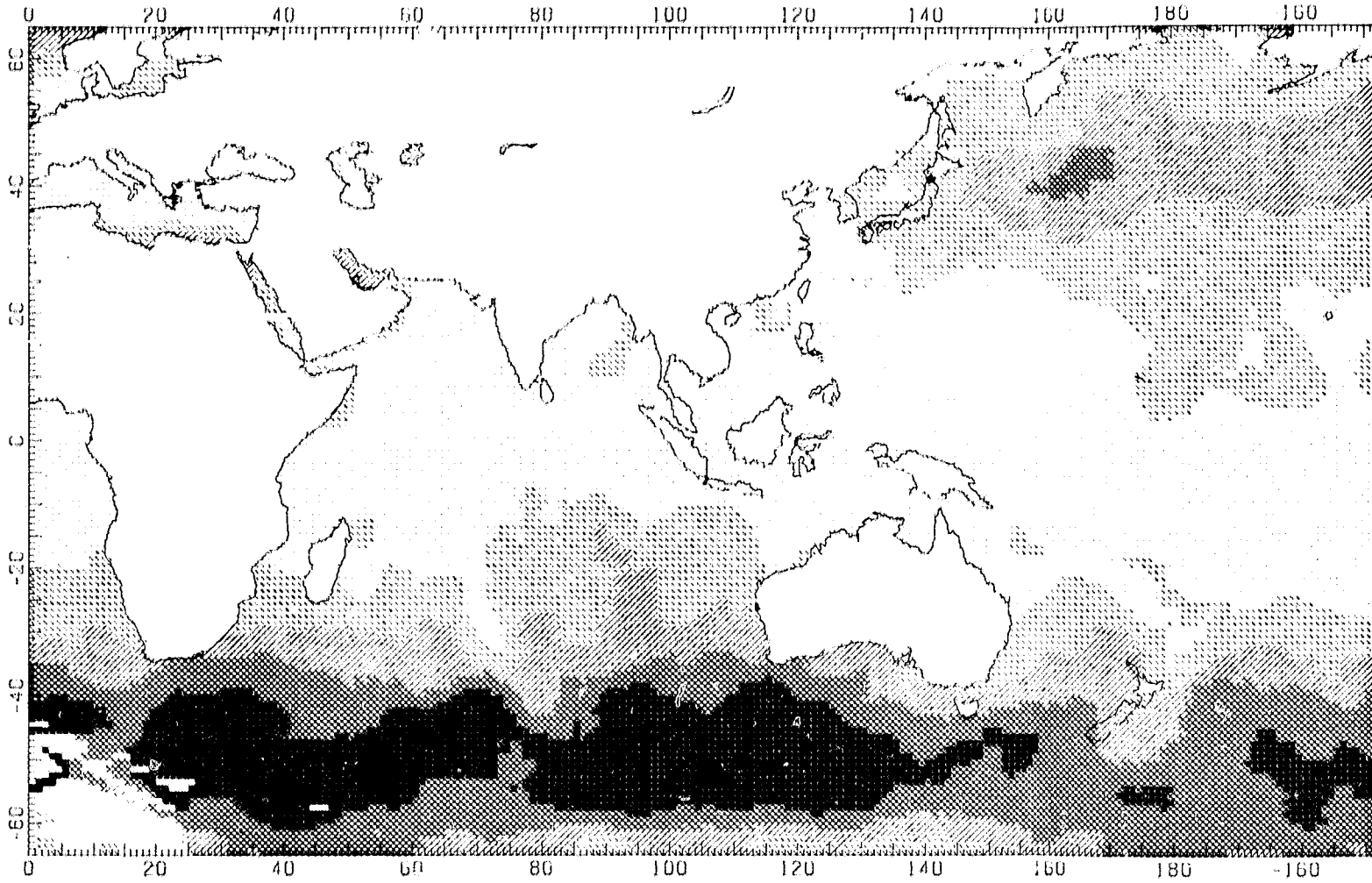


FOLDOUT FRAME

FOLDOUT FRAME

ORIGINAL PAGE IS
OF POOR QUALITY

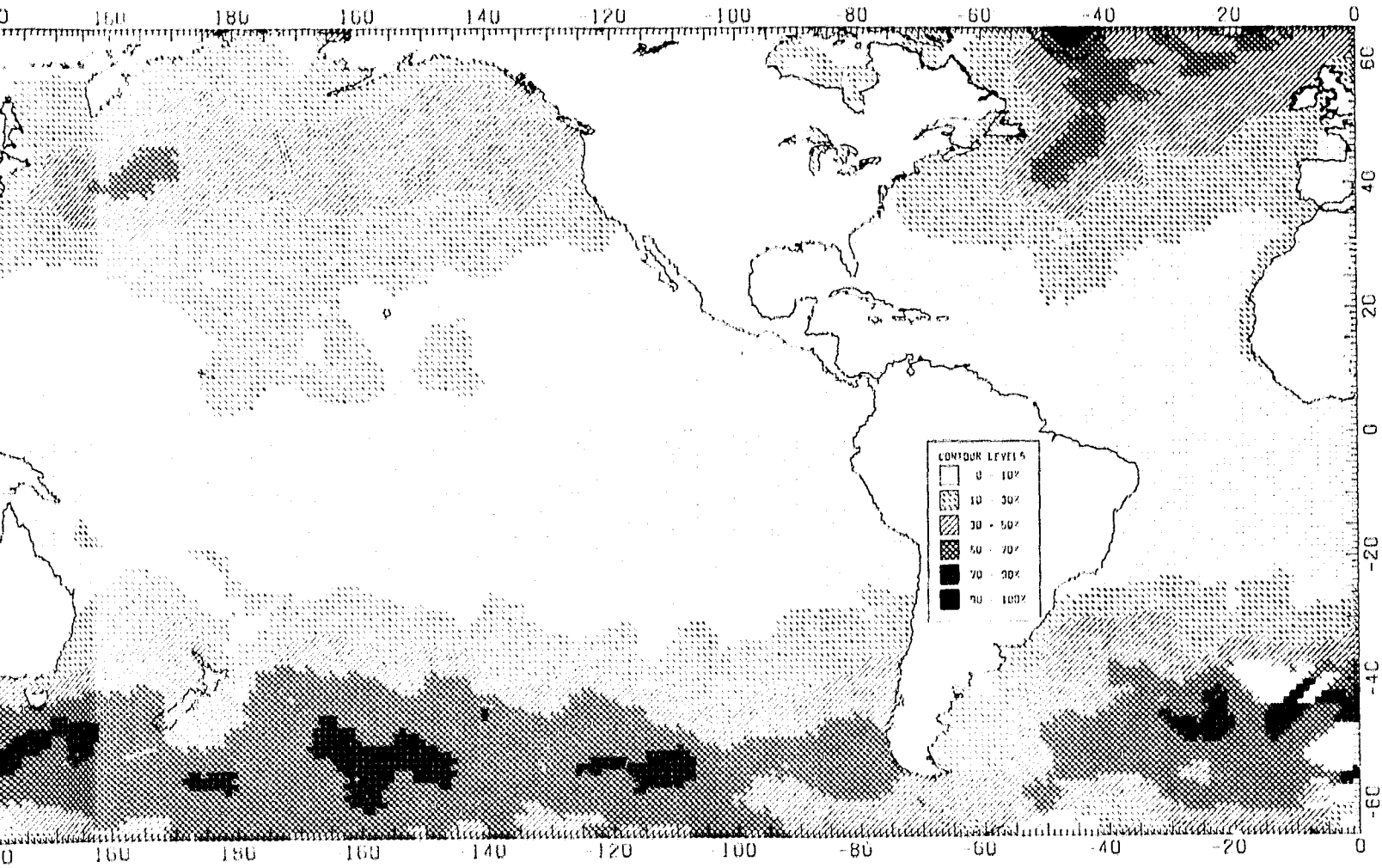




A.19 Entire Mission - Percent Significant Waveheight > 3.5 Meters

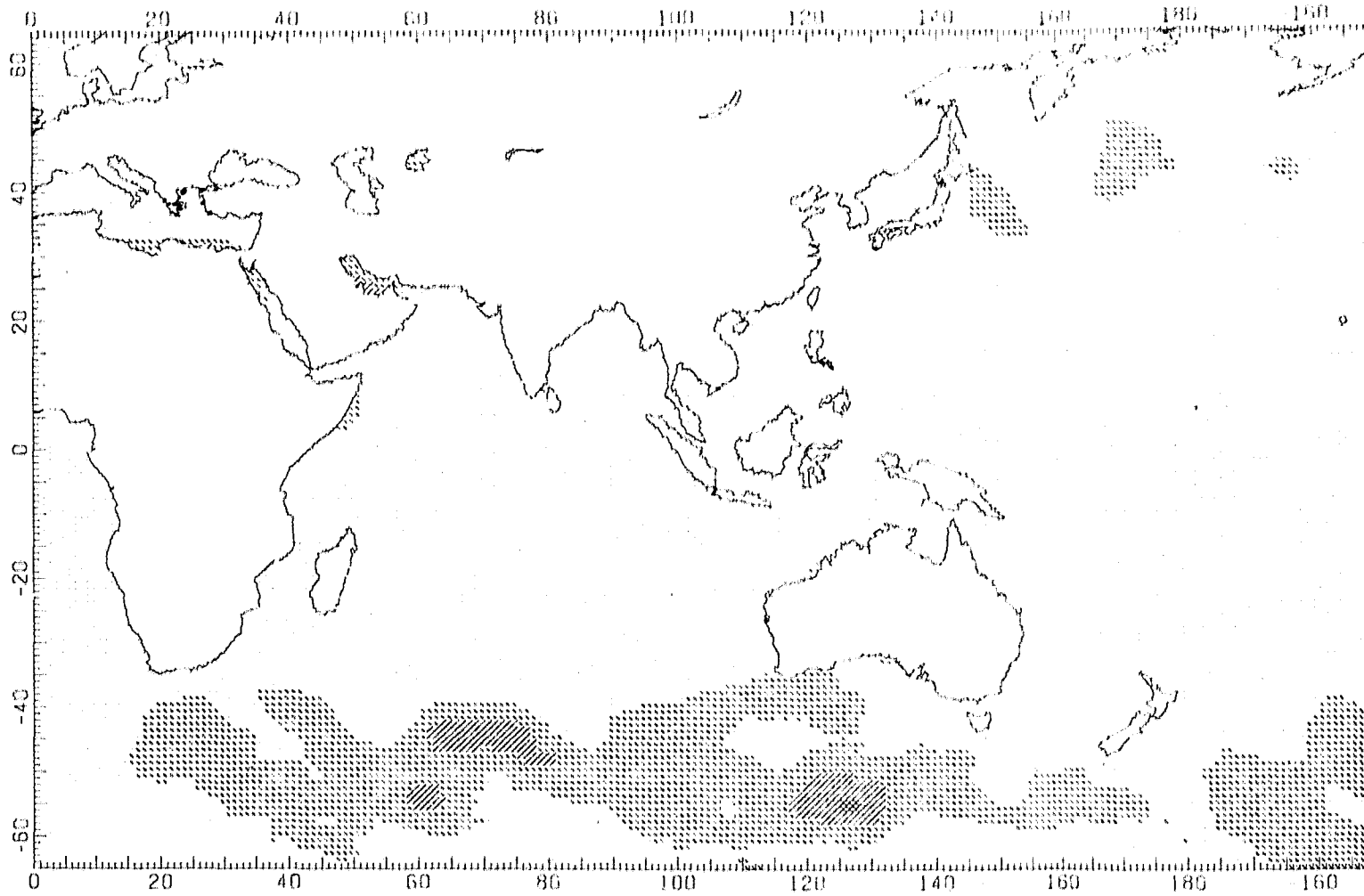


FOLDOUT FRAME

FOLDOUT FRAME

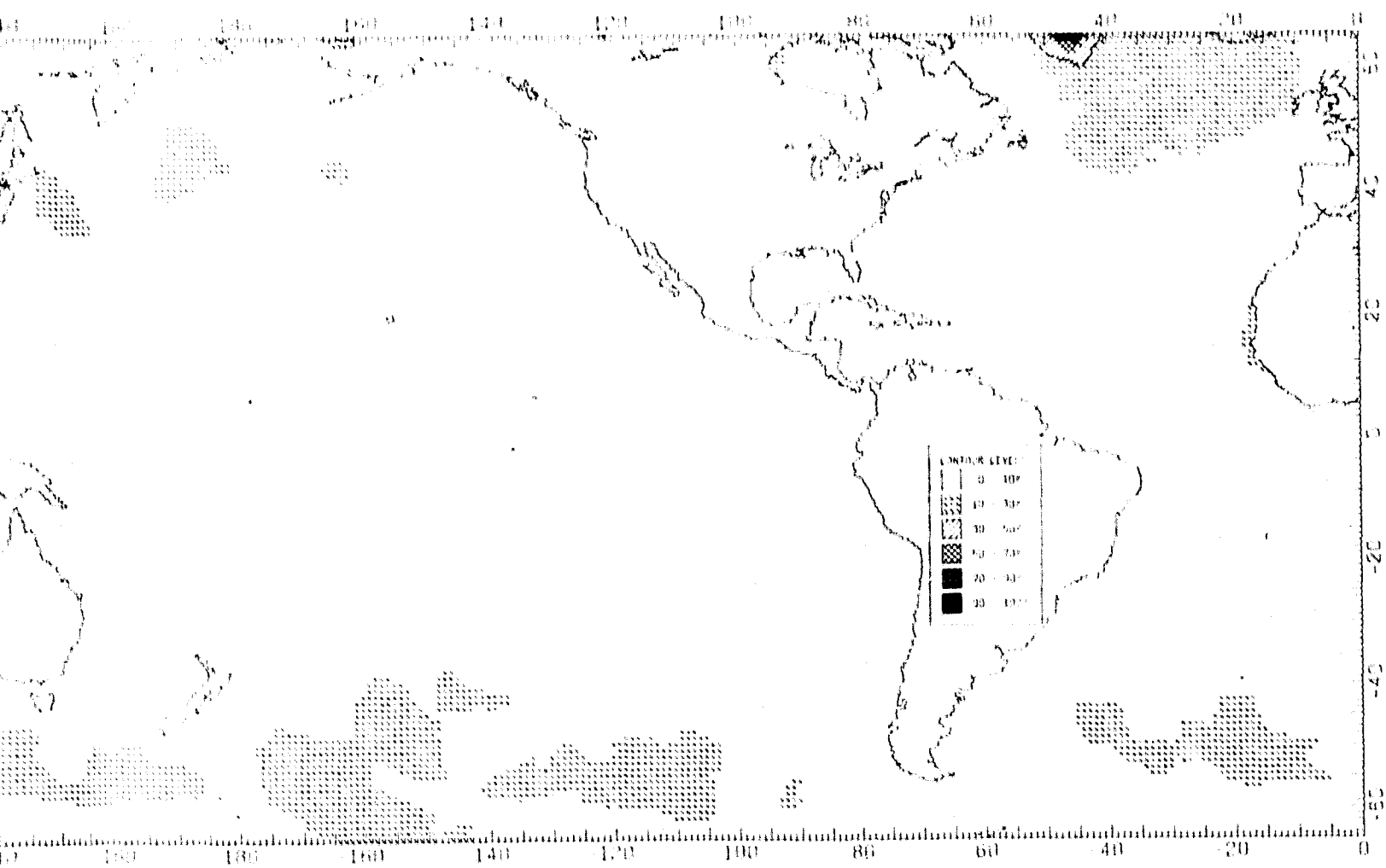



FOLDOUT FRAME

A.20 Entire Mission - Percent Significant Waveheight > 6.0 Meters

| 1. Report No. | 2. Government Accession No. | 3. Recipient's Catalog No. |
|---|---|---|
| NASA CR-156882 | | |

| 4. Title and Subtitle | 5. Report Date |
|---|---|
| A GLOBAL ATLAS OF GEOS-3 SIGNIFICANT WAVEHEIGHT DATA AND COMPARISON OF THE DATA WITH NATIONAL BUOY DATA | June 1981 |
| | 6. Performing Organization Code: 971.0 |
| 7. Author(s): J. D. McMillan | 8. Performing Organization Report No. |
| 9. Performing Organization Name and Address: EG&G Washington Analytical Services Center, Inc. P. O. Box 476 Pocomoke City, Maryland 21851 | 10. Work Unit No. |
| | 11. Contract or Grant No.: NAS6-2639 |
| 12. Sponsoring Agency Name and Address: NASA Wallops Flight Center Wallops Island, Virginia | 13. Type of Report and Period Covered: Contractor Report |
| | 14. Sponsoring Agency Code |

15. Supplementary Notes


16. Abstract

With the advent of satellite altimetry, it is now possible to estimate ocean wave characteristics with a high degree of accuracy. Specifically, the altimeter on board the Geodynamics Experimental Ocean Satellite (GEOS-3) sampled the radar return waveform, from which the ocean significant waveheight (the average of the heights of the one-third highest waves in a long sequence) at the subsatellite point could be estimates. This investigation determines the accuracy of the GEOS-3 significant waveheight estimates by comparing them with buoy measurements of significant waveheight. Then, a global atlas of the GEOS-3 significant waveheight estimates gathered during the entire mission of the spacecraft is presented and compared with data compiled by the U. S. Navy.

First, the GEOS-3 significant waveheight estimation algorithm is derived by analyzing the return waveform characteristics of the altimeter. It is shown that the difference between the waveform expected from a flat sea surface and the actual waveform observed returning from a non-flat sea surface can be analyzed to determine the magnitude of the significant waveheight. This technique employs a curve fitting procedure utilizing least squares estimation.

After the significant waveheight estimation algorithm has been derived, convergence considerations are examined. In particular, the rationale for a smoothing technique is presented and the convergence characteristics of the smoothed estimate are discussed. Then, a statistically representative sampling of GEOS-3 data is selected for comparison with buoy measurements and the accuracy of the GEOS-3 significant waveheight estimates is deduced, through statistical analysis, to be 50 cm.

Finally, the GEOS-3 significant waveheight estimates gathered during the entire mission of the spacecraft are assembled in the form of global atlas of contour maps. Both high and low sea state contour maps are presented, and the data are displayed both by seasons and for the entire duration of the GEOS-3 mission. The contour maps are then compared with contour maps compiled by the U. S. Navy and significant differences are found.


| 17. Key Words (Suggested by Author(s)) | 18. Distribution Statement |
|---|---|
| GEOS-3<br>altimeter<br>waveheight | Unclassified - Unlimited<br>STAR Category - 43, 48 |

| 19. Security Classif. (of this report) | 20. Security Classif. (of this page) | 21. No. of Pages | 22. Price* |
|---|---|---|---|
| Unclassified | Unclassified | 144 | |

*For sale by the National Technical Information Service, Springfield, Virginia 22151